The University of Leeds

Faculty of Medicine and Health

Leeds Institute of Cardiovascular and Metabolic Medicine

The Effect of Shear Stress on Weibel-Palade Bodies

Ashley Money

Submitted in accordance with the requirements for the degree of Doctor of Philosophy

December, 2023

Funded by the British Heart Foundation

Intellectual Property and Publication Statements

The candidate confirms that the work submitted is his own and that appropriate credit has been given where reference has been made to the work of others.

This copy has been supplied on the understanding that it is copyright material and that no quotation from the thesis may be published without proper acknowledgement.

The right of Ashley Money to be identified as Author of this work has been asserted by his in accordance with the Copyright, Designs and Patents Act 1988.

c 2023. The University of Leeds and Ashley Money

Acknowledgements

Firstly, I would like to thank my supervisor, Dr Lynn McKeown, for your guidance, support and ideas throughout this project. Your support through the covid-19 lockdown was invaluable, especially in facilitating new ideas and directions for the project when access to the lab was restricted. In the past year whilst I have been producing this thesis, your flexibility with meetings and advice on thesis writing has been extremely helpful. I really appreciate all that you have done.

I would also like to express my thanks to my secondary supervisor, Professor David Beech. I am grateful for all your support on the PhD programme as well as during our monthly meetings. Discussions with you, and Lynn, always challenged my thinking and encouraged me to think ahead with regards to the direction of the project and the end-goal. These discussions proved hugely beneficial in the long run.

To all the other members of the McKeown lab; Kat and Lucia for showing me the ropes when I first started; Sabina, Harriet and Ryan, it has been great working with you all and I am sure you will all be great scientists in the future.

Thank you to Kevin Cuthbertson, Charlotte Revill and Richard Foster (School of Chemistry, Leeds) for the Yoda1 analogues, including compound 2a. The Bioimaging Facility in the Faculty of Biological Science for your help with imaging, timely microscope repairs when they were down, and insightful training. Thanks to the University of Bristol proteomics facility for providing and analysing the proteomics data to support this project. Thanks also to Professor Hanjoong Jo (Emory University) for allowing me to analyse and use the data from the single-cell RNA sequencing experiments for use in this project.

To my partner, Chloe, I am incredibly grateful for your unwavering support, understanding and belief in me over the past 5 years. There’s no doubt I wouldn’t be in this position without you. Last but not least, a huge thanks to my family, mum, dad and Hayley, for believing in me and providing endless encouragement along the way.

Abstract

Background

Atherosclerosis is a focal disease, localised to arterial bifurcations and curvatures due to exposure of the endothelium to disturbed blood flow. The complex flow patterns in these regions of the vasculature promote atherosclerotic plaque development, partly by increasing the secretion of pro-inflammatory and pro-thrombotic components from endothelial cells. Many of these mediators reside in secretory organelles unique to the endothelium: Weibel-Palade bodies (WPBs). The untimely and unnecessary secretion of WPBs increases the susceptibility of the endothelium to atherosclerosis. The aim of this project is to investigate the effect of different types of flow on WPB morphology, cargo and function.

Methods and Results

High shear stress applied to cultured endothelial cells resulted in a decrease in WPB length compared to low oscillatory shear stress and static conditions. WPB number remained constant across all flow conditions. Single-cell RNA sequencing, coupled with proteomic analysis of the endothelial cell secretome, highlighted the impact of disturbed flow on both the gene expression of WPB cargo and associated genes, as well as the amount of protein secreted from the cells upon histamine stimulation. Additionally, HSS caused shorter vWF strings to form upon histamine stimulation and resulted in fragmentation of the Golgi apparatus, indicating a reduction of vWF function in regions exposed to HSS. Yoda1-evoked Piezo1 activation also leads to a shorter WPB population after 24 hours, and could be a useful tool to mimic and investigate the effects of shear stress of WPBs.

Conclusion

Disturbed flow results in longer WPBs and increased pro-inflammatory and pro-thrombotic mediators in endothelial cells, that may contribute to the focal progression of atherosclerosis in these areas. A better understanding of the molecular mechanisms that underlie these processes will provide avenues for the exploration of novel therapeutic targets in the treatment of cardiovascular disease.

Table of Contents

List of Figures

List of Tables

Abbreviations

ADAMTS13	A Disintegrin-like Metalloprotease domain with Thrombospondin type 1 motif, member 13
AMPK	AMP-activated Protein Kinase
Angpt1/Angpt2	Angiopoietin-1/Angiopoetin-2
ANOVA	Analysis of Variance
AP-1	Adaptor Protein-1
BSA	Bovine Serum Albumin
Ca^{2+}	Calcium
CD31	Cluster of Differentiation 31
CD63	Cluster of Differentiation 63
cDNA	Complementary Deoxyribonucleic Acid
cRFP	Common Repository of FBS Proteins
CT	Cycle Threshold
CVD	Cardiovascular Disease
EBM	Endothelial Basal Medium
EC	Endothelial Cell
ECM	Extracellular Matrix
EGM2	Endothelial Growth Medium-2
eNOS	Endothelial Nitric Oxide Synthase
ER	Endoplasmic Reticulum
ERK	Extracellular Signal-Regulated Kinase
ET-1	Endothelin-1
FAK	Focal Adhesion Kinase
FDR	False Discovery Rate
FGF	Fibroblast Growth Factor
FOV	Field of View
FoxO1	Forkhead box protein O1
GBF1	Golgi-specific Brefeldin A-resistance guanine nucleotide exchange Factor 1
GPCR	G-Protein Coupled Receptor
HAEC	Human Aortic Endothelial Cell
HMW	High Molecular Weight
HSS	High Shear Stress

HUVEC	Human Umbilical Vein Endothelial Cells
Igfbp7	Insulin growth factor binding protein-7
IL	Interleukin
kDa	(kilo) Daltons
KLF2/KLF4	Krüppel-like Factor-2/4
LDL(R)	Low Density Lipoprotein (Receptor)
LMW	Low Molecular Weight
LogFC	Log Fold Change
LOSS	Low Oscillatory Shear Stress
MAPK	Mitogen-Activated Protein Kinase
MFI	Mean Fluorescence Intensity
MS	Mass Spectrometry
MTOC	Microtubule Organising Centre
MyRIP	Myosin VIIA And Rab Interacting Protein
NO	Nitric Oxide
NOTCH	Neurogenic locus notch homolog protein
NS	Not Significant
NUCB1	Nucleobindin-1
PAR	Protease-Activated Receptors
PCA	Principal Component Analysis
PECAM-1	Platelet endothelial cell adhesion molecule
PFA	Paraformaldehyde
PI3K	Phosphoinositide 3-Kinase
PKA	Protein Kinase A
PLC	Phospholipase C
PMA	Phorbol 12-myristate 13-acetate
qPCR	Quantitative Polymerase Chain Reaction
(m)RNA	(messenger) Ribonucleic Acid
scRNAseq	Single Cell RNA Sequencing
SEM	Standard Error of the Mean
SMC	Smooth Muscle Cell
SPARC	Secreted Protein Acidic and Rich in Cysteine
TGN	Trans-Golgi Network
TMT	Tandem Mass Tagging

TNFα	Tumour Necrosis Factor Alpha
TRPV4	Transient Receptor Potential Vanilloid Subfamily 4
TTP	Thrombocytopenic Purpura
ULMW	Ultra-Large Molecular Weight
ULVWF	Ultra-Long von Willebrand Factor
UMAP	Uniform Manifold Approximation and Projection
VEGF	Vascular Endothelial Growth Factor
vWD	von Willebrand Disease
vWF	von Willebrand Factor
WPB	Weibel-Palade Body

Publications

Pedicini, L., Wiktor, SD., Simmons, KJ., **Money, A.**, McKeown, L. Affinity-based proteomics reveals novel binding partners for Rab46 in endothelial cells. Scientific Reports 11, Article number: 4054 (2021).

Money, A., Todd, HJ., Jo, H., Beech, DJ., McKeown, L. Low oscillatory shear stress regulates Weibel-Palade body size and vWF release. BioRxiv Preprint (2023).

Communications

The Effect of Flow on Weibel-Palade bodies. **Ashley Money**, David J Beech and Lynn McKeown. Physiological Conference, Aberdeen (2019).

The Effect of Flow on Weibel-Palade bodies. **Ashley Money**, David J Beech and Lynn McKeown. Dynamic Cell IV, Virtual Conference (2021).

Chapter 1 Introduction

Endothelial cells form a continuous monolayer, lining the internal surface of the vasculature. Their position in the vessel wall means they have a critical role in maintaining vascular homeostasis and integrity, acting as a tightly regulated barrier between the blood and surrounding tissues. The continuous exposure to haemodynamic forces induces morphological changes in endothelial cells, rendering certain areas of the vascular susceptible to atherosclerosis. This chapter provides an overview of endothelial cell biology and an introduction to shear stress and endothelial cell dysfunction. The focus then switches to Weibel-Palade bodies, their biogenesis, cargo and exocytosis, before summarising their clinical relevance. Finally, I discuss previous research investigating potential effects of shear stress on Weibel-Palade bodies and how this might render focal areas of the vasculature prone to endothelial dysfunction.

1.1 Endothelial cell biology

The human cardiovascular system comprises a complex network of arteries, veins and capillaries. The primary function of the cardiovascular system is to supply oxygenated blood to target organs and tissues, whilst pumping de-oxygenated blood and waste products to the respiratory organs. Arteries carry the oxygenated blood straight from the heart to the organs and have therefore evolved to cope with high pressures. Veins transport blood back to the heart and are designed to cope with lower pressures and prevent backflow with the presence of valves. The walls of arteries and veins both consist of 3 main layers (Figure 1.1). The tunica adventitia/externa is the outer layer of the blood vessel consisting of an elastic membrane and connective tissue that anchors the arteries to nearby tissues. The tunica media, the middle layer of the artery wall, is made up of a layer of smooth muscle cells (SMCs), much thicker in arteries than veins to cope with the high pressure from the heart. Finally, the tunica intima, a monolayer of cells known as the endothelium, which is in direct contact with the blood. The endothelium is often described as the largest organ in the body, with 10 trillion cells (Galley and Webster, 2004) that are all polarised, elongating with the flow direction in order to facilitate blood flow. As a result of this elongation, they are approximately 30-50 µm in length, 10-30 µm wide and 0.1-10 µm thick (Krüger-Genge *et al.*, 2019). Despite only being a single later of cells, they form

a semipermeable barrier, facilitating the transfer of molecules between the blood and the surrounding tissues and therefore playing a vital role in vascular biology and homeostasis (Galley and Webster, 2004). In addition, the endothelium produces a whole array of biologically active substances that perform a range of functions (Rubanyi, 1993; Cooke, 2000).

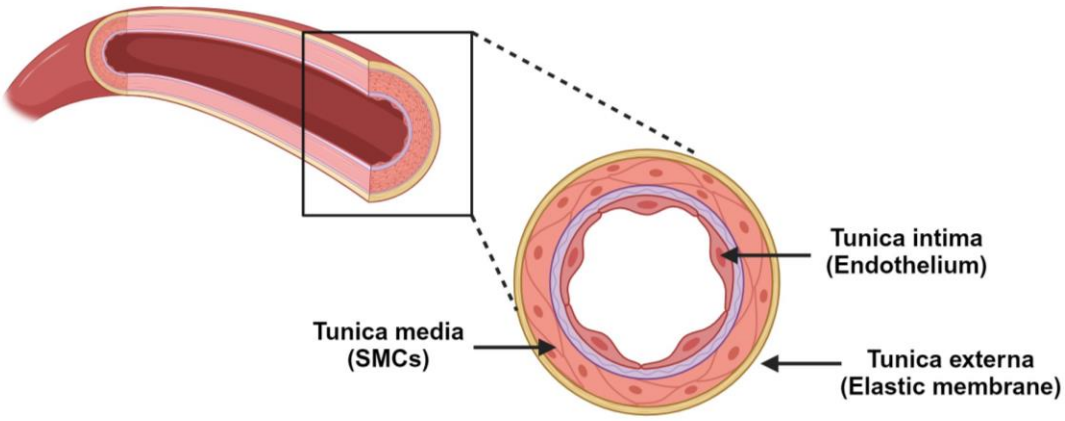

Figure 1.1 - Layers of the artery wall.
The arterial wall consists of the tunica intima, a single layer of endothelial cells in contact with the flowing blood, resting on a thin basement membrane composed of collagen and elastin. The tunica intima is supported by the next layer, the tunica media, a thick layer of SMCs, elastic tissue and collagen. Finally, the outermost layer of the artery wall is the tunica externa, comprised of an elastic membrane and connective tissue.

1.2 The role of the endothelium in the vasculature

The endothelium is optimally positioned to act as a mediator between the flowing blood and the surrounding tissues. It functions by responding to various chemical and physical signals, with varying responses depending on the type of stimulus. Under normal conditions, the general function of the endothelium is to facilitate blood flow. It does so by maintaining the blood in a fluid state and providing an anti-thrombotic surface that inhibits adhesion (Cooke, 2000). Under the appropriate stimulus, the endothelium can quickly switch to decrease blood flow through a variety of mechanisms (Gimbrone, Nagel and Topper, 1997).

1.2.1 Vascular tone

In order to maintain vascular homeostasis, the three layers of the vasculature work together to regulate the dilation and constriction of blood vessels that results in either increased or decreased blood flow respectively, also known as vascular tone. Vasodilation is known to be anti-inflammatory and anti-thrombotic, whereas vasoconstriction is associated with pro-inflammatory and pro-thrombotic effects (Cooke, 2000). The endothelium plays an important role in this regulation by detecting changes and responding by releasing factors that diffuse into the surrounding smooth muscle cells (SMCs) and mediate their contraction. A key factor released by endothelial cells is nitric oxide (NO), generated by endothelial NO synthase (eNOS) and L-arginine. It diffuses into the SMCs and leads to SMC relaxation and therefore vasodilation (Fleming, 2010). Laminar blood flow activates eNOS and therefore increases NO production (Corson *et al.*, 1996). This subsequently maintains the vascular wall in a quiescent state by inhibiting inflammation, cellular proliferation and thrombosis (Deanfield, Halcox and Rabelink, 2007). Vasoconstriction on the other hand, is induced by factors such as endothelin-1 (ET-1) and platelet-activating factor (PAF), which act to increase SMC contraction and restrict blood flow. Laminar blood flow decreases the levels of these factors and therefore acts to maintain homeostasis (Ando and Yamamoto, 2009).

1.2.2 Inflammation

The endothelium plays a crucial role in the body's response to inflammatory stimuli. It regulates inflammation by modulating the expression of adhesion molecules, such as selectins and integrins, on the cell surface. During this immune response, these adhesion molecules are more prevalent in the affected area, acting to recruit immune cells, facilitate attachment, rolling and subsequent transmigration of the immune cells into the surrounding tissues where they are required. Furthermore, endothelial cells contribute to the inflammatory cascade by releasing various cytokines into the bloodstream, amplifying the overall inflammatory response (Cines *et al.*, 1998).

1.2.3 Thrombosis

Under quiescent conditions, the endothelium plays a key role in maintaining normal, healthy blood flow. Under specific stimulus, such as vascular injury,

endothelial cells are required to induce blood clotting to reduce blood flow. In these instances, endothelial cells release vWF from storage organelles, known as Weibel-Palade bodies. vWF is highly multimerised and elongates upon exocytosis to form vWF strings that bind platelets from the blood. This ultimately leads to a clot and the reduction of blood flow. Similarly, the endothelium is responsible for releasing compounds that promote fibrinolysis, the process of breaking down blood clots, to resolve thrombotic events once they have occurred. Overall, the endothelium plays a key role in the regulation of thrombosis (Cines *et al.*, 1998).

1.2.4 Angiogenesis

Angiogenesis is the formation of blood vessels and requires migration, growth and differentiation of endothelial cells. Other than during developmental stages, the endothelium is a very quiescent cell type, maintained in this state by the autocrine action of signals such as VEGF, NOTCH, ANG-1 and FGFs (Carmeliet, 2005). Only 0.1% of all the endothelial cells are dividing at any time. In response to angiogenic stimulation such as in hypoxia or vascular injury, paracrine angiogenic signals such as VEGF, FGFs and Angiopoietin-2 are detected by ECs. This causes a switch to a proliferative state through the activation of a complex network of intracellular signalling pathways (Muñoz-Chápuli, Quesada and Angel Medina, 2004). An important factor in determining these responses in endothelial cells is the haemodynamic forces exerted on the cells by the flowing blood, one of which being the frictional force known as shear stress.

1.3 Shear Stress and Mechanotransduction

Endothelial cells have the ability to respond to not only humoral factors in the circulation, but also to mechanical forces exerted by blood flow and the cardiac cycle (Davies, Spaan and Krams, 2005). Mechanotransduction, the conversion of mechanical force into cellular signals, is vital for endothelial cell function and survival (Conway and Schwartz, 2013). Endothelial cells have evolved specialised mechanosensors to sense and adapt to their environment, influencing processes from embryonic development to adult physiology. Their position in the vasculature means they are exposed to three mechanical forces; pressure, circumferential stretch or tension, and shear stress (Traub and Berk,

1998), with the latter being the most significant due to its widespread effects on endothelial cell function.

Shear stress is the frictional force exerted by the flowing blood on the endothelial layer. It contributes to vascular health by regulating blood vessel tone, endothelial cell function, and the release of signalling molecules. Optimal shear stress is essential for maintaining the integrity and proper functioning of the vascular system (Davies, 2009). Physiological shear stress ranges from 1 to 70 dyn/cm^2, is proportional to the viscosity of the blood and the rate of blood flow, and varies depending on the architecture of the vessel (Tzima *et al.*, 2005; Davies, 2009). In straighter regions of the vasculature, blood flow is laminar, unidirectional and ordered, causing endothelial cells to undergo reorientation and alignment along their longitudinal axis parallel with the direction of blood flow (Dewey *et al.*, 1981) (Figure 1.2). Cell alignment in this manner promotes blood flow by reducing the resistance of the endothelium (Barbee *et al.*, 1995). Cells in these regions tend to be atheroprotective, expressing the well-characterised anti-atherogenic transcription factor, KLF2 (Dekker *et al.*, 2002; Parmar *et al.*, 2006). Endothelial cells expressing KLF2 exhibit anti-inflammatory, anti-thrombotic, anti-migratory, anti-fibrotic and anti-oxidant properties (Bhattacharya *et al.*, 2005; van Agtmaal *et al.*, 2012). It is therefore no surprise that atherosclerotic lesions rarely accumulate in regions of the vasculature exposed to laminar high shear stress (HSS).

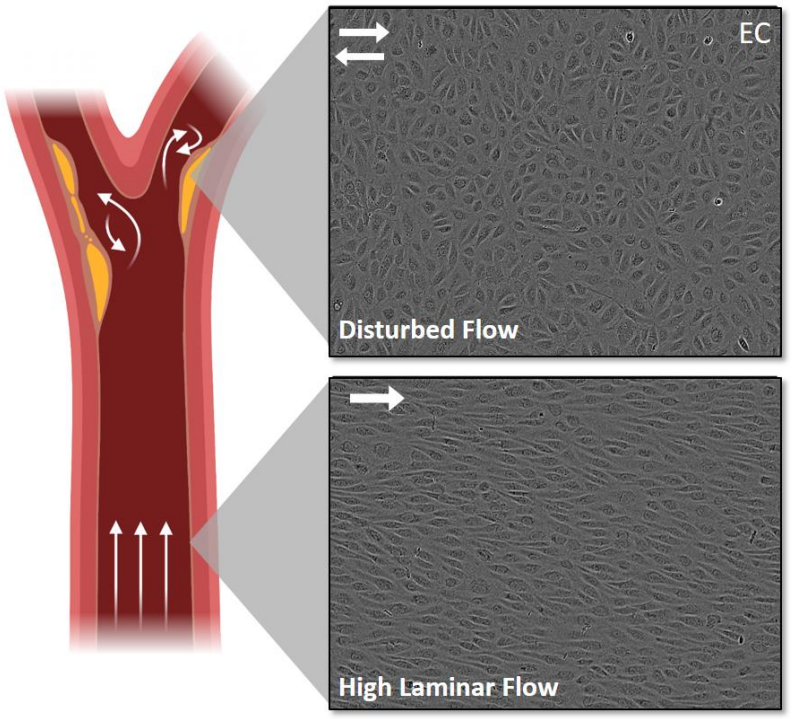

Figure 1.2 - Endothelial cell alignment at different regions of the vasculature.

Disturbed flow occurs at bifurcations and regions of abrupt curvatures, and results in non-aligned endothelial cells (top image). High laminar flow occurs at straight regions of arteries and results in aligned endothelial cells (bottom image). Arrows indicate the direction of flow (created with BioRender).

In contrast, bifurcations or abrupt curvatures in the vasculature cause blood flow to become disturbed and oscillatory, resulting in an overall decrease in shear stress (Ku *et al.*, 1985). Endothelial cells subjected to this type of flow do not reorient themselves, due to a lack of flow directionality, but instead adopt a cobblestone morphology as seen in cultured endothelial cells in the absence of flow (Figure 1.2). The cells sense the aberrant blood flow via mechanisms described previously, which ultimately leads to endothelial dysfunction and the increased prevalence of CVD such as atherosclerosis and thrombosis.

Endothelial cells sense shear stress with mechanosensors that are present on both apical and basal surfaces of the cells, as well as at cell-cell junctions. Important mechanosensors include platelet endothelial cell adhesion molecule (PECAM-1)/cluster of differentiation 31 (CD31), integrins, GPCRs and G-proteins. There are also a number of mechano-sensitive ion channels including

Piezo channels, TRPV4 channels and P2X4 purinoceptors. When endothelial cells are subjected to shear stress, these mechanosensors detect the mechanical forces and initiate intracellular signalling pathways. These pathways, in turn, regulate gene expression, cell morphology, and the release of signalling molecules. The ability of endothelial cells to sense shear stress is crucial for maintaining vascular homeostasis and adapting to changes in blood flow.

1.3.1 Integrins

Integrins are membrane-associated glycoproteins composed of α and β subunits, each featuring a large extracellular domain, a transmembrane spanning region, and a short cytoplasmic region. The extracellular domain binds to extracellular matrix (ECM) proteins, while the cytoplasmic domains interact with intracellular signalling molecules that modulate processes such as cytoskeletal organization, signal transduction, and cell motility (Shyy and Chien, 2002). The majority of integrins activate focal adhesion kinase (FAK) and Shc, which are crucial for initiating these signalling pathways. In response to shear stress, cells enhance their attachments to the ECM and neighbouring cells, a process initiated by the activation of FAK and the remodelling of focal adhesions in the direction of flow (Li *et al.*, 1999). Rho, a mediator of mechanical signalling, plays a significant role in organizing the actin cytoskeleton and regulating the activity of the Rho small GTPase family downstream of integrins. This activity is vital for cell alignment in response to shear stress (Tzima *et al.*, 2001).

1.3.2 Mechano-sensitive ion channels

A wide range of ion channels have been identified as being involved in shear stress sensing, including TRPV4 channels, P2X4 purinoceptors, and Piezo channels. Piezo1 and Piezo2, initially identified by Coste et al. (2010) as mechanically activated cation channels, have since become key proteins in mechanotransduction. Piezo1 is widely expressed throughout the body and is particularly significant in the context of shear stress due to its expression in endothelial cells. When these cells sense mechanical stimulation, such as stretching and shear stress, a conformational change in the Piezo1 structure results in the central pore opening, allowing cations, particularly Ca2+, to pass through (Zhao *et al.*, 2016). This leads to a cascade of intracellular signalling events that promote endothelial cell alignment, cytoskeletal rearrangements, and

gene expression changes, which help maintain vascular integrity and adapt to varying haemodynamic conditions. The primary role of Piezo1 is to selectively transport Ca^{2+} from the extracellular environment to the cytosol of endothelial cells in response to mechanical forces (Li *et al.*, 2014; Ranade *et al.*, 2014). This calcium influx can regulate downstream signalling pathways and influence vascular remodelling. Additionally, the activation of endothelial nitric oxide synthase (NOS3) is another critical response. The synthetic small molecule Yoda1 was identified when a library of approximately 3.25 million compounds were screened for their potential to activate Piezo1 or Piezo 2 (Syeda *et al.*, 2015). It was identified as a known activator of Piezo1, and has proven uses in studying the effects of shear stress on endothelial cells by mimicking mechanical forces and serves as a key tool to providing further insights into Piezo1's role in vascular biology.

1.3.3 GPCRs and G-proteins

G protein-coupled receptors (GPCRs) are implicated as mechanosensitive molecules. For example, fluid shear stress induces ligand-dependent conformational changes in the bradykinin B2 receptor in response to shear stress (Chachisvilis, Zhang and Frangos, 2006). Additionally, a large proportion of shear-responsive signalling pathways, such as ERK, AKT, and eNOS activation, rely on the lysophospholipid GPCR molecule, sphingosine-1-phosphate receptor 1. Many GPCRs present on the surface of endothelial cells activate intracellular G proteins and subsequently modulate a variety of signalling pathways. Several G proteins have also been shown to be rapidly activated upon the application of shear stress, independent of GPCR activation (Gudi, Clark and Frangos, 1996, p. 1; Chachisvilis, Zhang and Frangos, 2006). More specifically, the G protein Gαq/11 has been shown to associate with PECAM-1 in endothelial cells under laminar shear stress in vivo, but not under disturbed flow (Otte *et al.*, 2009). Similarly, in vitro, Gαq/11 and PECAM-1 are associated in unstimulated endothelial cells but rapidly dissociate in response to shear stress. Flow-mediated Ras activation has also been shown to be mediated by Gαq/11, implicating a role for G proteins in the activation of shear-induced MAPK signalling (Gudi *et al.*, 2003; Givens and Tzima, 2016). GPCRs and G proteins are proven components in the mechanotransduction of shear stress, playing key roles in maintaining vascular homeostasis and adapting to changes in blood flow.

1.3.4 Primary Cilia

Primary cilia are approximately 3-5 μm rod-like, non-motile structures that protrude from the luminal surface of endothelial cells. The body of the primary cilia are made from microtubules that are linked to the microtubular system of the cells and other components of the cytoskeleton. Mechanotransduction occurs are a result of bending of the primary cilia with shear stress and triggers a cascade of intracellular signalling events that influence endothelial cell function (Van der Heiden *et al.*, 2008). Their linked to the cytoskeleton implicates a role in cytoskeletal reorganisation under flow. Bending has also been shown in result in an influx of Ca^{2+}, leading to the activation of eNOS and therefore NO, implicating the primary cilia in the regulation of vascular tone (Nauli *et al.*, 2008). Interestingly, they are more apparent in regions of the vascular exposed to low or disturbed flow (Van der Heiden *et al.*, 2008), with exposure to laminar shear resulting in a rapid reduction of primary cilia (Iomini *et al.*, 2004). This indicates a correlation between the presence of flow-sensing primary cilia and atheroprone sites of the vasculature.

1.3.5 Glycocalyx

The endothelial glycocalyx, a layer of glycoproteins, hyaluronan, and proteoglycans like syndecan-1 and -4, plays a critical role in shear stress sensing. It forms an extended endothelial surface layer that includes plasma proteins, growth factors, and cytokines. The glycocalyx acts as a mechanosensor by dampening shear forces, with syndecans linking to the cytoskeleton to transfer these forces (Weinbaum, Tarbell and Damiano, 2007). Inflammation, induced by TNFα, reduces glycocalyx height, indicating its density is negatively regulated by endothelial inflammation (Henry and Duling, 2000). Knockout studies show that the absence of syndecans disrupts shear stress responses, actin dynamics, and leads to increased inflammation and atherosclerosis. Thus, the glycocalyx is essential in mechanotransduction, interacting closely with integrins to mediate endothelial responses to mechanical forces.

1.3.6 Caveolae

Caveolae are flask-shaped invaginations found in various cell types, including endothelial cells (ECs), where they are enriched due to exposure to mechanical stress. These structures are formed by caveolin (CAV1-3) and cavin (cavin1-3)

proteins, contributing to their stability and function in buffering cell membranes against mechanical stress. Studies in rat lungs demonstrated that increased perfusion of the vasculature led to increased protein tyrosine phosphorylation within caveolar compartments, particularly enriched with endothelial nitric oxide synthase (eNOS), critical for shear-induced eNOS activation (Victor Rizzo *et al.*, 1998; V. Rizzo *et al.*, 1998). Genetic evidence from Cav1 knockout mice revealed impaired vasodilation and increased arterial wall thickness, indicating caveolae's role in vascular function and adaptation (Givens and Tzima, 2016). Despite their response to shear stress, caveolae may not directly sense mechanical forces but rather serve as regulated structures involved in endothelial mechanotransduction pathways. Further research is needed to clarify their specific role in endothelial force sensing and signalling.

1.3.7 Junctional Mechanosensors

Endothelial cell function relies heavily on adhesion proteins such as Platelet Endothelial Cell Adhesion Molecule-1 (PECAM-1 or CD31) and Vascular Endothelial Cadherin (VE-Cadherin). PECAM-1 facilitates homophillic binding between cells at junctions, crucial for cell-cell adhesion in various tissues including endothelial cells. VE-Cadherin, linked to the cytoskeleton via ß-catenin, supports VEGF-dependent functions like vessel maturation and angiogenesis (Carmeliet *et al.*, 1999). Both proteins are integral to mechanotransduction pathways: PECAM-1 undergoes rapid tyrosine phosphorylation and ERK activation in response to shear stress, dependent on Fyn kinase (Chiu, McBeath and Fujiwara, 2008). VE-Cadherin and VEGFR2 also redistribute on the cell membrane under shear stress, forming clusters that activate PI3K/AKT signalling and enhance eNOS phosphorylation. Together with VEGFR2, CD31 and VE-Cadherin form a mechanosensory complex crucial for sensing both laminar and disturbed flow, influencing endothelial responses and inflammation in vivo (Chuntharpursat-Bon *et al.*, 2023).

1.4 Endothelial Dysfunction and Atherosclerosis

Endothelial dysfunction is used to describe endothelial cells that can no longer perform their normal function (Gimbrone Michael A. and García-Cardeña Guillermo, 2016). Normal endothelial function relies on a fine balance of opposing forces and effects, such as pro-inflammatory mediators and anti-inflammatory

mediators, or growth inhibiting factors and growth-promoting factors. Endothelial dysfunction occurs when there is an imbalance in one or more of these processes (Cooke, 2000). Risk factors such as hypertension, hypercholesterolaemia, smoking and diabetes, all increase susceptibility of arteries to endothelial dysfunction. Disturbed flow determines the localisation of this increased susceptibility to specific regions of the vasculature.

Atherosclerosis is a chronic disease of the artery walls, and begins with endothelial dysfunction. Endothelial cells that, under normal conditions, actively resist the adhesion of leukocytes, begin to express leukocyte adhesion molecules on their surface. This, unsurprisingly, leads to leukocyte adhesion from the flowing blood and promotes the early stages of atherogenesis (Libby, Ridker and Hansson, 2011). The adhered leukocytes, predominantly monocytes, extravasate into the intimal layer of the artery wall where they mature into macrophages and eventually lipid dense foam cells (Figure 1.3b). At this point, SMCs migrate into the media layer into the intima (Figure 1.3c), proliferating and producing extracellular matrix molecules such as collagen and elastin, that form a fibrous cap over the emerging plaque, now constituting a necrotic core consisting of foam cells and lipids (Basatemur *et al.*, 2019). The increasing size of the plaque in the artery wall causes narrowing of the lumen and therefore tissue ischaemia. Thrombosis typically occurs upon disruption of the fibrous cap that has formed over the plaque (Figure 1.3d). This results in release of coagulation proteins into the blood and the formation of a thrombus, which blocks the lumen and disrupts the flowing of blood (Libby, Ridker and Hansson, 2011).

The initiation and progression of atherosclerosis is facilitated by a diverse array of signalling pathways and proteins that are secreted from endothelial cells. A significant proportion of the proteins that contribute to atherosclerosis reside in endothelial-specific storage vesicles, Weibel-Palade bodies (WPBs). The next section of this chapter will provide an overview of WPBs and their role in atherosclerosis, later focusing on what we know about shear stress regulation of WPB biogenesis and function.

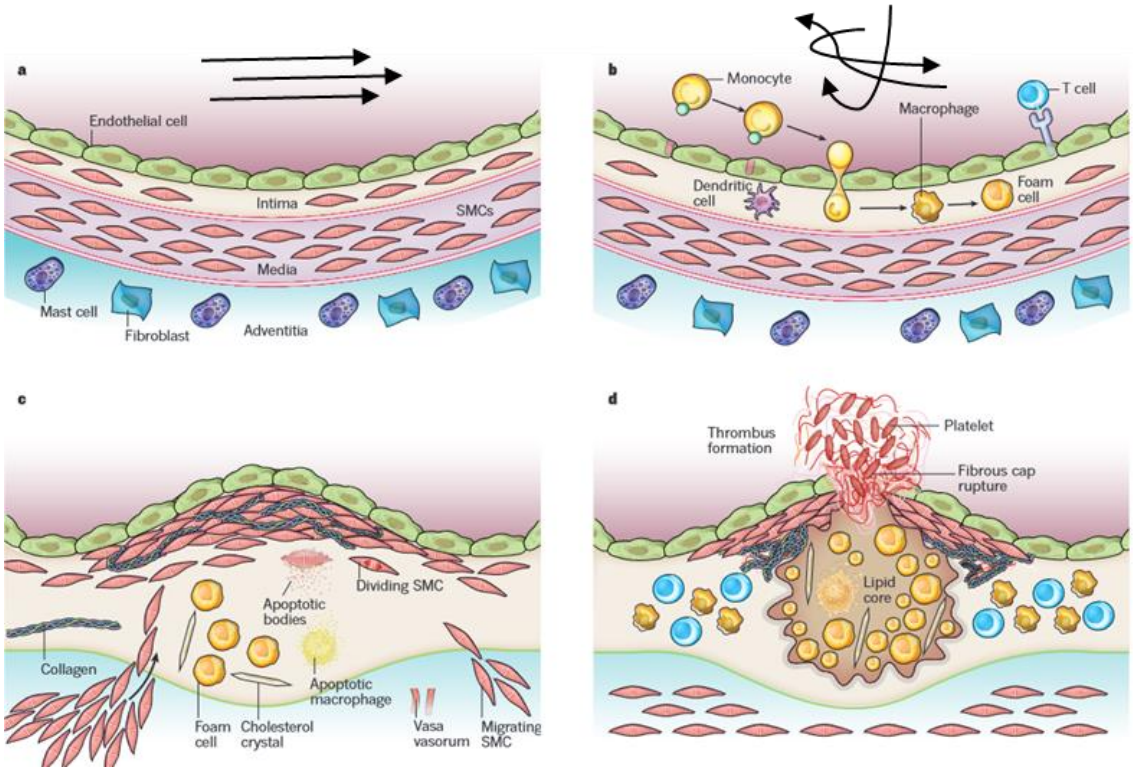

Figure 1.3 - Stages of atherosclerotic plaque development.

A) A normal artery with atheroprotective flow and a quiescent endothelium. All three layers of the artery wall are still intact. B) Under disturbed blood flow, the endothelial cells begin to express adhesion molecules on the cell surface leading to monocyte attachment and subsequent extravasation into the intimal layer of the artery wall. These monocytes mature into macrophages, taking in more and more lipids before evolving into a foam cell. C) At this stage, SMCs divide and migrate from the medial layer to the intimal layer, and synthesis of the matrices collagen, elastin and proteoglycans are increased. D) Lipids from dying macrophages and SMCs begin to accumulate in the form of a lipid core. The accumulation and size of the atherosclerotic lesion worsens, before the fibrous cap that has formed fractures, enabling the release of blood coagulation factors such as vWF, into the flowing blood. This results in the release of tissue factor and other members of the coagulation cascade, leading to thrombosis and a blood clot, impeding blood flow in that artery, and leading to serious downstream consequences as a result (This figure has been adopted from Libby P, Ridker PM & Hansson GK, 2011 with permission from the publisher. It has been adapted to show the direction of blood flow).

1.5 Weibel-Palade Bodies

Weibel-Palade bodies were first identified in 1964 by George Palade and Ewald Weibel when scanning a rat pulmonary artery using electron microscopy (Weibel and Palade, 1964). They observed long, rod-shaped structures residing in the endothelial cell cytoplasm, approximately 0.1 µm in width and up to 3 µm in length (Figure 1.4). Cross-sectional analysis showed a parallel arrangement of tubules along the longitudinal axis, enclosed by a close-fitting membrane. Despite these initial observations, the function of these novel endothelial organelles was not discovered for another 20 years.

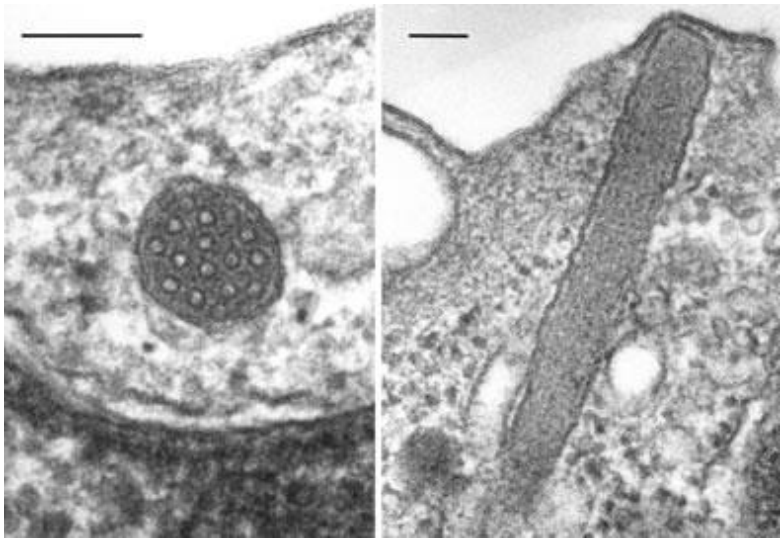

Figure 1.4 - WPB Morphology.
Electron micrographs (EM) of a transverse (left) and longitudinal (right) sections a WPB, showing the highly organised individual vWF tubules and their parallel alignment (Weibel, 2012). Scale bars = 0.1 µm.

The Wagner lab discovered that von Willebrand factor (vWF) was stored in WPBs in 1982 and was the most likely structure to form these tightly packed parallel tubules observed in electron microscopy images (Wagner, Olmsted and Marder, 1982). This was followed by the discovery of the leukocyte adhesion molecule P-selectin present in the membrane of WPBs in 1989 by the same group, and that of Roger McEver (Bonfanti *et al.*, 1989; McEver *et al.*, 1989). Since then, numerous other WPB cargoes have been identified (Table 1.1) with various functions. The combination of inflammatory and thrombotic mediators present in WPBs led Denisa Wagner to describe them as ‘the perfect first aid kit after an insult to the vasculature’. Given their vital role in endothelial cell biology,

extensive research has been dedicated to advancing our understanding of WPBs at every stage of their lifecycle.

1.5.1 WPB lifecycle

The WPB lifecycle begins with vWF synthesis and biogenesis of immature WPBs in the endoplasmic reticulum. These WPBs undergo maturation in the Golgi apparatus, incorporating essential cargo proteins before either constitutive release or storage in the cytoplasm of the endothelial cell. Upon stimulation, such as vascular injury, WPBs undergo exocytosis, releasing their contents into the vessel lumen to promote inflammation and thrombosis. After release, the remaining membrane components are recycled, allowing the endothelial cells to respond to future stimuli.

1.5.1.1 WPB Biogenesis

vWF synthesis is the first stage and driving force of WPB biogenesis. Endothelial cells devoid of vWF do not contain WPBs, and the heterologous expression of recombinant vWF in non-endothelial cell types results in the production of WPB-like granules, highlighting the importance of this protein in their biogenesis (Wagner *et al.*, 1991; Haberichter *et al.*, 2005). Initially synthesised as a 350 kDa monomer comprised of a signal sequence (22 residues), a pro-peptide (741 residues) and the mature protein (2050 residues), vWF undergoes various rounds of dimerisation, multimerisation and tubulation before forming nascent WPBs. Glycosylation occurs in the ER at 12 N-linked sites, before assembling into dimers through the formation of disulphide bonds between cysteine residues located in the C-terminal of the protein (Titani *et al.*, 1986; Voorberg *et al.*, 1991). At this stage the vWF exits the ER and enters the Golgi apparatus, undergoing carbohydrate modifications including the addition of O-linked sugar and maturation of the N-linked oligosaccharides (Wagner and Marder, 1984), before reaching the TGN. Here, N-terminal disulphide bonds form between vWF dimers, resulting in vWF multimers that are then cleaved leaving mature vWF and the propeptide (Voorberg *et al.*, 1990). Multimerisation is induced by a decrease in pH between the ER and the TGN, causing vWF multimers and propeptide to condense into tubules before protruding from the TGN in vesicles coated with clathrin and adaptor protein-1 (AP-1). The highest molecular weight multimers of vWF are sorted into WPBs, whereas less multimerised, low molecular weight

vWF is constitutively secreted once it has left the TGN. Importantly, low molecular weight vWF has 100 times less affinity for their platelet receptor than the highly multimerised vWF (Federici *et al.*, 1989; Michaux and Cutler, 2004). The characteristic elongated cigar-shape of WPBs is due to the multimerisation of several vWF quanta. This multimerisation is partly dependent on the morphology of the Golgi ribbon, a structure formed by the linkage of multiple piles of flat membrane cisternae, also known as Golgi mini stacks (Ferraro *et al.*, 2014). Under canonical circumstances, the Golgi mini stacks align to form a continuous ribbon, which allows for co-packaging of multiple vWF quanta into a single forming WPB. The more vWF quanta co-packaging that occurs, the longer the WPB. Those that are stored in WPBs undergo a series of maturation steps. Proteins are recruited to the membrane of newly formed WPBs, including P-selectin, the tetraspanin CD63 (Vischer and Wagner, 1993) and the small GTPases Rab3D and Rab27a, to name a few. The recruitment of Rab27a is considered the final step in WPB maturation due to its role in exocytosis, forming part of a complex that anchors WPBs to actin at the cell periphery (Hannah *et al.*, 2003).

1.5.2 WPB cargo

The primary function of WPBs is to prevent infection and to prevent bleeding after vascular injury by promoting inflammation and thrombosis. This is reflected in the continuously growing list of WPB cargo.

1.5.2.1 vWF

As described previously, the multimeric glycoprotein, vWF, is the main constituent of WPBs and is tightly packed into tubules organised a longitudinal array (Wagner, 1990). It is a well-characterised pro-coagulation protein that can be rapidly release into the vessel lumen, binding to platelets and Factor VIII to promote clotting. Upon vascular injury, this is exactly what the body needs in order to prevent blood loss. However, there is also a ‘dark side’ to this molecule, so much so that it has been described as the ‘Jedi knight of the bloodstream’ (Springer, 2014). When thrombosis occurs excessively or inappropriately, it can lead to serious complications such as heart attacks and strokes, often coinciding with sites of atherosclerotic plaque accumulation in the arterial walls.

vWF can be secreted from endothelial cells in the form of low molecular weight (LMW), high molecular weight (HMW), or ultra-large molecular weight (ULMW) multimers (Tsai *et al.*, 1991). While LMW multimers are constitutively secreted, a substantial proportion of plasma vWF consists of HMW multimers (Michaux and Cutler, 2004). These HMW and ULMW multimers form strings on the surface of the endothelium, and unravel under the force of the flowing blood. This reveals its monomers for multimeric binding to platelets to form a platelet plug (Springer, 2014, p. 201). vWF forms a complex with Factor VIII in the bloodstream, a pro-coagulation factor that acts as a co-factor in the activation of Factor X. This prevents its clearance and degradation, allowing it to perform it's normal function in the arterial layer.

The turnover of the WPB population is less than 24 hours (Kobayashi *et al.*, 2000). This relatively rapid turnover enables endothelial cells to fine-tune the contents of WPBs based on the cellular environment. The differential recruitment of cargo results in a non-homogeneous population of WPBs, exhibiting variations both within a cell and between different cells in the vicinity.

1.5.2.2 Angpt2

An example of a WPB cargo that is differentially regulated is the angiogenic factor, Angiopoietin-2, one of a family of growth factors involved in angiogenesis. Both Angpt1 and Angpt2 are ligands of the endothelial receptor tyrosine kinase Tie-2. Angpt1 mediated activation of Tie-2 exerts anti-inflammatory effects, regulating endothelial cell survival, blood vessel maturation (Suri *et al.*, 1996; Thurston *et al.*, 2000). Low-level Tie-2 activation as a result of Angpt1 binding contributes to a mature quiescent phenotype of the resting vascular endothelium (Fiedler *et al.*, 2004a). Angpt2 on the other hand, acts in an autocrine manner, binding to the Tie2 receptor with the same binding affinity, but with an antagonistic role. It's expression is tightly regulated and is triggered by inflammatory mediators such as thrombin and conditions such as hypoxia (Akwii *et al.*, 2019). Localisation of Angpt2 in WPBs enables a relatively long half-life of over 18 hours, and rapid secretion upon stimulation by compounds such as PMA, thrombin and histamine. The effects of Angpt2 and their localisation in WPBs demonstrates an important role in maintaining and disrupting vascular homeostasis (Fiedler *et al.*, 2004a).

1.5.2.3 P-selectin

P-selectin, a leukocyte adhesion molecule, is recruited to the membrane of WPBs during their biogenesis (McEver *et al.*, 1989). This 140 kDa single-chain glycoprotein is expressed in endothelial cells and circulating platelets. Upon stimulation, WPBs traffic to the cell membrane, leading to the expression of P-selectin on the cell surface. P-selectin, alongside other selectins, capture leukocytes from the flowing blood, causing them to roll on the surface of the endothelium. Subsequently, the leukocytes then bind to integrins, further slowing their movement and promoting extravasation into the arterial wall at the site of inflammation or vascular injury (Wagner and Frenette, 2008).

Interestingly, endothelial cells have the ability to transduce signals from the local microenvironment into a specific secretory response by tailoring the contents of individual WPBs (Schillemans *et al.*, 2019). P-selectin, for example, has only been observed in WPBs that are devoid of Angpt2, and these P-selectin containing WPBs have been shown to undergo different trafficking events based on the type of stimulus applied to the cells. This control over WPB contents allows endothelial cells to finely tune their secretory response to any injury or prevailing vascular conditions (Fiedler *et al.*, 2004a; van Agtmaal *et al.*, 2012; Miteva *et al.*, 2019).

1.5.2.4 Other cargoes

In addition to vWF, P-selectin and Angpt2, numerous other cargoes have been identified within WPBs. Moreover, further sets of proteins have been identified as likely candidates for WPB cargo through proximity proteomic analysis (van Breevoort *et al.*, 2012; Holthenrich *et al.*, 2019). A list of bona fide WPB cargo with their primary function can be found in Table 1.1. Here it is clear that all WPB cargo contribute to the overall function of WPBs and their cargo, which it to promote inflammation and thrombosis.

Component	Function	Reference
von Willebrand Factor (vWF)	Thrombosis – platelet aggregation	(Wagner, Olmsted and Marder, 1982)
P-selectin	Inflammation – leukocyte recruitment)	(Bonfanti *et al.*, 1989; McEver *et al.*, 1989)
Angiopoietin-2 (angpt2)	Angiogenesis	(Fiedler *et al.*, 2004b)
Endothelin-1 (ET-1)	Vasoconstriction	(Russell, Skepper and Davenport, 1998)
Endothelin converting enzyme	Vasoconstriction	(Russell Fraser D., Skepper Jeremy N., and Davenport Anthony P., 1998)
CD63/lamp3	Cell adhesion/migration (P-selectin co-factor)	(Vischer and Wagner, 1993)
IL-8	Inflammation – granulocyte adhesion/migration	(Utgaard *et al.*, 1998)
Tissue plasminogen activator (tPa)	Fibrinolysis	(Emeis *et al.*, 1997; Huber *et al.*, 2002)
Osteoprotegerin	Vascular homeostasis	(Zannettino *et al.*, 2005)
Eotaxin-3	Inflammation – eosinophil recruitment/migration	(Øynebråten *et al.*, 2004)
Alpha-(1,3)-fucosyltransferase	Glycosylation	(Schnyder-Candrian *et al.*, 2000)
IGFBP7	Angiogenesis	(van Breevoort *et al.*, 2012)
IL-6	Inflammation	(van Agtmaal *et al.*, 2012)

Table 1.1 – Bona fide WPB cargo.

1.5.3 Intracellular Transport

Following biogenesis, WPBs undergo a maturation phase during which they recruit several GTPases of the Rab family, namely, Rab27A (Hannah et al. 2003), several Rab3 isoforms (Knop *et al.*, 2004), Rab15, Rab33, Rab37 (Zografou *et al.*, 2012), and Rab46 (Miteva *et al.*, 2019). Rab GTPases play a fundamental role in the trafficking of intracellular organelles, including vesicle formation at the donor membrane, trafficking along the cytoskeleton, and vesicle fusion at the

acceptor membrane. As a result, they are often referred to as master regulators of vesicle trafficking (Stenmark, 2009). They act as molecular switches, cycling between their GDP-bound ‘off’ state and GTP-bound ‘on’ state, and regulate downstream effector proteins when in their GTP-bound state. Many of these effector proteins, such as MyRIP, Munc13-4, and Slp4-a, are recruited to WPBs and promote interaction with the cytoskeleton and/or plasma membrane (Nightingale *et al.*, 2009).

Rab46 was identified in our lab group as an unusually large GTPase, characterised by the presence of an extra Ca^{2+} sensing, EF-hand domain (Wilson et al. 2015. Previous work in the McKeown lab identified the role of Rab46 as coupling stimuli to the release of specific WPB cargo (Miteva *et al.*, 2019). More specifically, Rab46 is recruited to P-selectin-negative WPBs, and mediates histamine induced retrograde trafficking of a subset of WPBs containing Angpt2 towards the mitochondrial organising centre (MTOC). This retrograde trafficking is independent of Ca^{2+} and cAMP, but relies on Ca^{2+} to disperse WPBs from the MTOC (Miteva *et al.*, 2019). These findings suggest that endothelial cells can prevent the secretion of functionally unnecessary cargo by redirecting a subset of WPBs to the MTOC, whilst secreting functionally necessary cargo. Affinity-based proteomics has since been performed (Pedicini *et al.*, 2021), and identified dynein and ATPase Na+/K+ transporting subunit alpha 1 (ATP1α1) as Rab46 effector proteins. This, along with observations in previous experiments, reinforced evidence that retrograde trafficking of WPBs to the MTOC after histamine stimulation is dynein-dependent (Pedicini *et al.*, 2021). Rab46 is just one member of numerous Rab GTPases that play important roles in intracellular transport and facilitate the multi-faceted process of WPB exocytosis.

1.5.4 WPB Exocytosis

Endothelial cells secrete vWF via three routes: basal, constitutive and regulated. The level of multimerisation that occurs at the TGN determines which pathway is used. LMW vWF multimers traffic to the plasma membrane and are released immediately after synthesis via the constitutive pathway (Sporn, Marder and Wagner, 1986). The majority of this secretion occurs at the basolateral membrane. HMW and UHMW vWF multimers are condensed into tubules and stored in WPBs (Zenner *et al.*, 2007). Surprisingly, early studies indicated that the storage of vWF in WPBs was an incredibly inefficient process, with only 5 –

10% stored (Tsai *et al.*, 1991). A large proportion of this stored vWF is released via basal secretion at the apical endothelial surface, most likely facilitating a gradual turnover of the WPB population and supporting the reported half-life of WPBs of 24 hours (Kobayashi *et al.*, 2000; Giblin, Hewlett and Hannah, 2008). vWF that is not secreted as part of the basal pathway, resides in the cytoplasm and is secreted upon endothelial cell stimulation. Regulated exocytosis can be initiated by a wide range of physiological and pathological stimuli that use either Ca^{2+} or cAMP as intracellular second messengers that are coupled to ligand-gated receptors on the cell surface.

Ca^{2+} mediated stimuli, including histamine and thrombin, lead to the rapid release of large quantities of WPB cargo, promoting local inflammation and thrombosis, often in response to vascular injury. Histamine and thrombin use distinct common signalling pathway that converge at the same effector pathways to control WPB exocytosis according to the response required. More specifically, histamine and thrombin bind to GPCRs, namely H_1 and PAR1, respectively. This binding activates phospholipase C (PLC), which cleaves membrane bound phosphatidylinositol 4,5-bisphosphate (PIP_2), initiating the phosphatidylinositol pathway. This pathway leads to an elevation in cytoplasmic Ca^{2+}. The increased Ca^{2+} forms a complex with calmodulin and the small GTP-binding protein Ral, triggering cytoskeletal rearrangements that precede the rapid exocytosis of WPBs (Vischer Ulrich M., Barth Holger, and Wollheim Claes B., 2000).

In contrast, cAMP mediated stimuli, such as epinephrine and vasopressin, acts systemically to induce a slow, sustained release of WPBs, whilst concurrently enhancing endothelial barrier function (Schillemans *et al.*, 2019). Both epinephrine and vasopressin act on GPCRs of the G_s subtype, the β_2-adrenergic receptor and the vasopressin V2 receptor, respectively (Vischer and Wollheinn, 1997; Kaufmann *et al.*, 2000). This results in the activation of cAMP-dependent protein kinase A (PKA), which then activates a host of downstream signalling pathways, including phosphorylation events of components of the WPB exocytotic machinery. Once these pathways are activated, WPBs traffic to the plasma membrane where they can secrete their contents.

In addition to the control endothelial cells exhibit on the cargo of WPBs and selective exocytosis, they can also regulate the type of fusion event at the plasma membrane that governs the amount of WPB cargo exocytosed. Stimulated

exocytosis of WPBs involves full fusion with the plasma membrane, as well as compound fusion. That is, the fusion of WPBs with each other as well as with the plasma membrane (Pickett and Edwardson, 2006). These types of fusion result in complete expulsion of WPB cargo and are often seen in response to vascular injury. The study by Babich et al. (2008) discovered that WPB fusion in endothelial cells is not always an all-or-nothing event. The latter stages of WPB exocytosis can result in a "long lingering kiss," allowing effective release of smaller molecules like cytokines while retaining von Willebrand Factor (VWF) within the collapsed WPB (Babich *et al.*, 2008). This state enables endothelial cells to tailor their response to different stimuli, releasing content with a lower VWF-to-cytokine ratio, potentially promoting a less thrombotic and more inflammatory response, often seen in the early stages of atherosclerosis for example. An additional level of regulation has been identified, involving the recruitment of an actomyosin ring after stimulation with specific secretagogues (Nightingale *et al.*, 2018). Actomyosin ring recruitment is positively correlated with the efficiency of vWF release, increasing vWF string length without influencing leukocyte recruitment.

1.5.5 Clinical relevance of WPBs

WPBs hold substantial clinical importance in vascular health. Dysregulation of WPBs is implicated in various vascular disorders, including von Willebrand Disease (vWD), thrombotic events, atherosclerosis, and inflammatory conditions.

Von Willebrand disease is primarily a hereditary disorder, affecting approximately 1% of the population, but can also be acquired. The hereditary form of the disease has three types. Type 1 comprises 70-80% of cases and is characterised by a decrease in vWF levels, resulting in an impaired ability to form a clot leading to an increased bleeding tendency (James *et al.*, 2007). Type 2 comprises 20-30% of cases and does not affect the amount of vWF in the bloodstream but arises as a result of impaired vWF function. Type 3 vWD is the most infrequent and is characterised by almost complete deficiency of vWF in the circulation, affecting between 0.1 – 5 per million (Eikenboom, 2001; Sadler *et al.*, 2006).

Studies in vWD have shown that patients with vWD have a decreased prevalence of CVD compared to the general population (Sanders *et al.*, 2013, p. 201). Even accounting for age, gender, diabetes, obesity, smoking and hypertension, the risk

of acute coronary syndromes is 15% lower in vWF patients compared to the general population. Conversely, patients with elevated levels of vWF in the circulation have an increased risk of cardiovascular complications, such as coronary heart disease and stroke (Whincup *et al.*, 2002; Wieberdink *et al.*, 2010). vWF therefore is an attractive therapeutic target for the treatment of cardiovascular disease, and their important role in the lifecycle of vWF renders them a potential therapeutic target in the search for treatments.

Understanding the role of WPBs provides insights into vascular pathophysiology and offers potential avenues for therapeutic interventions, particularly in the development of drugs targeting haemostasis and inflammation.

1.6 Shear Stress and WPBs

1.6.1 Shear stress and WPB Synthesis

The abundance of cytoplasmic components has been shown to govern the size of cellular organelles (Goehring and Hyman, 2012, 2012). In line with this observation, the availability of vWF is a fundamental determinant of WPB number and size (Ferraro *et al.*, 2014). siRNA mediated reduction of vWF protein levels results in a significant decrease in the number of WPBs, whereas overexpression in non-endothelial cells evokes the production of pseudo WPBs (Wagner *et al.*, 1991). vWF availability is therefore a crucial factor in the rate and success of WPB biogenesis. Numerous studies have highlighted how shear stress influences variations in vWF expression (Aird *et al.*, 1997). Initial vWF staining of rat aortic endothelial cells and porcine intima identified a differential expression of vWF in distinct endothelial cell populations based on their position in the vasculature (Rand *et al.*, 1987; Senis *et al.*, 1996a). More specifically, endothelial cells exposed to disturbed blood flow at the intercostal orifices exhibited homogenous and elaborate vWF staining compared to the heterogeneous staining pattern observed in endothelial cells exposed to laminar flow (Senis *et al.*, 1996a). The initial response of the endothelial cell to shear stress is to change their structural organisation or function of pre-existing proteins, followed by delayed *de novo* protein synthesis (Hough *et al.*, 2008). Several studies have described a significant increase in vWF mRNA expression following prolonged exposure to flow (Dekker *et al.*, 2002; Hough *et al.*, 2008). Dekker et al. (2002) observed a 2.4-fold increase in vWF mRNA expression after prolonged (7 day)

exposure to high pulsatile flow compared to static conditions. VWF's response to flow is not surprising based on the discovery of a flow regulated polymorphic GT repeat element at position -2124 of the vWF gene. The study found increased vWF promoter activity upon exposure to high shear stress (15 dyn/cm^2) for 6 hours (Hough *et al.*, 2008). This was accompanied by a 1.84-fold increase in endogenous vWF mRNA expression after extended exposure to flow for 26 hours. At first, an increase in the expression of the pro-atherogenic vWF in response to atheroprotective shear stress seems counterintuitive. Dekker et al. however, discovered that the increase in vWF expression as a result of high KLF2 expression (a flow responsive transcription factor), meant WPB distribution in endothelial cells were more homogeneous, as opposed to the heterogeneous distribution of WPBs in endothelial cells not exposed to any form of shear stress (Dekker *et al.*, 2006). The homogeneous distribution is much more representative of that found in a quiescent endothelium. Decreased expression and heterogeneous distribution of vWF in sites of disturbed flow could indicate less storage of vWF in WPBs and more basal release, contributing to the pro-atherogenic phenotype associated with these cells. Indeed, vWF$^{-/-}$ / LDLR$^{-/-}$ double knockout mice models lacking vWF at these predisposed sites exhibit reduced prevalence of atherosclerosis (Methia *et al.*, 2001). The direct effect of disturbed flow on vWF and its promoter identified at position -2124 is yet to be determined, but it is possible to speculate that there are other flow-regulated elements of the vWF protein outside of this promoter region.

Single vWF molecules are initially multimerised and packed into individual 'quanta' (Ferraro *et al.*, 2014). Interestingly, the size of individual vWF quanta (0.5 µM) remains the same irrespective of vWF availability, so the change in length therefore relies on the number of vWF quanta co-packaged in a WPB. Packaging of vWF quanta may be dependent on the effects that flow exerts on other cellular structures such as the Golgi (Ferraro *et al.*, 2014). Reduction of the high molecular weight (HMW) vWF observed in longer WPBs reduces the platelet adhesive properties of vWF strings, potentially reducing the risk of atherogenesis (Ferraro *et al.*, 2016). Mechanical forces such as shear stress therefore have the ability to regulate WPB biogenesis via the differential expression and availability of vWF quanta for packaging into nascent WPBs. This results in altered WPB size, number and haemostatic capabilities of the cell. Further work is required to

determine the direct effect of laminar and disturbed flow on vWF expression in endothelial cells, in particular how this alters vWF quanta copackaging.

1.6.2 ER-Golgi Transport

As well as vWF availability, WPB biogenesis is also dependent on correct post-translational trafficking and transport of vWF from the ER to the Golgi. The Golgi apparatus is a dynamic organelle responsible for sorting cargo received from the ER, packaging cargo into vesicles for either storage in the cytoplasm or targeting vesicles for secretion depending on the type of cargo. Efficient trafficking between the ER and Golgi is critical to ensure the steady availability of vWF for copackaging into nascent WPBs.

A protein responsible for ER-Golgi trafficking is the ADP-ribosylation factor (ARF) guanine nucleotide exchange factor (GEF), Golgi Brefeldin A Resistant Guanine Nucleotide Factor 1 (GBF1) (Lopes-da-Silva *et al.*, 2019), which regulates the retrograde transport of COPI vesicles and therefore the recycling of membrane proteins required for WPB biogenesis. Depletion of this GBF1 results in slower trafficking of vWF to the TGN for packaging (Lopes-da-Silva *et al.*, 2019). The slow arrival of vWF results in more time to co-package vWF quanta into single nascent WPBs. The result is extra-large WPBs, which remain in the perinuclear region close to the Golgi. These WPBs are devoid of any post-Golgi cargo such as Rab27a, and therefore do not respond to agonists and are not secreted. Interestingly, phosphorylation of GBF1 is highly dependent on AMP-activated protein kinase (AMPK) expression, a kinase whose expression is regulated by shear stress (Dixit *et al.*, 2008). More specifically, high shear stress (12 dynes/cm^2) causes sustained phosphorylation of AMPK on Thr172. Increased AMPK phosphorylation is concurrent with increased GBF1 phosphorylation, which in turn permits a ‘normal’ rate of anterograde vWF trafficking, and therefore limits the excessive copackaging observed in GBF1 depleted cells (Lopes-da-Silva *et al.*, 2019). It is therefore possible to speculate that in cells exposed to low shear stress or disturbed flow patterns, there is reduced AMPK phosphorylation, reduced GBF1 phosphorylation, and therefore somewhat slower anterograde trafficking of vWF. This would result in more vWF quanta copackaging and longer, more ‘adhesive’ WPBs, increasing the susceptibility of predisposed sites of the vasculature to atherosclerosis (Figure 1.5).

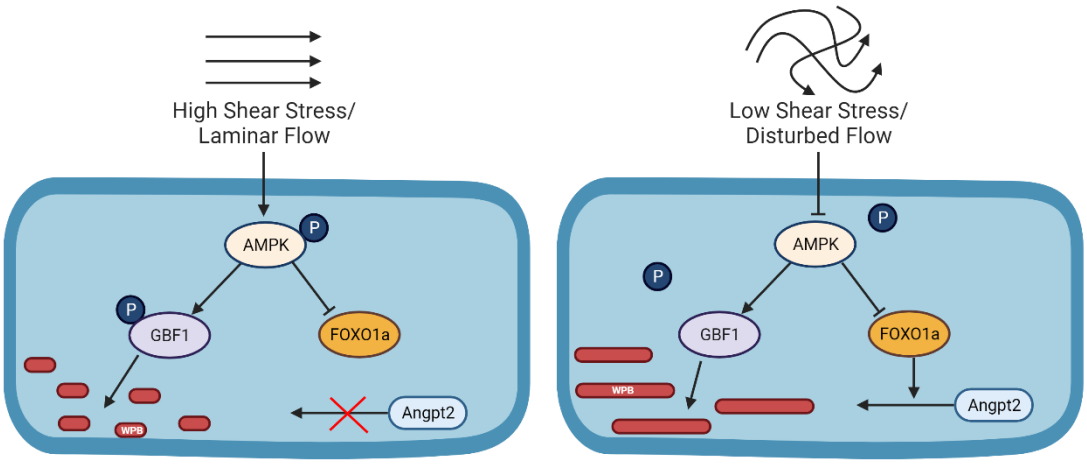

Figure 1.5 – Shear stress and AMPK signalling.
Schematic to highlight the effect of different types of shear stress on AMPK signalling, and the resulting effect on WPB size via GBF1 phosphorylation. High shear stress also reduces copackaging of Angpt2 in WPBs via its regulation of FoxO1a (created with BioRender).

In addition to the regulation of GBF1 phosphorylation, high shear stress also results in the AMPK-dependent phosphorylation and the subsequent degradation of FoxO1a, a regulator of a number of endothelial genes including the WPB constituent, Angiopoietin-2 (Angpt2) (Dixit *et al.*, 2008). Angpt2 is a growth factor known to induce angiogenesis and vascular remodelling, promoting atherogenesis in endothelial cells (Maisonpierre *et al.*, 1997). Shear stress induced phosphorylation of AMPK could reduce the Angpt2 content of WPBs by degrading FoxO1a. Concurrently, a reduction of Angpt2 was also apparent in endothelial cells overexpressing the flow regulated transcription factor, KLF2 (characteristic gene expression of cells exposed to high shear stress) (van Agtmaal *et al.*, 2012).

In summary, shear stress could determine the length of WPBs at the stage of anterograde vWF trafficking from the ER to the Golgi, at which point the phosphorylation of GBF1 could play a crucial role. GBF1 is regulated by AMPK, a kinase which is well documented to be regulated by shear stress. Regulation of AMPK by shear stress could be an important contributing factor in WPB biogenesis based also on its regulation of the WPB constituent, Angpt2. Further work is required to determine whether shear stress regulates any other contributing factors in the complex ER-Golgi vWF transport pathway.

1.6.3 Trans-Golgi Network Morphology

After the formation of very large vWF multimers in the cis-Golgi, the vWF reaches the TGN for packaging into WPBs. The TGN consists of multiple mini stacks of flat membrane cisternae that link together to form a Golgi 'ribbon'. The study by Ferraro et al., (2014) demonstrated that the architecture of the Golgi apparatus alters the size of WPBs. More specifically, an intact Golgi ribbon enables vWF quanta to co-package into nascent vesicles, resulting in the characteristic elongated rod shape of WPBs. Unlinking of the Golgi ribbon by treatment with reagents such as nocodazole and statins result in an inability of the Golgi to co-package vWF quanta and therefore the generation of a population of short or mini-WPBs. Statins cause Golgi dispersion, and have also been shown to increase the expression of the flow regulated transcription factor, KLF2 (Sen-Banerjee Sucharita et al., 2005).

Virus-mediated overexpression of KLF2 also results in the production of mini-WPBs and an increase in the number of WPBs (van Agtmaal et al., 2012). If KLF2 was responsible for WPB length and number, knockdown of this flow-regulated transcription factor should ablate these changes. Ferraro et al., (2016) however, found that knockdown of KLF2, despite rescuing the number of WPBs, did not completely rescue the WPB length. That is, KLF2 knockdown cells showed a modest increase in WPB size, and partially rescued the WPB size reduction found in statin treated cells. As a result, it was concluded that KLF2 plays only a partial and not a major role in the statin-mediated WPB size reduction. KLF2 knockdown had no effect on the Golgi morphology. It is possible to speculate that rescuing WPB length with KLF2 knockdown was impossible in this model due to the drastic disruption of the Golgi complex observed in the statin treated cells, and it may have rescued the length had a more modest and more physiological treatment/experimental model been used.

1.6.4 Coat Formation

There is substantial evidence that WPB biogenesis is highly regulated by the availability of the major WPB coat proteins – clathrin and adaptor protein 1 (AP1) (Lui-Roberts *et al.*, 2005). When the function of clathrin and AP1 is inhibited, mini-WPBs, similar to those seen with statin treatment, are observed as opposed to the characteristic WPB elongated rod-like shape (Lui-Roberts *et al.*, 2005).

Interestingly, the vWF positive mini-WPBs generated in AP1 deficient endothelial cells do not recruit P-selectin (speculating that the folding of vWF into tubules - which does not occur in AP1 deficient cells - forms a P-selectin binding site within this protein) or Rab27a. Of interest in this context, is the inhibition of AP1 by shear stress and the transcription factor, KLF2 (Lan, Mercurius and Davies, 1994; Das *et al.*, 2006). An increase in KLF2 activity, such as in cells exposed to atheroprotective high shear stress, inhibits AP1 expression, resulting in a population of mini-WPBs which are devoid of the inflammatory receptor, P-selectin and Rab27a (Lui-Roberts *et al.*, 2005). As a result, there is a possibility that high shear stress reduces the thrombotic propensity of endothelial cells by depleting AP1 expression, and therefore generates shorter, anti-thrombotic/less adhesive WPBs. The lack of Rab27a recruitment to these mini-WPB throws doubt on this theory however, as Rab27a is vital in the regulated exocytosis by recruiting multiple effector molecules. It is therefore important to take into account, the observations in the studies mentioned are the most extreme examples i.e. complete AP1 deficiency (Das *et al.*, 2006). In vivo, it is likely that KLF2 will induce a subtle reduction of AP1, which could ultimately lead to either a higher proportion of mini-WPBs or WPBs which are generally shorter in length and therefore less thrombotic (Figure 1.6).

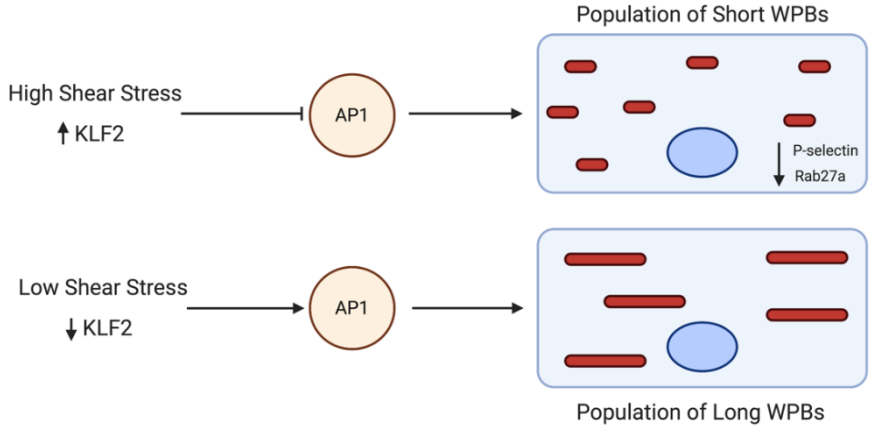

Figure 1.6 - Shear stress regulation of AP-1 and effects on WPB length.
High shear stress and elevated expression of KLF2 inhibits AP1. This results in a lack of coat formation on WPBs and a population of short WPBs devoid of P-selectin and Rab27a. Low shear stress and downregulated KLF2 expression results in higher AP1 expression. This results in a population of long WPB, containing P-selectin and Rab27a (created with BioRender).

1.6.5 Trafficking

The trafficking of nascent WPBs post-Golgi budding depends on the secretory pathway to which they are targeted. There are 3 main secretory pathways for vWF; constitutive; basal and regulated. The simplest form is constitutive secretion of low molecular weight (LMW) vWF multimers on the endothelial basolateral membrane (Schillemans *et al.*, 2019). This occurs independent of secretagogue stimulation and does not involve packaging of vWF into WPBs. Basal secretion occurs at the apical side of the cell, independent of stimulation and involves microtubule-dependent trafficking of immature WPBs directly to the plasma membrane from the Golgi (Giblin, Hewlett and Hannah, 2008). In the absence of stimulation, vWF secretion predominantly occurs via the basal secretory pathway (Giblin, Hewlett and Hannah, 2008), however this is directed towards constitutive secretion when a component involved in WPB biogenesis is depleted, such as AP-1. Lui-Roberts et al. (2005) observed an increase in constitutive secretion upon AP-1 knockdown, but this was accompanied by a complete ablation of regulated vWF secretion. The inhibition of AP-1 that occurs in high shear stress conditions, as mentioned previously, could therefore direct more vWF towards constitutive secretion of LMW multimers basolaterally, as opposed to basal secretion apically or the storage of HMW multimers in WPBs, decreasing the thrombotic potential of the cells.

The agonist-induced regulated secretory pathway involves the rapid secretion of HMW vWF multimers from mature WPBs into the vessel lumen and occurs in response to high level stimulation such as histamine and thrombin. This regulated secretory pathway relies on the availability of a readily available pool of mature WPBs in the cytoplasm of the cell. In order for this to occur, nascent WPBs must migrate from the perinuclear region towards the cell periphery where they can undergo a maturation process. This movement requires anchoring to the cytoskeleton, a critical component of which is the small GTPase, Rab27A. Rab27a facilitates the anchoring of WPBs to the actin cytoskeleton via a complex also including myosin, myosin Va and MyRIP (Nightingale *et al.*, 2009). MyRIP acts as a negative regulator of exocytosis, opposed by the binding of Rab27a to Slp4-a, which acts as a positive regulator (Bierings *et al.*, 2012). The pronounced structural changes in the cytoskeleton when endothelial cells are exposed to shear stress, mainly the alignment of stress fibres in the direction of flow (Birukov

et al., 2002; Manneville *et al.*, 2003) and the dependence on these cytoskeletal elements for WPB maturation, may lead to the assumption that shear stress affects WPB trafficking within the cell. In addition, flow has an effect on the positioning of many cellular structures, such as the MTOC (Tzima *et al.*, 2003) and the Golgi (Coan *et al.*, 1993), thereby one would presume that the polarisation of trafficking is altered. However, despite these large alterations in cytoskeletal elements, in the absence of stimulation, Dragt et al. revealed no change in the WPB distribution after prolonged exposure to laminar shear stress. They documented a slight increase in the proportion of WPBs upstream of the nucleus under flow but this was negligible when taking into account the morphological changes of the cell after exposure to shear stress (Dragt *et al.*, 2012).

1.6.6 Exocytosis

Galbusera et al. (1997) observed an increase in vWF secretion into the cell culture media after sudden exposure of endothelial cells to a moderately high laminar shear stress (8 dyn/cm^2) for 6 and 15 hours, the first indication *in vitro* that flow affects vWF secretion. Several mechanisms have been described to regulate the stimulated release of cargo from endothelial cells so that secretion is functionally coupled to the stimulant. Release of distinct cargo is controlled either at the level of the plasma membrane or stimulants, such as histamine, which can induce differential trafficking of subpopulations of WPBs carrying cargo superfluous to the response away from the plasma membrane (Miteva *et al.*, 2019). Firstly, endothelial cells can regulate their response to certain stimuli by utilising different modes of exocytosis at the plasma membrane. A lingering kiss fusion event involves transient fusion with the plasma membrane, allowing only small molecular weight molecules such as chemokines and cytokines out of the cell (not vWF) before returning to the cytoplasm of the cell (Babich *et al.*, 2008). The study by Babich et al. demonstrated that the proportion of lingering kiss fusion events was increased during low-level stimulation (25%). This raises the possibility that low-level activation induced by disturbed flow could promote lingering kiss exocytosis to promote inflammation, as opposed to full fusion which would lead to thrombosis. One peptide that is small enough to pass through a lingering kiss fusion pore is angiopoietin-2 (Angpt2). Angpt2 contributes to angiogenesis and inflammation (Fiedler *et al.*, 2006), promoting atherogenesis.

Angpt2 has been shown to be downregulated in cells overexpressing KLF2, a transcription factor upregulated by high shear stress (van Agtmaal *et al.*, 2012). Disturbed flow may therefore increase the levels of Angpt2 in endothelial cells, and the mild activation of this flow may induce more release of Angpt2 by lingering kiss fusion events. Other types of exocytosis involve full fusion or compound fusion. Full fusion of a single WPB involves the exocytosis of all the contents into the vessel lumen. There is evidence to suggest that long length WPBs recruit an actin ring to aid exocytosis of the ultra large vWF strings found in this subset of WPBs (Nightingale *et al.*, 2011; McCormack, Harrison- Lavoie and Cutler, 2020). The role of shear stress in reshaping other actin structures in endothelial cells (Birukov *et al.*, 2002), raises the possibility that shear stress affects actin ring recruitment, and could therefore influence which subset of WPBs are secreted.

Regulation of secretion can also occur through differential trafficking of subpopulations of WPBs. Histamine has been shown to rescue exocytosis of WPBs containing Angpt2, but not P-selectin, by diverting them to the MTOC. This stimulated trafficking is dependent on the Rab GTPase, Rab46, as well as dynein and microtubules (Miteva *et al.*, 2019). In addition to the effect of shear stress on these cytoskeletal elements, Rab46 expression was shown to be necessary for Angpt2 recruitment to WPBs in a manner similar to the flow responsive transcription factor KLF2 (van Agtmaal *et al.*, 2012). This raises the question as to whether there is a relationship between shear stress, Rab46 expression and WPB cargo recruitment.

There is therefore evidence that WPBs can fine-tune their secretory response to stimulation by regulating the exocytosis of their WPBs, and shear stress is likely to affect one or all of these modes of exocytosis based on either the cargo of the WPBs targeted for secretion or the mode of exocytosis. Upon exocytosis, the ability of vWF to form strings on the surface of endothelial cells relies on the presence of blood flow to cause the unfolding of vWF multimers.

1.6.7 VWF String Formation

In the event of full fusion with the plasma membrane, vWF leaves the endothelial cells in the form of UL vWF strings. The highly multimerised vWF tubules found in WPBs unfold in the presence of shear stress (Siedlecki *et al.*, 1996) and remain

anchored to the endothelial cells from which they originate. VWF string length represents its ability to bind to platelets i.e. the longer the string the more platelets it can recruit. String length is determined by the size of WPBs from which they originate (Ferraro *et al.*, 2016). A population of short WPBs results in a higher proportion of short vWF strings on the surface of endothelial cells on exocytosis, reducing the cells ability recruit platelets. Based on the various effects of shear stress on mechanisms known to regulate WPB size, for example AP1, shear stress may regulate the thrombotic potential of different areas of the endothelium by altering the size of WPBs and therefore the length of vWF strings formed.

Once formed on the endothelial surface, vWF strings are quickly cleaved via the circulating metalloprotease enzyme, ADAMTS13. ADAMTS13 evokes flow induced cleavage of vWF strings, a critical anti-thrombotic process that requires high shear stress in order to open the cleavage site (Reininger, 2015). There is evidence that the D'D3 domain of vWF binds to P-selectin on the endothelial cell surface to anchor the full length of the vWF string to the cell surface upon exocytosis. This increases the tensile stress exerted by shear stress on the vWF string and therefore promotes ADAMTS13 cleavage (Michaux *et al.*, 2006). This tensile stress also increases upon platelet binding to the vWF string, due to the extra drag forces (Reininger, 2015). Once released from WPBs and cleaved by ADAMTS13, studies have shown that shear stress induces conformational changes in circulating vWF, exposing the A2 domain and therefore promoting further cleavage of HMW multimers into LMW multimers (Bortot *et al.*, 2019). This is particularly apparent in patients with severe aortic stenosis, which causes excessive high shear stress conditions and therefore unnecessary cleavage of HMW multimers. This often leads to acquired von Willebrand disease (aVWD) due to a reduced ability of vWF to form a clot (Jilma-Stohlawetz *et al.*, 2016; Kellermair *et al.*, 2020). The shear-dependent conformational change of vWF that enables cleavage by ADAMTS13 may be reduced at sites of the endothelium experiencing disturbed flow patterns. Reduced vWF cleavage by ADAMTS13 is linked to thrombotic thrombocytopenic purpura (TTP) and inflammation (Dong *et al.*, 2002). Low shear stress could therefore increase the propensity of specific regions of the endothelium to atherosclerosis and thrombosis by preventing ADAMTS13 cleavage of vWF strings from the endothelial cell surface after WPB exocytosis.

1.6.8 Mechanotransduction and WPBs

The mechanotransduction of stimuli to a biological signal occurs via multiple mechanisms as described in section 1.3. The response of endothelial cells to shear stress is dependent on both the magnitude and flow pattern of the medium i.e. laminar, pulsatile, oscillatory or turbulent. The response can also be characterised based on whether it is an immediate, short-term or long-term response. The immediate response (within seconds) involves ion channel activation that results in the production of reactive oxygen species. Short-term activation (1-2 hours) involves the activation of transcription factors such as NFκB and AP1, and matrix proteins such as focal adhesion kinases. Long-term responses (24-48h) occurs when cells have reached equilibrium with their new environment, and features the reorganisation of the actin cytoskeleton and focal adhesions to align with the flow direction (Davies, Robotewskyj and Griem, 1994; Galbraith, Skalak and Chien, 1998).

Whilst the molecular mechanisms regulating vWF release have been extensively studied, the mechanotransduction mechanisms that occur upstream of the shear-mediated release, and specific mechanotransduction pathways linked to the long-term response of WPBs remains unclear. Fluid shear stress is known to induce vWF release proportionate to its magnitude by modulating intracellular calcium levels (Galbusera *et al.*, 1997). One study proposed a link between the endothelial glycocalyx (EGC) and the release of WPB/vWF in response to shear stress (Choi and Lillicrap, 2020). This proposed link arose following evidence of mechanotransduction-mediated roles of the EGC in haemostatic processes such as NO production and embryonic stem cell differentiation, however this link is yet to be proven (Pahakis *et al.*, 2007; Nikmanesh, Shi and Tarbell, 2012).

Another study has shown that hypertensive stretch induces the exocytosis of WPBs in endothelial cells via VEGFR2. This modulates two signalling pathways; a rapid and strong PLCγ1/Ca^{2+} mediated activation and a weaker but longer lasting Akt/NO/NSF signalling pathway (Xiong *et al.*, 2013). As stretch is also a mechanical stimuli, the role of VEGFR2 in the triad complex with CD31 and VE-Cadherin (described in section 1.3.7), implicates this junctional mechanosensor in activating intracellular signalling pathways that result in WPB exocytosis in response to shear stress. Further research is required to elucidate these pathways fully.

1.7 Summary

This chapter summarises the pivotal role of endothelial cells in maintaining vascular homeostasis. It describes the mechanisms by which endothelial cells become dysfunctional, especially as a result of shear stress, and how this results in atherosclerosis. Endothelial cell mechanosensors play an important role in sensing shear stress and transducing these mechanical stimuli into downstream effects. Many of these signalling pathways may regulate WPBs, the endothelial-specific storage vesicle considered the ‘vascular first-aid kit’. There is evidence that dysregulation of specific aspects of the WPB lifecycle could increase susceptibility of specific regions of the endothelium to atherosclerosis. Research is needed to establish whether there is any connection between physiological shear stress and WPBs, an area that provides the basis for this project.

1.8 Aims and Objectives

Aim

The aim of this project is to optimise an *in vitro* method for studying WPBs under flow, analysing the effects of different flow conditions on WPBs at various stages of their lifecycle.

Understanding whether different rates of shear stress regulate WPBs, and the mechanisms underlying these changes, will provide an insight into the level of WPB contribution to the focal nature of atherosclerosis. Insights into the mechanisms that underlie these changes will aid in the search for therapeutic targets for the treatment of cardiovascular disease.

Hypothesis

Disturbed flow results in a population of WPB mediated pro-thrombotic and pro-inflammatory endothelial cells that increases the susceptibility to atherosclerosis.

Objectives

1. Optimise an *in vitro* flow model to study the effects of shear stress on WPBs.
2. Observe the effects of shear stress on WPB morphology and function.
3. Explore any potential mechanisms that contribute to the shear stress dependent regulation of WPBs (if present).

Chapter 2 - Materials and Methods

2.1 Reagents

Reagent	Solvent	Stock Concentration	Working Concentration	Supplier
Histamine	H_2O	100 mM	150 µM	Sigma
PMA	DMSO	5 mM	1 µM	Promega
Yoda1	DMSO	10 mM	0.5 – 1 µM	Tocris
Dooku1	DMSO	10 mM	10 µM	UoL Chemistry
Compound 2a	DMSO	10 mM	10 µM	UoL Chemistry

Table 2.1 - List of reagents

2.2 Cell Culture

2.2.1 HUVEC

Pooled human umbilical vein endothelial cells (HUVECs) (PromoCell) were maintained in Endothelial Cell Basal Medium (EBM-2) supplemented with Endothelial Growth Medium-2 SupplementPack (PromoCell). Cells were maintained at 37^{o}C and 5% CO_2 in a humidified incubator. Cells were grown to confluency before passage and used between passages 1-5.

2.2.2 HAEC

Pooled human aortic endothelial cells (HAECs) (PromoCell) were maintained in Endothelial Cell Growth Medium MV2 supplemented with Growth Medium MV2 SupplementPack (PromoCell). Cells were maintained at 37^{o}C and 5% CO_2 in a humidified incubator. Cells were grown to confluency before passage and used between passages 1-5.

2.3 Ibidi Pump System

HUVECs were plated on Ibidi µ-slide $I^{0.4}$ Leur (IbiTreat) at a concentration of 7.5 x 10^5 cells/ml and incubated at 37^{o}C and 5% CO_2 until confluent (18-24 h). To subject the cells to flow, each Ibidi µ-slide was connected to a fluidic unit, with reservoirs containing approx. 15 ml EGM-2. Based on the parameters input into the Ibidi software, the media was flowed over the cells in a either a continuous

unidirectional manner (HSS) or alternating direction every second due to electrically controlled valves within the fluidic unit (LOSS). In this instance, HUVECs were then exposed to either high unidirectional shear stress (HSS; 10 dyn/cm^2), low oscillatory shear stress (OSS; 2 dyn/cm^2, oscillating at 1 Hz) or static conditions concomitantly with daily media change for 48 hours on the static slide.

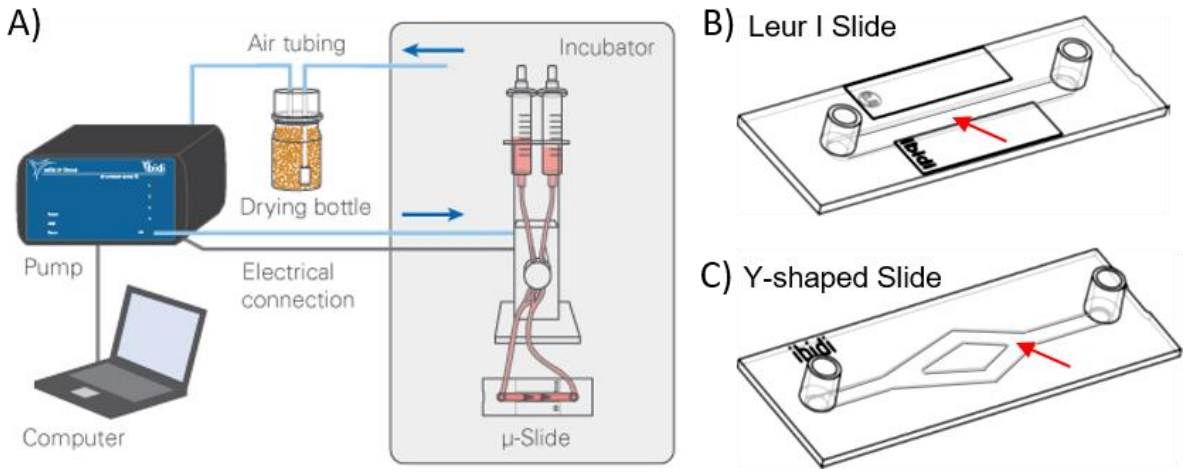

Figure 2.1 - The Ibidi pump system and slides used for flow experiments.
A) The Ibidi software controlling the pump, which is connected to the fluidic unit inside the incubator. B) Ibidi µ-slide I Leur used to mimic straight arteries. C) Ibidi µ-slide y-shaped used to mimic an arterial bifurcation. HUVECs are cultured in the central channel (indicated by red arrows).

2.4 RT-qPCR

2.4.1 RNA Extraction

Total RNA was extracted from fresh cells using high pure RNA isolation kit (Roche) as per manufacturer's instructions. Briefly, the cell culture media was removed, the cells were washed with PBS before shearing with 200 µl lysis buffer and adding to a spin column. For each sample, 90 µl of DNase incubation I and 10 µl of DNase was added to the column and centrifuged again. Following three washing steps the RNA was eluted with 15 µl elution buffer, quantified using the Nanodrop and stored at -80°C or used immediately in reverse transcription.

2.4.2 Reverse Transcriptase PCR

Complimentary DNA (cDNA) was synthesised using a High Capacity RNA-to-cDNA RT kit (Applied Biosystems). 100 ng of RNA was mixed with 5 µl 2x RT buffer, 1 µl 20x enzyme mix and nuclease-free water to make a 10 µl total reaction volume. Non-reverse transcribed control solutions were prepared and tested in parallel. The solutions were mixed, centrifuged and incubated for 1 hour at 37°C followed by 5 minutes at 95°C, producing in cDNA that is ready for use in real-time qPCR application or short-term storage at 4°C.

2.4.3 qPCR

RT-qPCR was carried out using SYBR Green I (Bio-Rad) on a LightCycler (Roche). Each reaction had a 10 µl total volume and contained: 5 µl of 2x iTaq™ Universal SYBR® Green Supermix (containing antibody-mediated hot-start iTaq DNA polymerase, dNTPs, $MgCl_2$, SYBR Green I dye, enhancers and stabilisers), 0.75 µl of forward primer (0.375 µM), 0.75 µl of reverse primer (0.375 µM), 1 µl cDNA and 2.5 µl nuclease-free water. Real-time PCR primers (Table 2.2) were designed using the Primer3-BLAST tool (https://www.ncbi.nlm.nih.gov/tools/primer-blast/). DNA amplification started with 10 minutes at 95°C, followed by 40 cycles with 10 seconds at 95°C and 60 seconds at 60°C. The relative abundance of target genes amplified by RT-qPCR were calculated relative to the housekeeping gene, GAPDH. GAPDH was selected as an appropriate housekeeping gene because it is not regulated by shear stress (Diamond *et al.*, 1990).

Target	Primer Sequence (5' – 3')
h-KLF2	**F**: GTCCTTCTCCACTTTCGCCA **R**: ACAGGATGAAGTCCAGCAGC
h-ANGPT2	**F**: CAAATGCTAACAGGAGGCTGGT **R**: CAGGTGGACTGGGATGTTTAGA
h-SELP	**F**: TGCAAAGGCATAGCATCACTTC **R**: TGTCCATTGTCCTGAAGGTCTG
h-VWF	**F**: TTCCCGACAAGGTGTGTGTC **R**: GCCTTCATGCAGAACGTAAGTG

Table 2.2 - RT-qPCR primers.

2.5 vWF String Formation

HUVEC were plated on Ibidi µ-slide $I^{0.4}$ Leur (IbiTreat) and subjected to HSS, LOSS and static conditions as described previously in section 2.2, with an additional static slide to act as a control. After 48h of each condition, the cells were stimulated with 150 µM histamine for 10 minutes at 2.5 dyn/cm^2 (37^{o}C, 5% CO_2). The additional static slide plated was exposed to 1 µM PMA for 10 minutes at 2.5 dyn/cm^2 (37^{o}C, 5% CO_2), acting as a positive control. After 10 minutes of stimulation, each slide was transferred to a new fluidic unit containing 4% PFA, which was applied at 2.5 dyn/cm^2 for 10 minutes at room temperature. Slides were then used for immunofluorescent staining (without permeabilisation) as described previously in section 2.6 and imaged on the confocal microscope.

2.6 Immunocytochemistry

After 48 hours of exposure to shear stress, cells were fixed with 4% paraformaldehyde (PFA) for 10 min at room temperature, washed with PBS and then permeabilised with 0.1% Triton-X solution for 10 minutes. Cells were incubated with primary antibody (in PBS; see Table 2.3 for primary antibodies) for 1 h, then washed with PBS and incubated with the relevant species-specific fluorescent dye-conjugated secondary antibody for 30 mins (in PBS; see table 3 for secondary antibodies). Cells were washed with PBS and incubated with HOECHST 33342 (Cell signalling) (nuclear stain) for 7 minutes before being mounted with Ibidi mounting medium. Cells were imaged using the Deconvolution microscope.

Primary Antibody	Species	Working Dilution	Supplier
Anti-vWF	Mouse	1:200	DAKO
Anti-vWF	Rabbit	1:100	DAKO
Anti-GM130	Mouse	1:200	BD Biosciences
Anti-Angpt2	Goat	1:100	R&D Systems
Anti-CD31	Rat	1:50	R&D Systems

Table 2.3 - Primary antibodies used for immunofluorescence.

Secondary Antibody	Species	Working Dilution	Supplier
AlexaFluor594 anti-mouse IgG	Mouse	1:300	Jackson ImmunoResearch Labs
AlexaFluor594 anti-rabbit IgG	Rabbit	1:300	Jackson ImmunoResearch Labs
AlexaFluor488 anti-rat IgG	Rat	1:300	Jackson ImmunoResearch Labs

Table 2.4 - Secondary antibodies used for immunofluorescence.

2.7 Microscopy

2.7.1 IncuCyte ZOOM

After cessation of flow, the IncuCyte ZOOM (Essen Bioscience) was used to image the cells on the Ibidi slides. 32 images at different regions of the channel were taken and cell orientation analysis (section 2.8.1) performed on ImageJ Fiji.

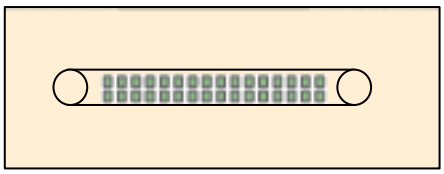

Figure 2.2 - Areas of the Ibidi µ-slide I Leur imaged on the IncuCyte ZOOM. Each individual green box represents a single phase-contrast image captured. Total of 32 images per slide.

2.7.2 Wide-Field Deconvolution Microscopy

Two wide-field deconvolution microscopy systems were used:

Initially, the DeltaVision deconvolution system (Applied Precision) was used to image cells on an Olympus IX-70 inverted microscope. 10-focal planes at 0.2 µm per Z-stack were taken for each image using Roper CoolSNAP HQ charge-coupled device camera. Re-iterative deconvolution (5x) was performed on the z-stacks using an algorithm to restore out of focus light (deconvolution) from one plane of a z-stack to another. The filter sets used were as follows: DAPI; FITC and TRITC. The objectives used were 40x/1.35 oil or 60x/1.4 oil. All imaging was

performed at room temperature. Image acquisition and processing was performed using the proprietary SoftWoRx software.

Secondly, deconvolution microscopy was performed on an Olympus inverted microscope supported by CellSense deconvolution systems, using the same parameters, camera and re-iterative deconvolution methods as the one used previously.

2.7.3 Confocal Microscopy

High-resolution microscopy was performed using an inverted confocal laser-scanning microscope, Zeiss LS880. Images were captured using a 20x air objective for vWF string analysis or 63× oil objective for Golgi analysis and 405-nm diode, Argon/2 (458, 477, 488, and 514 nm), HeNe 543 nm, and HeNe 633 nm lasers. Due to the size of the vWF strings, a tile scan was used (2x2) to capture a sufficient area. All the images were acquired and processed with Zen software. All imaging was performed at room temperature.

2.8 Image Processing and Analysis

Maximum intensity projections were generated using DeltaVision SoftWoRx or Zeiss Zen software and subsequently analysed in ImageJ Fiji. ImageJ macros were used (see appendix) for the quantification of WPB number and Feret, vWF string length and Golgi fragmentation.

2.8.1 Cell Orientation Analysis

Using ImageJ software, images were rotated to the direction of applied shear stress processed using a Difference of Gaussian plugin to define cell edges. Automated quantification of cell orientation relative to the direction of shear stress was determined using OrientationJ software, also an ImageJ plugin (http://bigwww.epfl.ch/demo/orientation/). OrientationJ produced a histogram of all local angles in each image. A Gaussian distribution curve was fitted to each arising histogram. The mean frequency maximum at the mode of the distribution of each condition was determined.

2.8.2 WPB Length and Number of WPBs/cell

Channels were split and background subtracted from the TRITC/vWF channel. A local threshold followed by particle analysis was applied to determine the number

of WPBs per image and the length of each individual WPB in the image. To determine the number of WPBs/cell, the total number of WPBs in the image was divided by the number of nuclei present in the image. Ten images per condition per repeat were analysed.

2.8.3 WPB Polarisation

WPB polarisation was quantified using the Feret angle of WPBs using the same ImageJ macro as in section 2.8.2 to automate the analysis. The angle data is based on the angle between the Feret line and a horizontal line. As a result, a Feret angle closer to 0 or 180 indicates that the WPB is polarised with the direction of the flow.

2.8.4 WPB Distribution

Initially, a distance map based on cell nuclei was created using StarDist ImageJ plugin (https://imagej.net/plugins/stardist). The WPBs (identified using a macro, see appendix) in the corresponding red channel were then superimposed on the distance map and the mean gray value of each WPB was quantified. The higher the mean gray value. the closer the WPB to the cell periphery.

2.8.5 vWF String Quantification

vWF strings were analysed using an ImageJ macro (see appendix). Briefly, channels were split and a local threshold applied to the red/vWF channel followed by particle analysis to determine the number and length of vWF strings present. Five images per condition per repeat were analysed.

2.8.6 Golgi Fragmentation

Golgi fragmentation was analysed by counting the number of Golgi objects per image (see appendix for ImageJ macro). Briefly, channels were split and a local threshold applied to the channel used to image the Golgi, dividing this value by the number of cells in the image to give the number of objects per cell.

2.8.7 Mouse aorta extraction and staining

Animal use was authorised by the University of Leeds Animal Ethics Committee. In order to observe the effect of shear stress on WPBs in vivo, the aortic arch and descending aorta of C57/B mice were flushed with PBS fixed with 4% PFA. Once fixed, aortas were extracted and permeabilised with 0.1% Triton X-100 before

blocking for 1 hour with 5% donkey serum. Aortas were then incubated overnight at 4ºC with primary antibody (Table 2.3) followed by incubation with relevant species-specific fluorescent dye-conjugated secondary antibody for 1 hour (Table 2.4). The whole aortas (including the arch) were then cut longitudinally to expose the lumen, and mounted on a cover slip, en face, with fluoromount (containing DAPI) before imaging with confocal microscopy.

2.9 Single Cell RNA Sequencing

scRNAseq FastQ data files generated in Andueza et al. 2020 were obtained from the NCBI BioProject repository (accession number PRJNA646233). Data files were downloaded and stored using the University of Leeds High Performance Computing system – arc3. Arc3 was also used to process the data with Cell Ranger Software, aligning sequencing reads to the mouse reference genome with STAR aligner. H5 files were generated which were then processed using Seurat R package to visualise the data. The code used to analyse the data was kindly made available with the study by Andueza et al. 2020 (https://github.com/JoLab-Emory/SingleCell). Briefly, a quality control step was performed, removing low quality cells and doublets based on a threshold of unique feature counts, discarding those with less than 200 or more than 7600 feature counts. Cells with lower than 10% of mitochondrial counts were also discarded. Datasets were then merged, normalised, scaled, clustered and visualised by Uniform Manifold Approximation and Projection (UMAP).

2.10 Yoda1 addition

Dooku1 and compound 2a (Evans *et al.*, 2018) were synthesized at the University of Leeds and solubilised in DMSO. HUVECs were plated on Ibidi 8-well slide (IbiTreat) at a concentration of 50,000 cells/ml and incubated at 37ºC and 5% CO_2 until confluent (18-24h). Cells were pre-incubated with DMSO, Dooku1 (1 µM), Dooku1 (5 µM), or compound 2a for 30 mins. Yoda1 was then added to each of the wells either in the presence of Dooku1 (10 µM) or compound 2a (10 µM), or separately. Cells were then fixed at stained at 4 different time points: 5 minutes, 30 minutes, 2 hours and 24 hours. Immunofluorescent staining and high-resolution microscopy was performed as described previously.

2.11 Proteomics Analysis

Shear stress experiments using HUVECs were performed for 48 hours, as described in section 2.3. After 48 hours, the cell culture media was collected, centrifuged for 5 minutes at 400 *g* to pellet any cells. The supernatant was then transferred to a fresh tube before centrifugation for 5 minutes at 2000 *g* to pellet cell debris. The supernatant was then frozen at -80^{o}C. EGM-2 media containing histamine was then added to the flow apparatus and 2.5 dyn/cm^{2} flow was applied to all three slides for 10 minutes. The resulting media was also collected, centrifuged as described previously and frozen at -80^{o}C. All frozen media samples were then sent to University of Bristol proteomics facility for downstream proteomic analysis.

The method of quantitative proteomic analysis used was Tandem Mass Tagging (TMT). Samples were depleted of BSA and equal volumes of each depleted sample was used for TMT analysis. Samples were labelled within the Bristol proteomics facility, fractionated and analysed by nano-LC MSMS using the SPS-MS3 approach on an Orbitrap Fusion Tribrid mass spectrometer. Fragmentation of the isobaric tag released low molecular mass reporter ions which were used to quantify the peptides. Protein quantitation was based on the median values of multiple peptides identified from the same protein, resulting in highly accurate protein quantitation between samples.

To perform conditional comparisons, the LogFC was calculated based on the difference between the mean Log2 normalised protein abundances for each condition, followed by a t-test also performed on the Log2 normalised protein abundances. The resulting *p*-value was FDR corrected (*q*-value). Proteins were compared to 3 databases; the Uniprot Human database, the Uniprot Bovine database and against a 'common contaminants' database. Those matching exclusively with the cRFP database and exclusively with the contaminant database were removed from Table 4.1. Those matching with the human database but with a ‘TRUE’ contaminant identification should be treated with caution.

2.12 Statistical Analysis

All averaged data are presented as mean ± SEM. Outliers were removed using a Grubb’s test and equal variance confirmed. Shapiro-Wilk normality test was

used to determine whether data was drawn from a normally distributed population. Normally distributed data was assessed for significance with a two sample t-test when comparing two data groups, or one-way ANOVA coupled with Bonferroni post hoc test when comparing three or more data groups. Data not drawn from a normally distributed population was assessed for significance with either Mann-Whitney U test or Kruskal Wallis test depending on the number of data groups. Statistical significance was considered to exist at probability $p < 0.05$ (### < 10^{-15}, *** < 0.001, ** < 0.01, * < 0.05). Where comparisons lacked an asterisk or marked NS, no significant difference between groups was observed. OriginPro 2020 software and R studio was used for data analysis and presentation. *n* = represents the number of independent biological repeats (for fluorescent microscopy - each independent repeat included 5-10 technical replicates i.e. individual images).

Chapter 3 – Shear stress affects WPB size, cargo and gene expression.

3.1 Introduction

Endothelial cells line the vessels of arteries and are therefore constantly exposed to shear forces by the flowing blood. In order to study the effect of these shear forces on endothelial cells specifically, an *in vitro* flow system is required to mimic these forces in a more controlled and measurable environment. In this instance, a commercially available system known as the Ibidi pump system (Ibidi GmbH, Germany) was opted for. The system comprises an air pump, a laptop with the Ibidi pump software, fluidic units with media reservoirs and channel slides on which cells are cultured (Figure 3.1). This is a closed system meaning long-term experiments can be carried out without having to top-up or refresh the cell culture media, whilst sterility is maintained. The cells can also be fixed, fluorescently stained and imaged in the Ibidi channel slides. The Ibidi software provided with the pump allows the shear rates to be precisely defined and maintained throughout the entirety of the experiment. Although the system is relatively well established, optimisation was required to ensure it was a suitable system to observe WPBs.

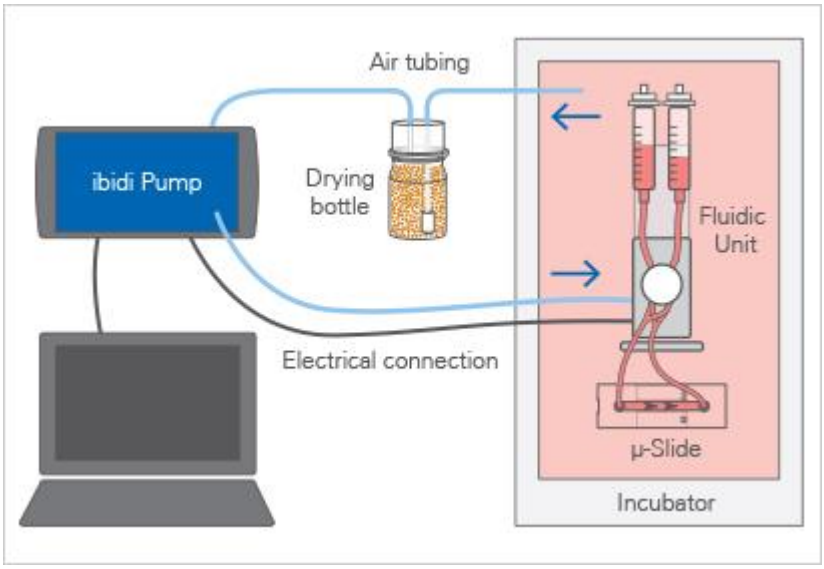

Figure 3.1 - Ibidi Pump System.

3.2 Optimisation of an *in vitro* flow system

Endothelial cells by their nature align with the direction of the flowing blood. In vitro, previous studies have shown that this occurs anywhere from 12 to 24 hours (Galbraith, Skalak and Chien, 1998). In order to ensure this was a suitable model for studying WPBs, I carried out a number of optimisation experiments to determine the most suitable shear stress value, length of time for exposure to shear stress, seeding density and optimal channel height. In order to do these optimisation experiments, the alignment of the cells with the direction of the flow was used to quantify the effectiveness of each condition/parameter.

The initial parameter assessed was the duration of exposure to flow required for achieving uniform alignment of cells. HUVECs were exposed to high uniform laminar shear stress (HSS) for 0, 24 and 48 hours before phase contrast imaging on the IncuCyte (Figure 3.2). HUVECs exhibited no alignment at 0h, as anticipated. At 24h, slight alignment with the direction of flow was observed, with significantly more alignment at 48h. Subsequent observations at 72h showed no further improvement in alignment. As a result, it was concluded that 48h was the optimal timeframe to achieve the desired cellular response.

The next parameter assessed was the seeding density and therefore confluency of the cells prior to exposure to flow. HUVECs were seeded onto the channel slides at a range of concentrations and exposed to HSS (Figure 3.3). Quantification of alignment indicated that a concentration of 5 x 10^5 cells/ml seeding density was optimal under these shear stress conditions. Fewer cells resulted in an incomplete monolayer by the end of the experiment. Too many cells limit the available space for the cells to alter their morphology in order to align with the direction of flow.

At this point, the HUVECs aligned with the direction of flow, however alignment was not uniform. The Ibidi channel slides are available at different channel heights and can be used with perfusion sets with varying diameters, features which can affect the shear stress perceived by the cells. Upon further evaluation of the parameters used, with the red perfusion set and 0.8 mm channel slide, 10 dyn/cm^2 was the upper limit of the range in terms of shear rate and pressure. Upon changing to a smaller channel height, 0.4 mm, the pressure and shear rate were in the middle of the acceptable range. With these parameters, the

endothelial cells aligned more uniformly with the direction of flow (Figure 3.4), and it was therefore decided these would be the optimal parameters.

Blood Vessel	Shear stress (dyn/cm^2)
Arterial	5 – 60
Venous	1 – 10
Ascending aorta	12
Descending aorta	5 – 8
Large vein	5
Small vein	11

Approximate values taken from (Taylor, 1975; Papaioannou *et al.*, 2006)

Approximate values taken from (Chaterjee, Shampa, 2018)

Table 3.1 - Shear stress values depending on site in vasculature

It is important to note that the 0.4 mm Ibidi channel has half the volume of the 0.8 mm channel, 100 µl compared to 200 µl. The seeding density therefore also changed as half the number of cells/ml were being plated onto the slides. As a result, 5 x 10^5 cells/ml (5 x 10^4 cells/slide) on the 0.4 mm slide was deemed an insufficient concentration. 7.5 x 10^5 cells/ml (7.5 x 10^4 cells/slide) was more optimal and gave highly uniform alignment and was therefore chosen as the optimal concentration for seeding density on these cells.

Once the HSS condition had been optimised, representing atheroprotective flow, an atheroprone flow condition was required. Atheroprone flow tends to be a lower velocity and disturbed due to bifurcations and curves in the arteries. As a result, low oscillatory shear stress (LOSS) was used to mimic disturbed blood flow found in these regions. LOSS on the Ibidi pump system means the blood flow is relatively low velocity (2 dyn/cm^2) and constantly switches direction after a specified time interval (1 Hz) (Mahmoud *et al.*, 2016). The final condition was a static control, in which no flow was applied but the media was refreshed daily. To confirm the flow conditions, cell alignment and expression of the atheroprotective KLF2 transcription factor (Figure 3.6) was measured in each of the conditions after 48h. HUVECs and HAECs exposed to HSS aligned with the direction of flow. HUVECs exposed to LOSS and static conditions showed no alignment and retained their cobblestone morphology. KLF2 mRNA expression was significantly higher in cells exposed to HSS compared to LOSS and static conditions,

consistent with previous literature (Dekker *et al.*, 2002). A summary of the optimisation parameters used is shown in Table 3.2.

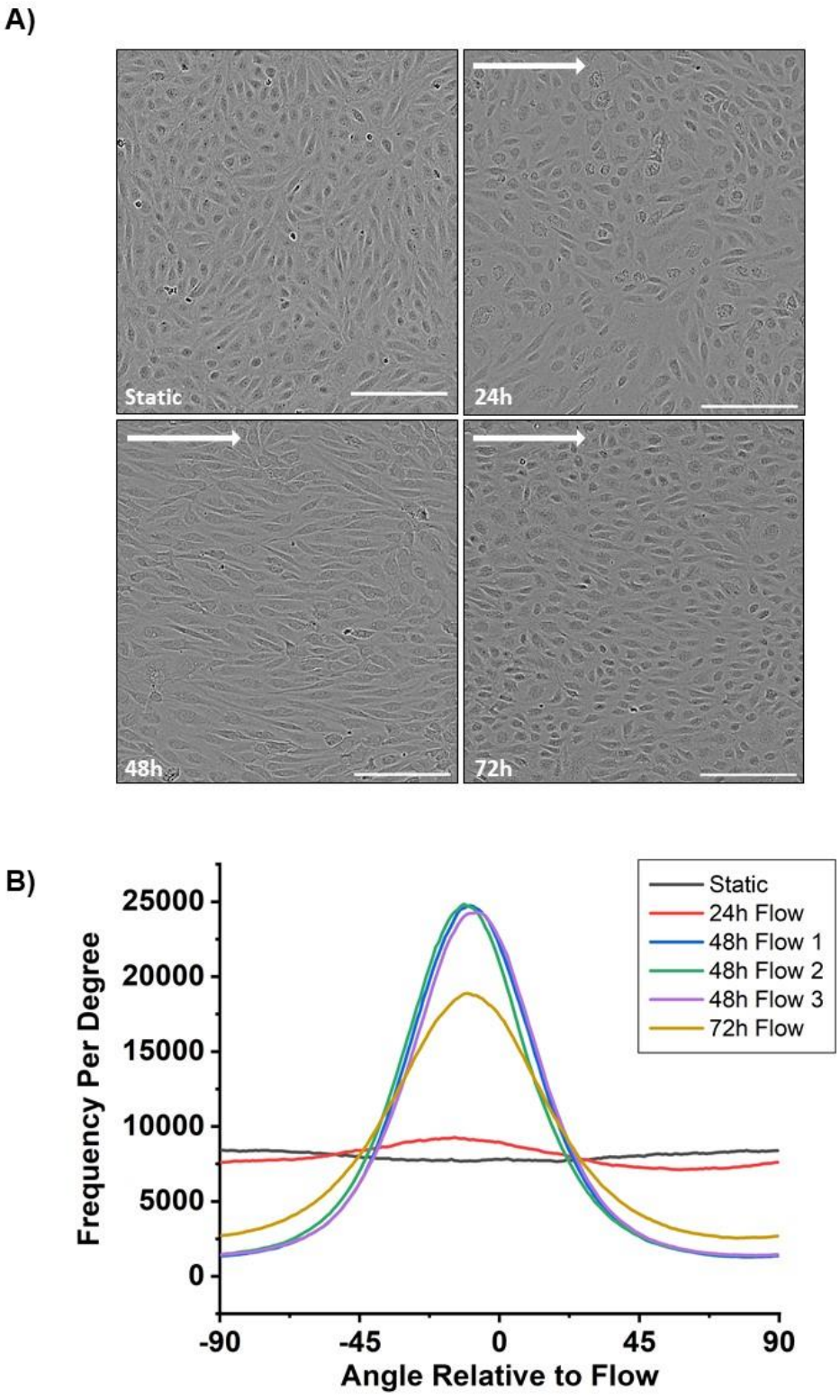

Figure 3.2 – HUVECs showed highest alignment with the direction of flow at 48h.

A) Representative images from each time point using the IncuCyte ZOOM. Arrows indicate direction of flow. Scale bar = 200 µm. B) Histogram to show the alignment of HUVECs relative to the direction of HSS flow (10 dyn/cm^2). *n = 1.*

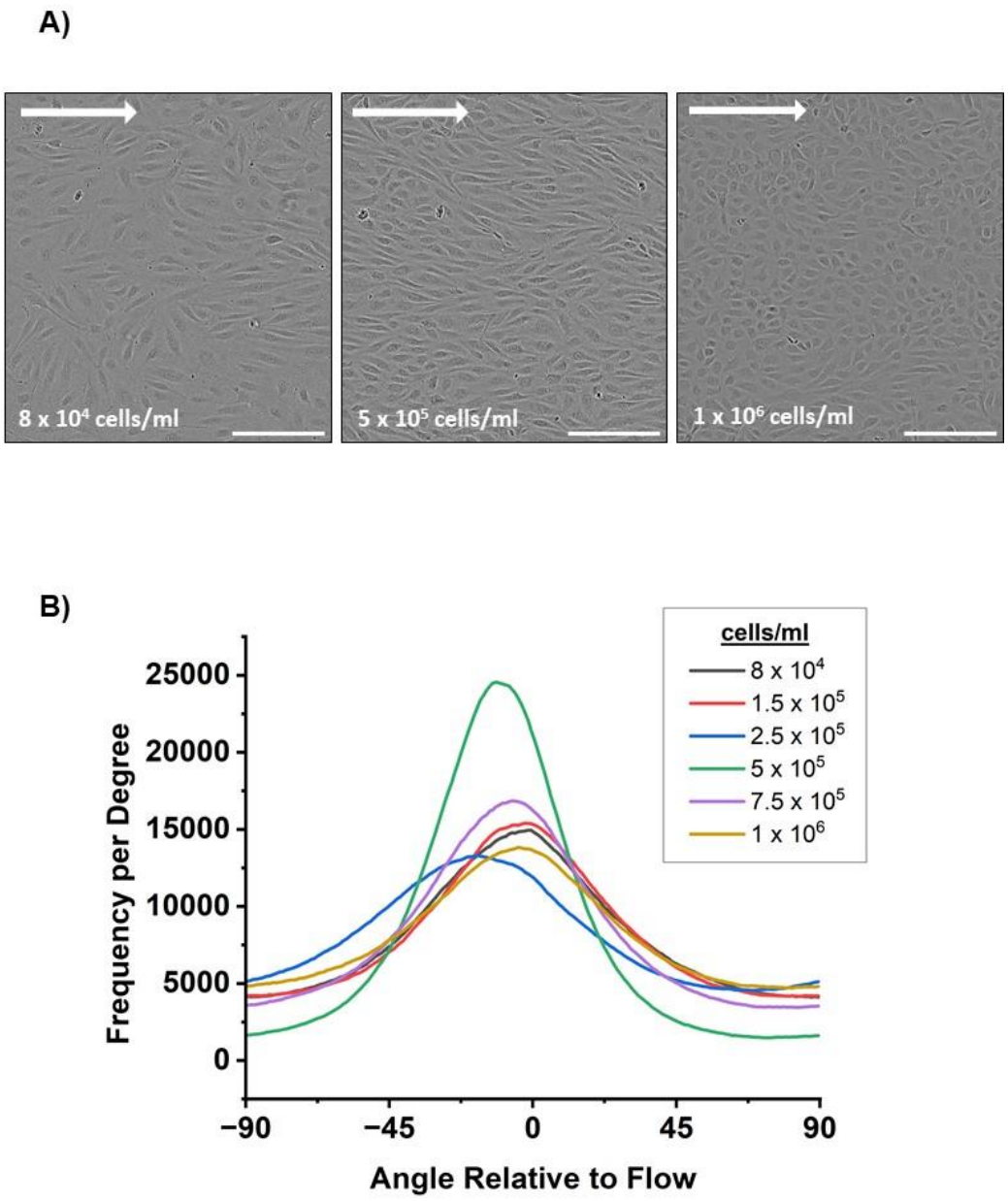

Figure 3.3 – Seeding density of HUVEC affects alignment after application of flow.

A) Representative images from each Ibidi µ-slide I 0.8 Leur channel (IbiTreat) using the IncuCyte ZOOM. Arrows indicate direction of flow. Scale bar = 200 µm. B) Histogram to show the alignment of HUVECs in each channel relative to the direction of flow. *n = 1.*

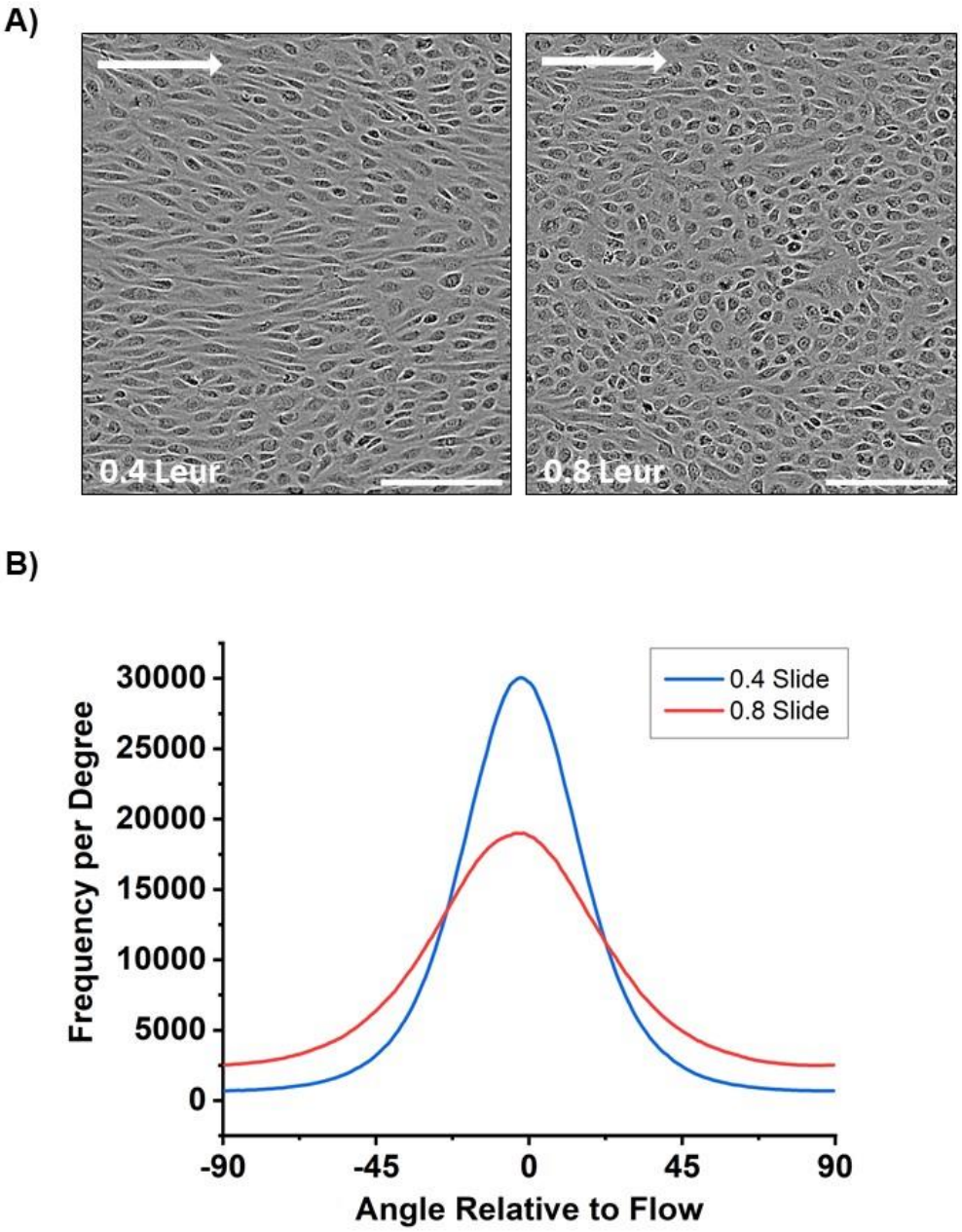

Figure 3.4 – Channel height determines HUVEC alignment to flow, irrespective of shear stress value.

A) Representative images from Ibidi µ-slide I 0.4 Leur (left) and 0.8 Leur (right) channels using the IncuCyte ZOOM. Arrows indicate direction of flow. Scale bar = 200 µm. B) Histogram to show the alignment of HUVECs in each channel relative to the direction of flow. *n = 1.*

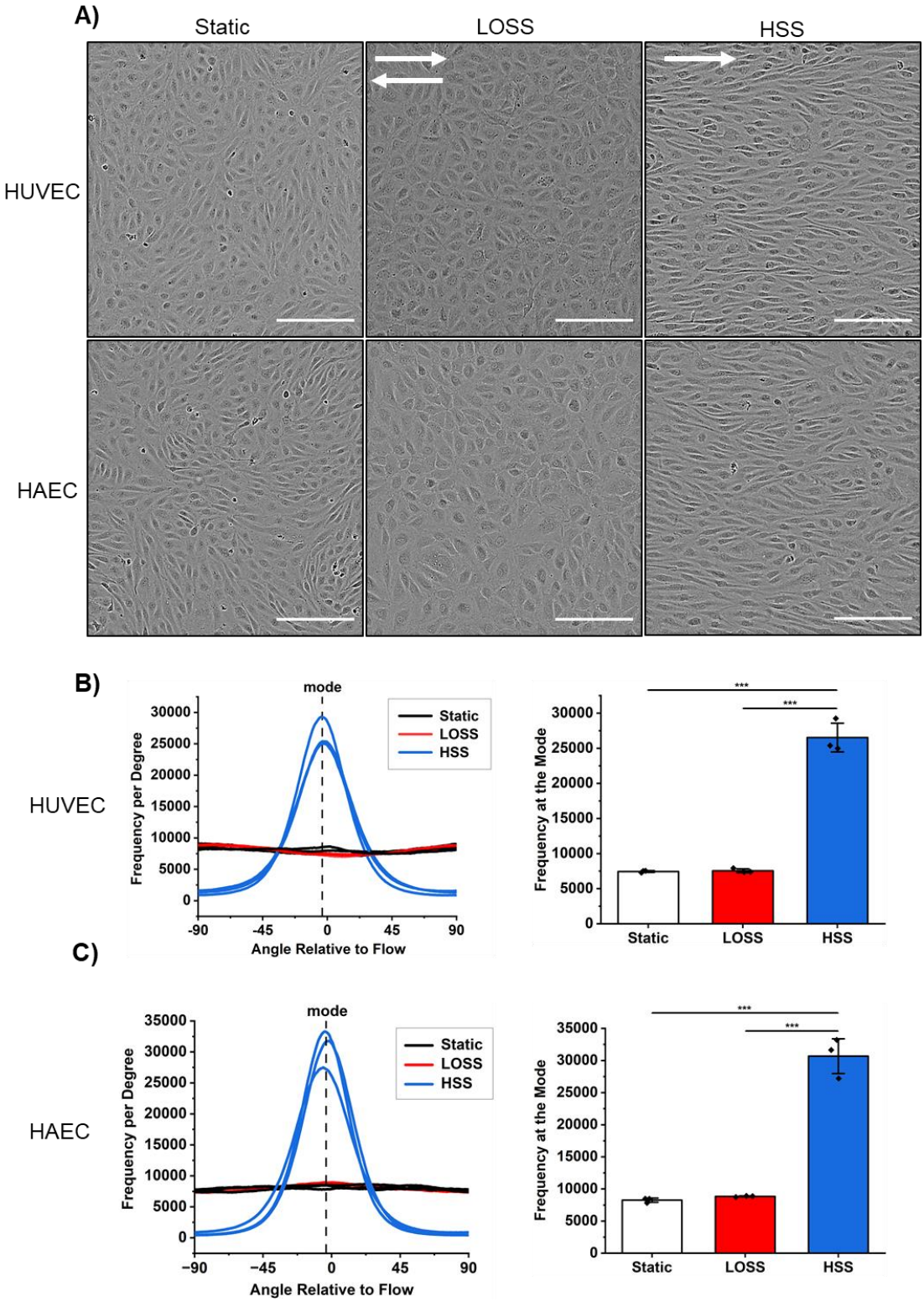

Figure 3.5 - Endothelial cell alignment under different flow conditions.
A) Representative images from each condition using the IncuCyte ZOOM. Arrows indicate direction of flow. Scale bar = 200 µm. B) and C) Histograms to show the alignment of HUVECs and HAECs relative to the direction of flow and frequency at the mode of each histogram. *n* = 3 for each condition. Bars represent mean ± SEM. *** $p < 0.001$ by one-way ANOVA with Bonferroni post-hoc test.

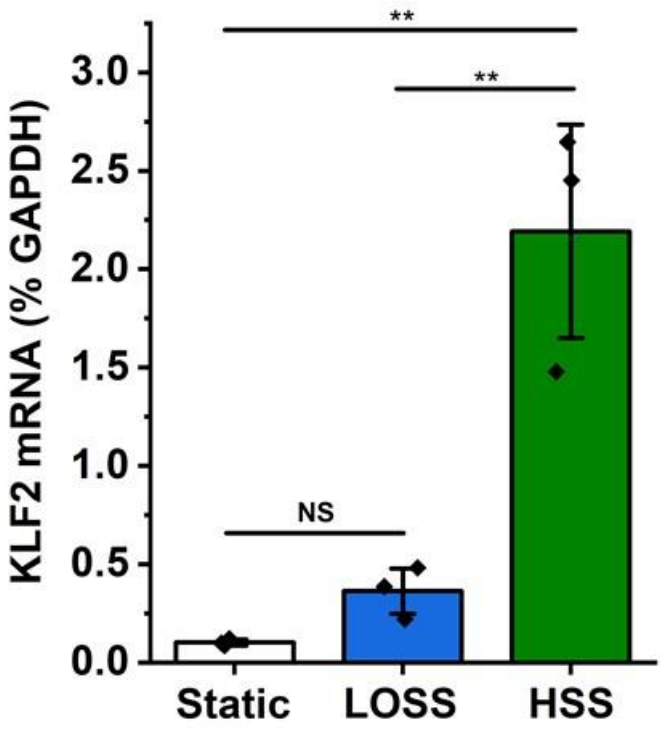

Figure 3.6 – HUVEC KLF2 mRNA expression between different flow conditions.

Graph of quantitative PCR change in cycle threshold (ΔCT) analysis (± SEM) of KLF2 mRNA expression in each shear stress condition. Expression was measured as a percentage of the housekeeping gene control (GAPDH). $n = 3$ for each condition. Bars represent mean ± SEM. ** $p < 0.01$ by one-way ANOVA with Bonferroni post-hoc test.

Channel	Condition	Perfusion Set	Shear Stress (dyn/cm2)	Increment of shear stress	Pressure (mbar)	Flow rate (ml/min)	Plating concentration (cells/ml)	Length of time for attachment	Confluence prior to flow	Flow Period (hours)	Alignment
Ibidi I Leur 0.8	HSS	Red	12	None	91.8	47.97	250,000	24h	Yes	48	Little Alignment
Ibidi I Leur 0.8	HSS	Red	12	2 + 5 (30m each)	91.8	47.97	80,000	24h	No	48	Little Alignment
Ibidi I Leur 0.8	HSS	Red	12	2 + 5 (30m each)	91.8	47.97	150,000	24h	No	48	Little Alignment
Ibidi I Leur 0.8	HSS	Red	12	2 + 5 (1h each)	91.8	47.97	250,000	2h	No	48	Little Alignment
Ibidi I Leur 0.8	HSS	Red	12	2 + 5 (1h each)	91.8	47.97	500,000	2h	No	48	Moderately Aligned
Ibidi I Leur 0.8	HSS	Red	12	2 + 5 (1h each)	91.8	47.97	750,000	2h	Yes	48	Little Alignment
Ibidi I Leur 0.8	HSS	Red	12	2 + 5 (1h each)	91.8	47.97	1,000,000	2h	Yes	48	Little Alignment
Ibidi I Leur 0.8	HSS	Red	12	2 + 5 (1h each)	91.8	47.97	500,000	24h	90%	48	Little Alignment
Ibidi I Leur 0.8	HSS	Red	12	2 + 5 (1h each)	91.8	47.97	500,000	24h	90%	24	No Alignment
Ibidi I Leur 0.8	HSS	Red	10	2 + 5 (1h each)	67.9	39.97	500,000	24h	90%	48	Moderately Aligned
Ibidi I Leur 0.8	HSS	Red	10	2 + 5 (1h each)	67.9	39.97	500,000	24h	90%	72	Moderately Aligned
Ibidi I Leur 0.4	HSS	Red	10	5 (1h)	17	10.55	500,000	24h	90%	48	Highly Aligned
Ibidi I Leur 0.4	HSS	Red	10	5 (1h)	17	7.6	750,000	Overnight	Yes	48	Highly Aligned
Ibidi I Leur 0.4	LOSS	Blue	2 (oscillating - 1Hz)	None	22.2	2.11	750,000	Overnight	Yes	48	No Alignment
Ibidi I Leur 0.4	LSS	Blue	2	None	22.2	2.11	750,000	Overnight	Yes	48	Little Alignment

Table 3.2 - Optimisation parameters of Ibidi pump system.

3.3 High shear stress results in a population of shorter WPBs

Once the Ibidi pump system had been optimised and the flow parameters established, the effect of the different flow conditions on WPBs could be investigated. We hypothesised that high shear stress would result in a population of shorter WPBs, resulting in less thrombotic, atheroprotective endothelial cells located in regions of the vasculature exposed to this type of blood flow. After 48h exposure to flow, and based on the mean Feret's diameter, WPBs were significantly shorter in HUVECs exposed to HSS (0.81 ± 0.03 μm) compared to WPBs in HUVECs exposed to LOSS (1.08 ± 0.01 μm) and static conditions (1.16 ± 0.02 μm) (Figure 3.7 A, B). The change was also observed in HAECs exposed to HSS (0.84 ± 0.03 μm), LOSS (0.99 ± 0.002 μm) and static conditions (1.17 ± 0.05 μm) (Figure 3.8 A, B). Interestingly, WPBs in HAECs exposed to LOSS were also significantly shorter than WPBs in static HAECs, but not to the same extent as in HSS. Cumulative frequency graphs of total WPBs in each condition shows a clear shift to a population of shorter WPBs in HSS conditions compared to LOSS and static in both populations of cells (Figure 3.7 C, Figure 3.8 C). Binned analysis of WPB length shows peaks in WPB counts at distinctive lengths (~0.65, ~0.95 and ~1.25 μm) (Figure 3.7 D, Figure 3.8 D). Ferraro et al. 2014 showed distinct peaks in binned WPB length analysis at 0.5 μm intervals based on the size of individual vWF quanta packaged into nascent WPBs at the Golgi apparatus. Although not as distinct here and slightly different to 0.5 μm, this data indicates an increase in WPBs at specific length intervals in both HUVEC and HAEC. With a more high-throughput model as used in Ferraro et al. 2014, these peaks may become more apparent.

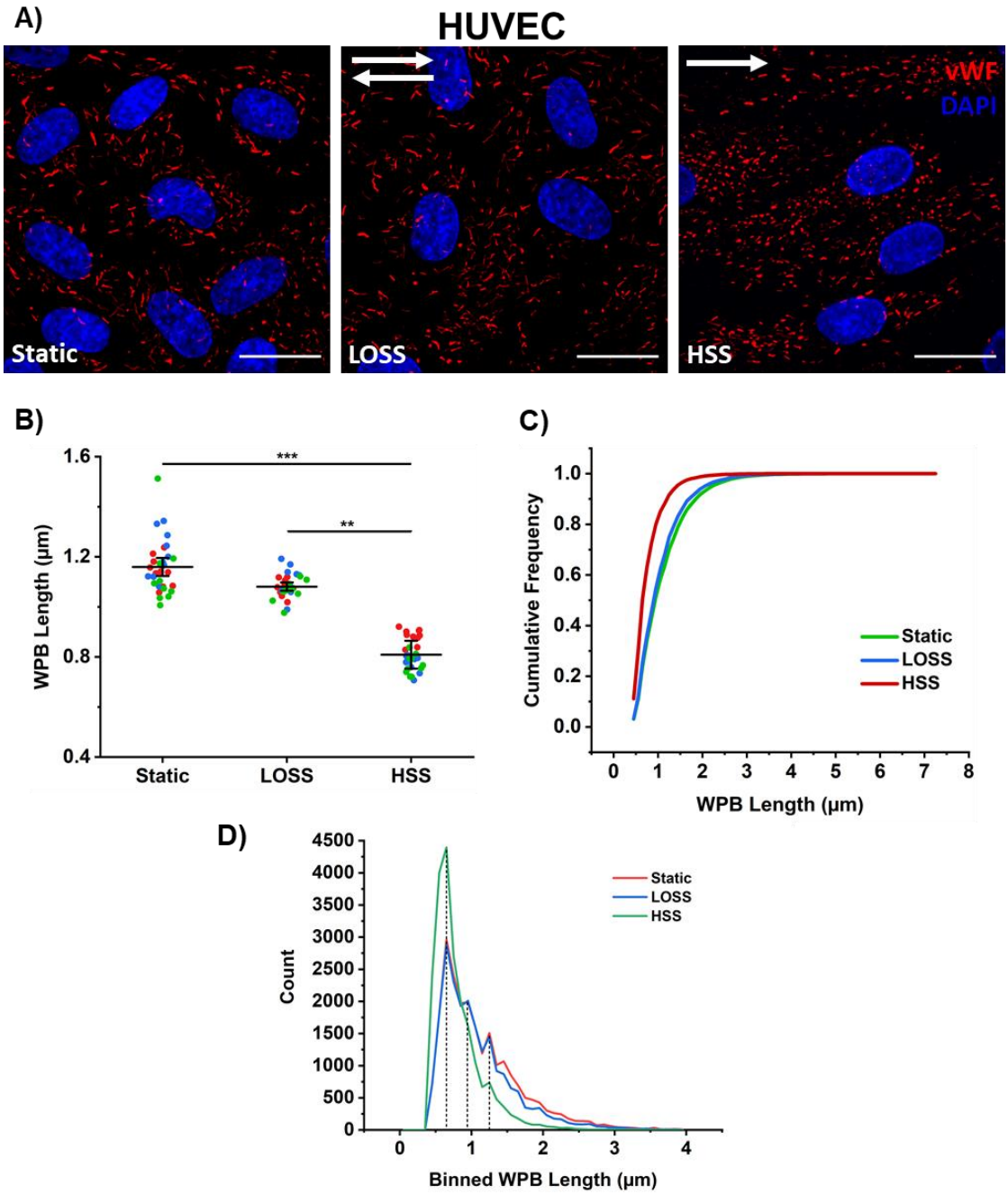

Figure 3.7 - WPB length in HUVEC under different flow conditions.

A) Representative images (x60 objective) of WPBs (vWF: red) from each flow condition. Scale bar = 20 µm. B) Super plot to show mean WPB length ± SEM in each condition, *n* = 3. Each data point represents the mean WPB length from one image (10 images per condition, per repeat). Each colour represents a separate repeat. C) Cumulative Frequency graph of WPB length of all WPBs measured (65599). ** $p < 0.01$, *** $p < 0.001$. D) Histogram to show frequency of counts in binned WPB lengths of all WPBs measured (bin size = 0.1 µm**).**

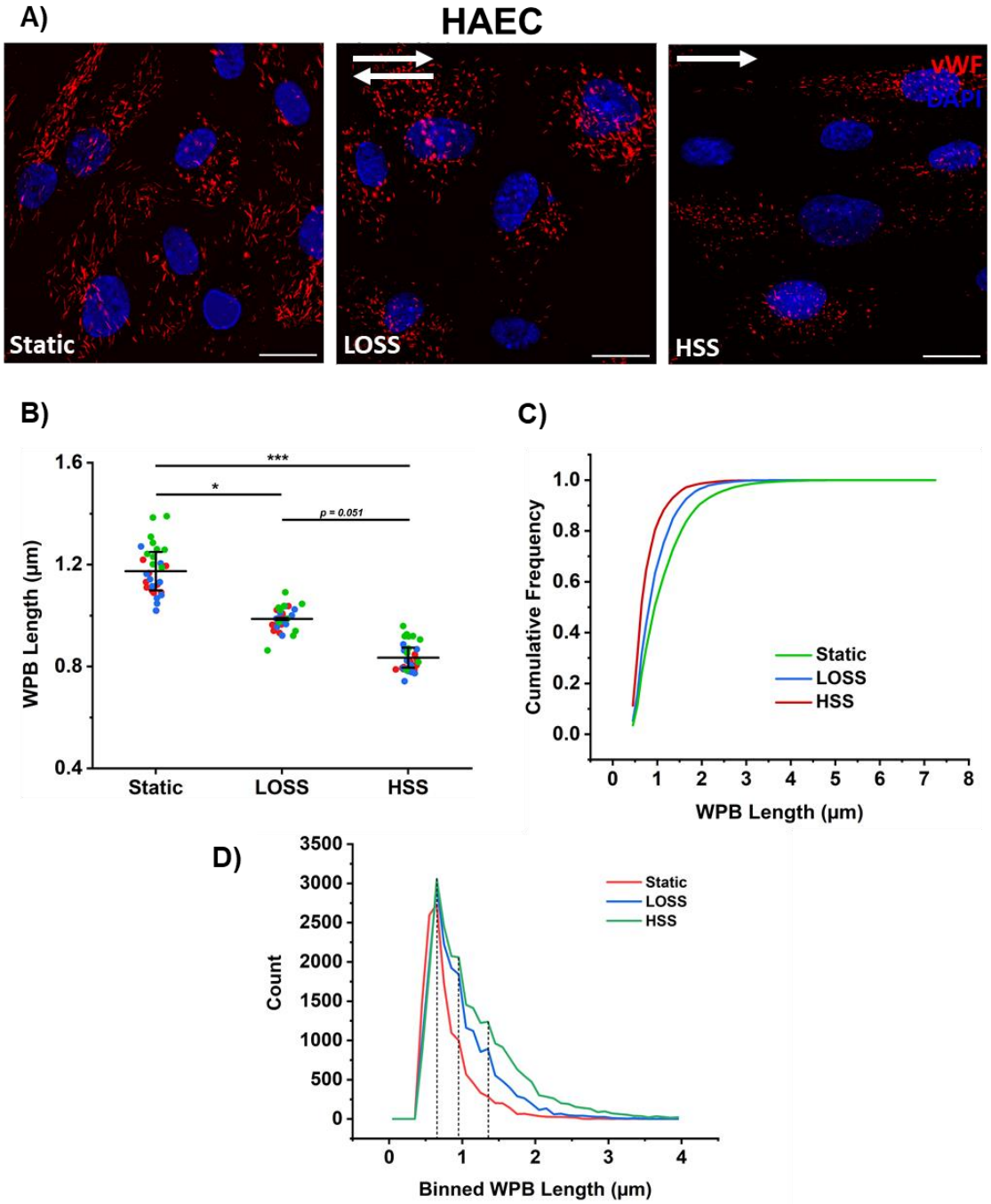

Figure 3.8 - WPB length in HAEC under different flow conditions.

A) Representative images (x60 objective) of WPBs (vWF: red) from each flow condition. Scale bar = 20 µm. B) Super plot to show mean WPB length ± SEM in each condition, *n* = 3. Each data point represents the mean WPB length from one image (10 images per condition, per repeat). Each colour represents a separate repeat. C) Cumulative Frequency graph of WPB length of all WPBs measured (56316). * $p < 0.05$, *** $p < 0.001$. D) Histogram to show frequency of counts in binned WPB lengths of all WPBs measured (bin size = 0.1 µm**).**

3.4 WPB size remains the same in different regions of Ibidi y-shaped slide

The Ibidi y-shaped slide incorporates a channel that branches into two separate channels just after the channel inlet before converging again just before the outlet. This results in regions of unidirectional flow and regions of non-unidirectional flow designed to mimic bifurcations found in the vasculature and therefore providing a more physiological model. Close to the inlet and outlet where there is just one channel (regions 1 and 6), the flow is uniform at its highest rate of shear stress. In the straight regions (regions 3 and 4) of each channel arm after the bifurcation, the flow remains uniform but the shear stress is half that of regions 1 and 6. At regions 2 and 5, the flow is non-uniform due to the change of direction and convergence of flow from the two arms of the channel. It is important to note however, that this flow is not described as disturbed because the flow is still unidirectional and in the same plane.

We hypothesised that the endothelial cells in regions of the slide exposed to non-uniform flow would contain a population of WPBs that were longer than those in cells exposed to unidirectional flow. At 20 dyn/cm^2, there was no significant change in WPB size observed at each of the regions identified in both HUVECs and HAECs (Figure 3.9).

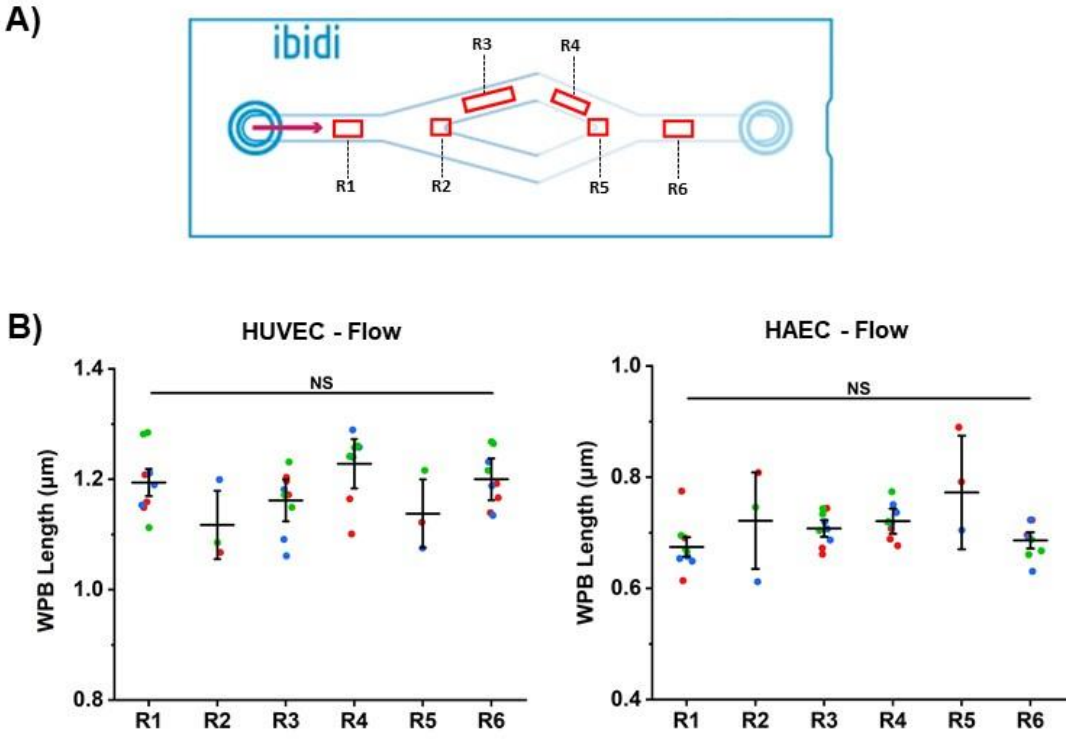

Figure 3.9 – HUVEC and HAEC WPB size remains the same in different regions of Ibidi y-shaped slide.

A) Different regions of the Ibidi y-shaped slide used to observe WPBs. R1 and R6 = 20 dyn/cm^2 uniform flow, R2 and R5 = low, non-uniform flow, R3 and R4 = 10 dyn/cm^2 uniform flow. B) Scatter plots to show average WPB lengths in each of the regions highlighted in both HAEC and HUVEC under flow. *n* = 3, NS = not significant.

3.5 WPB number did not change in the different flow conditions

In addition to WPB size, the number of WPBs in the cells gives an indication of the inflammatory state and thrombotic propensity of a cell population. The higher the number of WPBs per cell, suggests more vWF is ready to be released upon stimulation and therefore, the higher the thrombotic propensity.

WPB number was measured in three ways: 1) the number of WPBs per field of view. This gives an indication of the overall number of WPBs within an image, however, does not consider the number of cells present in each image. 2) the number of WPBs per cell. This measurement involves dividing the total number of WPBs in the field of view by the number of nuclei in the image. 3) the percentage of cells containing WPBs. This involves quantifying the number of cells containing vWF as a percentage value of the total number of nuclei in the field of view.

Hypothesis: cells exposed to LOSS and static conditions will have more WPBs per cell compared to HSS due to the pro-inflammatory stimulus.

There was no significant difference in the number of WPBs across all three methods of quantification between HSS, LOSS and static conditions in both HUVECs and HAECs. HUVECs exposed to HSS contained an average of 711 WPBs/FOV and 74 WPBs/cell, compared to 706 WPBs/FOV and 66 WPBs/cell in LOSS conditions and 768 WPBs/FOV and 71 WPBs/cell in static conditions (Figure 3.10 A, B). HAECs exposed to HSS contained an average of 510 WPBs/FOV and 21 WPBs/cell, compared to 627 WPBs/FOV and 26 WPBs/cell in LOSS conditions and 811 WPBs/FOV and 26 WPBs/cell in static conditions (Figure 3.10 A, B).

Although there was no change in WPB number between each flow condition, there was a notable decrease in the number of WPBs/cell in HAEC compared to HUVEC. This was not surprising, as WPBs are known to be distributed heterogeneously across the vascular tree (Gebrane-Younès *et al.*, 1991), with varying levels of vWF expression observed based on the tissue (Yamamoto *et al.*, 1998). HUVECs are a cell population with a reliably high number of WPBs, whereas cells from the aorta are known to have less. Surprisingly, in one study of the porcine aorta, no vWF was observed (Gebrane-Younès *et al.*, 1991). In this flow model, initial observations of WPBs/FOV indicate little change in the WPB

number. Once the number of WPBs/cell was quantified, the difference between the two cell populations became apparent. The WPBs/FOV remained the same because a different microscope was used for HUVECs compared to HAECs resulting in different sizes of fields of view (HUVEC FOV = 103.2 µm, HAEC FOV = 221.87 µm). In HUVECs the average number of WPBs/cell was 70, compared to 24 WPBs/cell in HAECs. In addition, when quantifying the percentage of cells containing WPBs, 99.8% of HUVECs contained WPBs across the conditions compared to 87% of HAECs. When calculating the number of WPBs per WPB positive cells, HUVECs contain the same 70 WPBs/cell whereas HAECs contain 27 WPBs/cell. This is still a large difference between the two, and indicates that in HAECs, the proportion of WPB positive cells is decreased, as well as the total number of WPBs in the cells containing them.

WPB number provides an insight into the WPB population of cells in different conditions. Although the number did not differ significantly between flow conditions, the change between HUVEC and HAEC show that there are differences based on origin of the cells, with those derived from the aorta containing fewer WPBs/cell compared to cells from the umbilical vein. The reduced percentage of cells containing WPBs in HAEC also highlights heterogeneity of the cells in terms of WPBs. Why do some cells contain WPBs and others don’t? Could this heterogeneity extend to other WPB cargo? Single cell RNA sequencing is one method that can be used to identify changes of gene expression across a cell population at the single cell level. RNA seq analysis could also inform how flow conditions could alter WPB size by changing expression levels of recruited cargo.

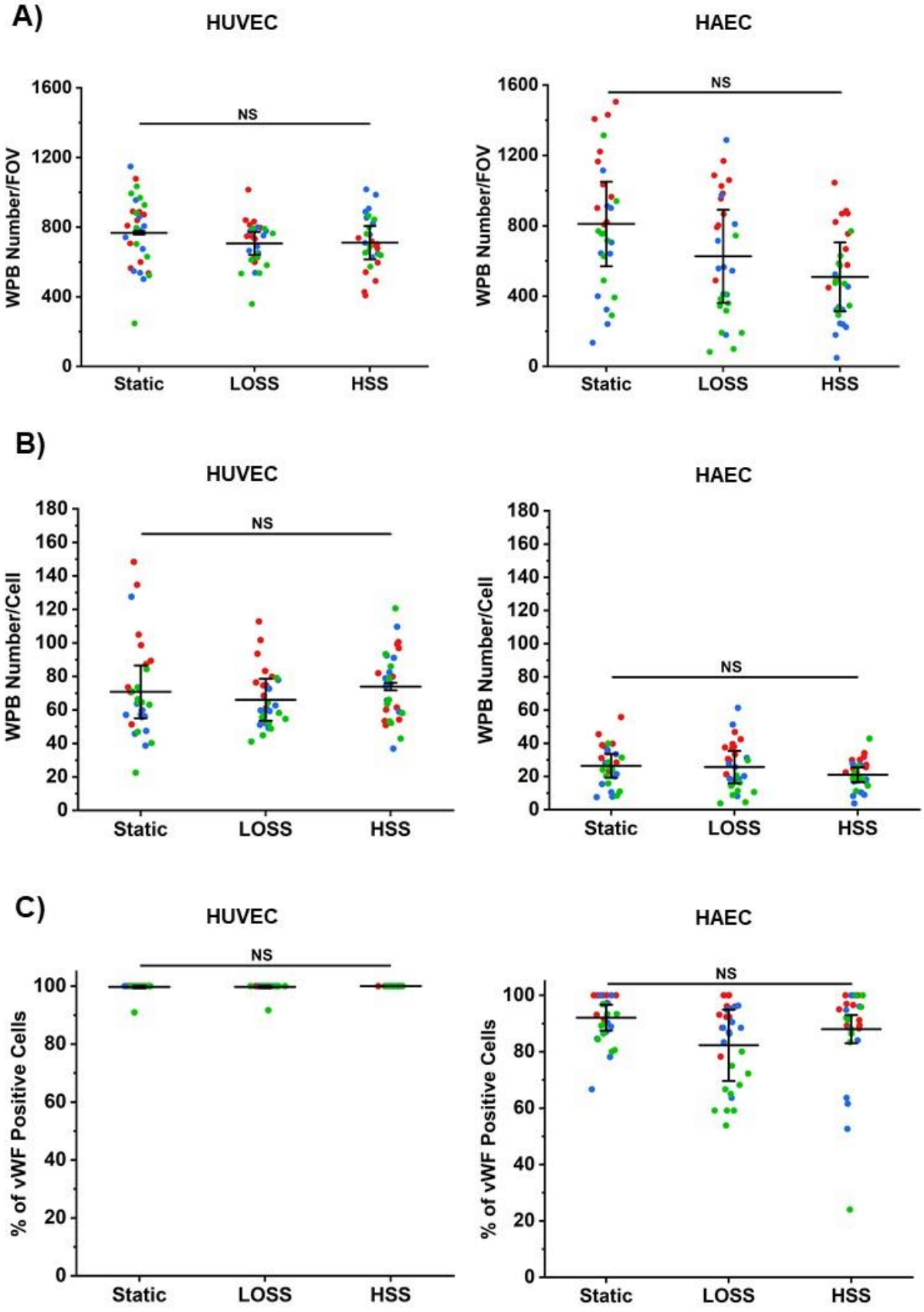
A)
HUVEC
HAEC
WPB Number/FOV
1600
1200
800
400
0
NS
Static
LOSS
HSS
B)
HUVEC
HAEC
WPB Number/Cell
180
160
140
120
100
80
60
40
20
0
NS
Static
LOSS
HSS
C)
HUVEC
HAEC
% of vWF Positive Cells
100
80
60
40
20
0
NS
Static
LOSS
HSS

Figure 3.10 – WPB numbers in HUVEC and HAEC do not change under different flow conditions.

A) Mean Number of WPBs per Field of View (FOV) in each image. Total of 10 FOVs in each condition per repeat. B) Number of WPBs per cell, based on the total number of cells (nuclei) in each image. C) Percentage of vWF positive cells compared to the total number of cells (nuclei) in each image. All super plots show mean ± SEM. *n* = 3, NS = not significant by one-way ANOVA with Bonferroni post-hoc test.

3.6 WPB morphology in different regions of the mouse aorta

The endothelial cells lining the aorta are subjected to both laminar high shear stress in straight sections and disturbed flow, similar to LOSS, in regions with a bifurcations or an abrupt curvature such as the aortic arch. As discussed previously, disturbed flow tends to be the site of atherogenesis, and we hypothesise that this is partly due to changes in WPB morphology and function. *In vitro* findings demonstrated the effect of defined flow rates on WPB length, number and cargo. *In vivo*, flow rates are more variable and dependent on numerous other parameters such as the viscosity, pressure and vessel architecture. We hypothesised that endothelial cells in regions of the mouse aorta subjected to HSS would contain a population of WPBs that were shorter in length compared to WPBs in cell exposed to disturbed flow. The mouse aorta was therefore extracted from wild-type C57/black mice, fixed and immunofluorescent staining performed en face with CD31 and vWF primary antibodies. Confocal images of the inner curvature of the aortic arch were captured to represent the region exposed to disturbed flow, as well as regions of the descending aorta to represent regions exposed to high laminar flow.

CD31 staining shows alignment of cells in regions exposed to high laminar shear, compared to non-aligned cells in regions exposed to disturbed flow, as expected (Figure 3.11). Initial observations indicate WPBs in regions of HSS are shorter than their counterparts in cells exposed to disturbed flow. vWF staining in general appears more ‘patchy’ and conglomerated in specific locations in the aortic arch, compared to relatively uniform staining in the descending aorta. Whether this is due to endothelial cell activation during the extraction process, or a direct result of the types of flow, is yet to be determined. Further optimisation is required with the method and imaging to accurately measure WPB size, however, these initial findings suggest that the changes in WPB length observed in our in vitro model may mimic those observed in vivo.

A limited number of aortas were successfully images due to challenges encountered in the extraction method. The difficulties mainly arose in preserving the aorta’s structure adequately during the staining and mounting steps, which is crucial for identifying regions with aligned and non-aligned cells. Consequently, only a single example is presented here.

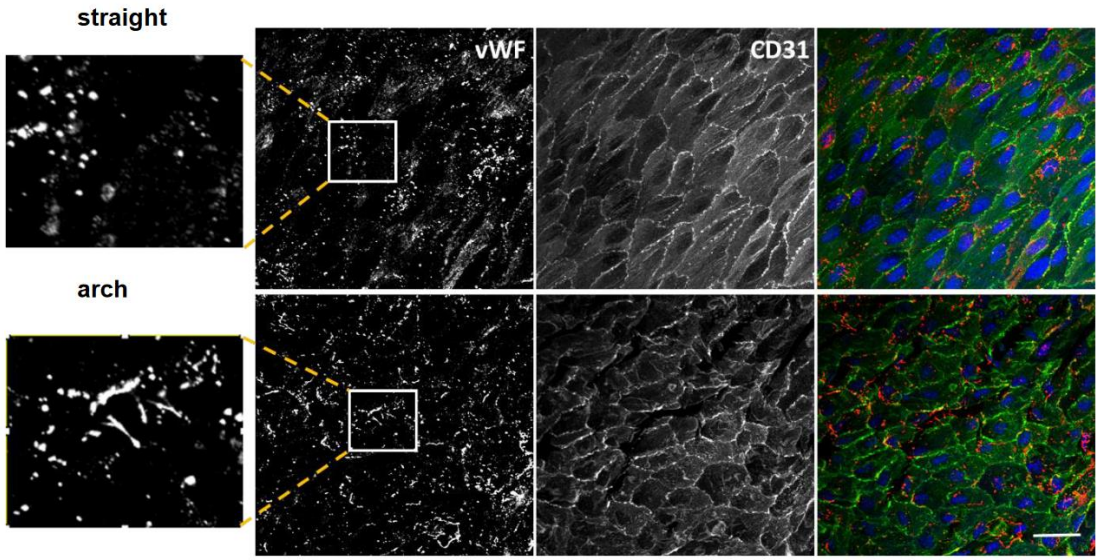

Figure 3.11 - Change in WPB morphology observed in endothelial cells of the mouse aortic arch.

WPBs (vWF: red) and CD31 (green: cell membrane) were examined by en face immunostaining of endothelial cells lining the mouse aorta. The boxes depict the regions of interest on the vWF image that is magnified to the left. The CD31 staining demonstrates the alignment of the cells in the arched regions versus the straight regions. Scale bar = 30 µm.

3.7 Single cell RNA sequencing of endothelial cells from mouse carotid arteries highlights changes in gene expression of WPB cargoes

The study by the Hanjoong Jo research group (Andueza *et al.*, 2020) used single cell RNA sequencing (scRNA-seq) to show that disturbed flow (d-flow) induced gene expression changes resulting in a transition of endothelial cells from an anti-inflammatory and anti-atherogenic phenotype to a pro-inflammatory and pro-atherogenic phenotype. Many of the proteins encoded by these genes are stored in WPBs, so we utilised this dataset to further investigate changes in gene expression of bona fide WPB cargo and additional WPB associated proteins of interest (see appendix).

In the study, scRNA-seq was performed on endothelial-enriched cell samples extracted from the mouse carotid arteries. Mice have two carotid arteries, left (LCA) and right (RCA), which meant two flow conditions could be created within the same mouse. The LCA was partially ligated to induce disturbed flow (d-flow), whilst the RCA was left untouched with stable flow (s-flow). Cells were extracted after 2 days and 2 weeks and scRNA-seq was performed, resulting in 4 conditions (2D-R, 2W-R, 2D-L, 2W-L) (Table 3.3).

LCA		**RCA**	
2 days	2 weeks	2 days	2 weeks
2D-L	2W-L	2D-R	2W-R

Table 3.3 - scRNA-seq - 4 different flow condition abbreviations.

As described in (Section 2.9), cells were initially clustered by UMAP based on well-known gene markers. This resulted in the identification of a range of cell types, including smooth muscle cells, macrophages, dendritic cells, monocytes, fibroblasts and endothelial cells (Figure 3.12). Within the endothelial cell cluster, 8 distinctive endothelial cell clusters were identified across the 4 conditions. These were characterised by the size of each cluster in each condition, and using gene markers known to be up and down-regulated in different types of flow (Table 3.4). Based on the cluster size in each flow condition, E1-E4 consisted of

endothelial cells mostly exposed to s-flow (2D-R and 2W-R). Clusters E5 and E7 were mostly endothelial cells exposed to acute d-flow (2D-L), whilst E6 and E8 contained cells exposed to chronic d-flow (2W-L). In terms of gene marker expression, cluster E2 had the highest levels of the known mechanosensitive genes (KLF2 and KLF4) (Figure 3.12). This cluster was therefore labelled as most representative of endothelial cells in s-flow. Cluster E8 had the highest level of thrombospondin-1, a gene known to be upregulated in d-flow, and was a cluster not present in s-flow conditions but appeared after 2 weeks exposure to d-flow (Figure 3.12). E8 was therefore labelled as the most representative of endothelial cells in chronic d-flow. The other clusters sat somewhere in the middle of these 2 extremes (Table 3.4).

Endothelial Cell Cluster	Characterisation of Flow
E1	S-flow (low sensitivity to flow)
E2	Highest levels of known mechanosensitive genes (KLF2/KLF4)
E3	Second highest levels of known mechanosensitive genes (KLF2/KLF4)
E4	S-flow (low sensitivity to flow)
E5	Acute d-flow
E6	Chronic d-flow
E7	Acute d-flow
E8	Chronic d-flow (highest level of Thsp1)

Table 3.4 – Characterisation of endothelial cell clusters.
UMAP identified 8 endothelial cell clusters which were characterised based on gene marker expression and appearance/disappearance of distinct clusters after exposure to different flow types.

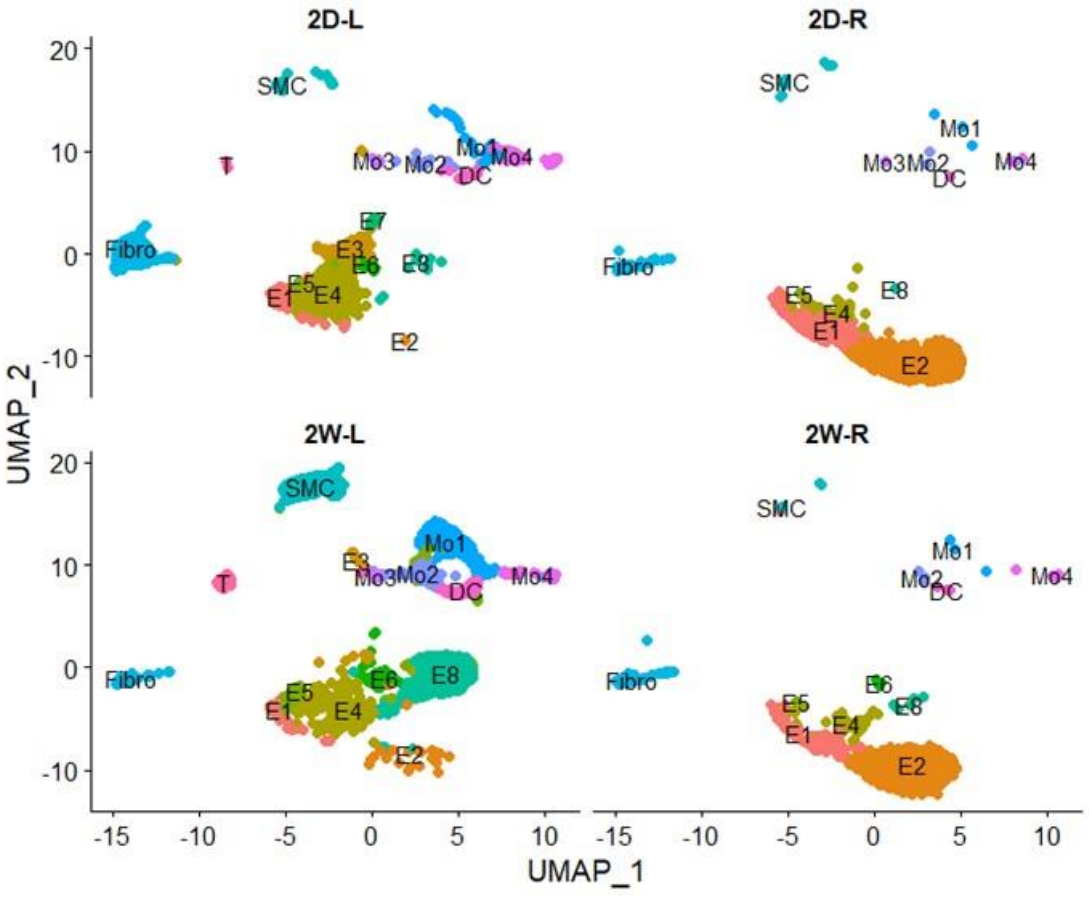

Figure 3.12 – UMAP showing the clusters of cells in each condition.

Firstly, the expression of bona fide WPB cargoes (Table 1.1) were investigated in each endothelial cell cluster. Figure 3.13 shows the expression of WPB cargoes in each endothelial cell cluster (E1-E8). The expression of **vWF** and P-selectin (**Selp**) was not significantly different between E2 and E8 clusters. Angiopoietin-2 (**Angpt2**) was downregulated in s-flow conditions (as expected) (Figure 3.13). The expression levels of these 3 genes were consistent with the expression of genes quantified with RT-qPCR after exposure to HSS, LOSS and static conditions for 48h in the Ibidi pump system (Figure 3.15) suggesting that the *in vitro* model reflects the *in vivo* data in terms of gene expression. Having confirmed similar levels of gene expression between the RNA-seq dataset and that seen in the Ibidi pump system, the other WPB cargoes were investigated. There were significant differences in the expression of endothelin-1 (Edn1), insulin growth factor binding protein 7 (Igfbp7), Angiopoietin-2 (Angpt2), CD63 and tissue plasminogen activator (Plat) between E2 and E8 clusters (Figure 3.15).

Expression of the potent vasoconstrictor, **endothelin-1** (Edn1), was increased in chronic d-flow (E8) compared to s-flow (E2), and a significantly higher number of cells were Edn1 positive (99% compared to 69%, respectively). This is consistent with previous studies, which suggest endothelin-1 is downregulated in laminar shear stress conditions (Morawietz *et al.*, 2000). Expression of the endothelin converting enzyme, Ece1 however, was not significantly different.

Igfbp7 is a secreted protein belonging to the low-affinity family of insulin-like growth factor binding proteins (100-fold lower affinity compared to members of the high affinity family) (Jin *et al.*, 2020). It binds strongly to insulin, which results in inhibition of insulin receptor phosphorylation. Expression was significantly upregulated in d-flow (E8) compared to s-flow (E2), with an increase in the percentage of Igfbp7 positive cells (95% compared to 71%, respectively). This finding is consistent with previous studies, which showed that KLF2 overexpression resulted in down-regulation of Igfbp7 localised to WPBs (van Breevoort *et al.*, 2012). It is suggested that Igfbp7 binds directly to vWF and is therefore co-packaged at the point of WPBs. The change in Igfbp7 expression is independent of VWF, as the expression of vWF did not change.

Angiopoietin-2 is a well characterised angiogenic factor known to be regulated by shear stress (Chlench *et al.*, 2007). In this instance, d-flow induced

upregulation of Angpt2 expression compared to s-flow. In s-flow, almost no cell was Angpt2 positive (0.01%) compared to 55% of cells after exposure to d-flow.

CD63, a member of the tetraspanin family, regulates the surface levels of membrane proteins. In particular, previous studies have shown it is essential in clustering of P-selectin at the cell surface in order to recruit leukocytes to endothelial cells (Doyle *et al.*, 2011). In this dataset, Cd63 was significantly downregulated in s-flow compared to d-flow, but almost every cell in both conditions was Cd63 positive (97% compared to 98%, respectively).

Plat encodes the tissue-type plasminogen activator protein, a key enzyme involved in fibrinolysis and the breakdown of blood clots. It is colocalised to vWF in WPBs (Huber *et al.*, 2002). Plat was downregulated after exposure to d-flow, with 33% of cells Plat positive compared to 62% in s-flow. This result is consistent with the lesser likelihood of clots forming in regions of s-flow i.e. the higher the expression of Plat, the quicker the breakdown of any clots that form and therefore less chance of a blockage.

The results from the scRNA-seq dataset in Andueza *et al.*, 2020 highlights the heterogeneity of WPB gene expression in the endothelial cell population, with 8 distinct endothelial cell clusters expressing different levels of each WPB cargo gene. More specifically, it shows that there are significant differences in the expression of WPB cargo genes in different types of flow. All appear to be consistent with a lesser thrombotic, inflammatory phenotype in s-flow compared to d-flow.

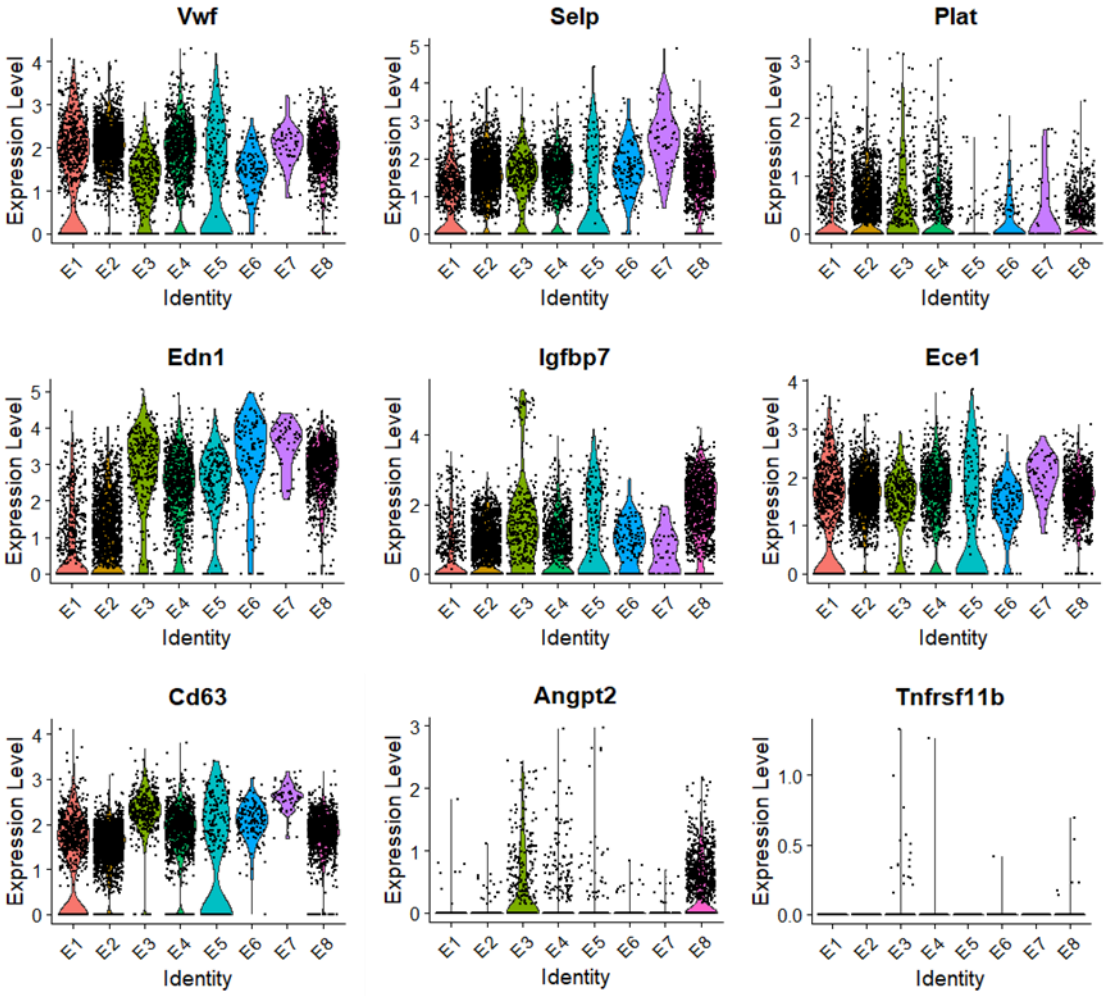

Figure 3.13 – Violin plots to show bona fide WPB cargo gene expression in each endothelial cluster (E1-E8) identified in the scRNA-seq dataset.

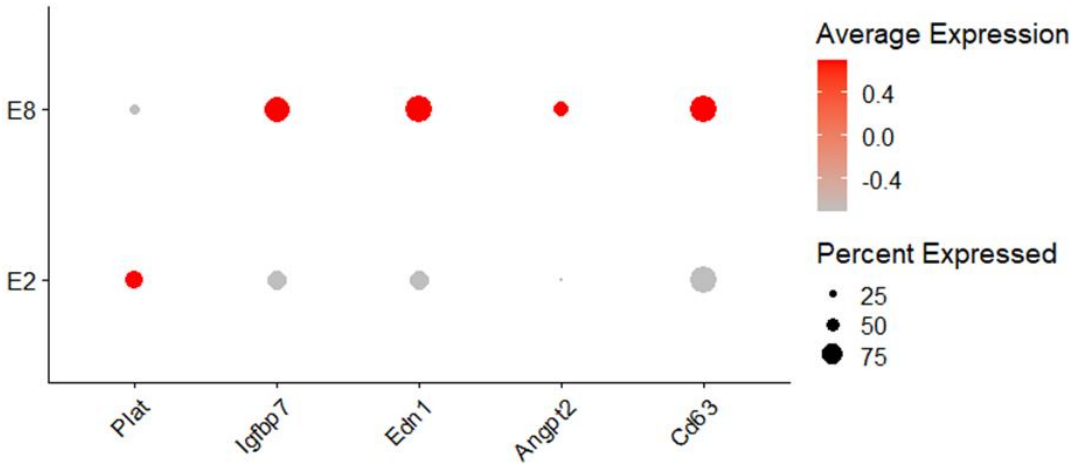

Figure 3.14 - Dot plot to show the average and percentage expression difference of significantly different WPB cargo genes between s-flow (E2) and chronic d-flow (E8). Statistical analysis was performed based on the non-parametric Wilcoxon rank sum test using Seurat's differential expression testing in R.

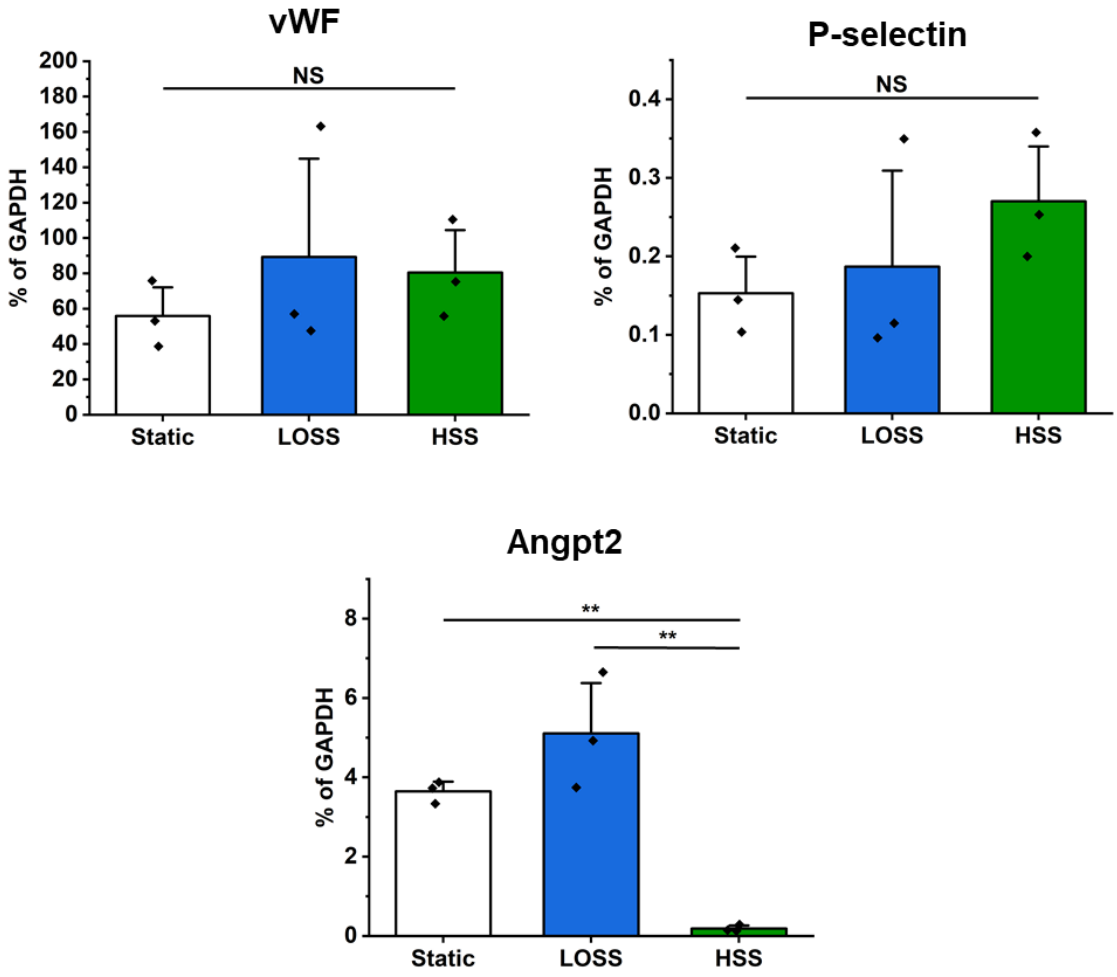

Figure 3.15 - mRNA expression of vWF, P-selectin and Angiopoietin-2 in different flow conditions of Ibidi pump system using RT-qPCR.

Graphs of quantitative PCR change in cycle threshold (ΔCT) analysis (± SEM) of vWF, P-selectin and Angiopoietin-2 mRNA expression in each shear stress condition. Expression was measured as a percentage of the housekeeping control (GAPDH). n = 3 for each condition. Bars represent mean ± SEM. * p < 0.05 by one-way ANOVA with Bonferroni post-hoc test.

3.8 WPB Cargo

Single-cell RNA-seq and RT-qPCR provide insights into gene expression changes under different flow conditions, however this doesn't always correlate with changes in translate protein levels. To explore any changes in protein levels, fluorescent staining and imaging was performed and quantified using mean fluorescent intensity (MFI) values.

3.8.1 Angiopoietin-2

The expression of Angpt2 in known to be regulated by different types of flow (Tressel *et al.*, 2007; Andueza *et al.*, 2020). Under atheroprotective conditions, such as HSS, the flow responsive transcription factor KLF2 is overexpressed and Angpt2 levels are downregulated (van Agtmaal et al. 2012). This is thought to contribute to vessel stabilisation because there is a higher Angpt1 to Angpt2 ratio which leads to a reduction in inflammation and vascular remodelling. Here, I show that HSS induces a significant reduction in the mean fluorescence intensity of Angpt2, compared to Angpt2 expression in HUVECs exposed to LOSS conditions (Figure 3.16). While the data implies that there is no significant difference in Angpt2 levels in WPBs between HSS and static conditions, this observation is influenced by the considerable variability in Angpt2 intensity observed in cells cultured under static conditions. However, the overall trend suggests increased Angpt2 levels under static conditions compared to HSS. This finding is consistent with previous research showing that Angpt2 levels are reduced in endothelial cells exhibiting an atheroprotective phenotype, but increased under disturbed flow conditions (Fiedler *et al.*, 2004a; Chlench *et al.*, 2007).

3.8.2 Von Willebrand Factor

Given its prominence in WPBs and its essential role in their biogenesis and morphology, we hypothesised that exposure to HSS would lead to reduced vWF expression compared to LOSS and static conditions. We assessed the mean fluorescence intensity (MFI) of vWF across HSS, LOSS, and static conditions (Figure 3.16). Surprisingly, there were no statistically significant differences in vWF MFI among these flow conditions. This indicates that, despite observed changes in WPBs under high shear stress, the overall quantity of vWF within endothelial cells remained consistent. This suggests a potential adaptation of

cells to flow conditions, maintaining a relatively stable pool of vWF in the cytoplasm across varying flow conditions. Further investigation into any alterations in secreted vWF will be crucial in determining whether the functional aspects of vWF change in response to these diverse flow conditions.

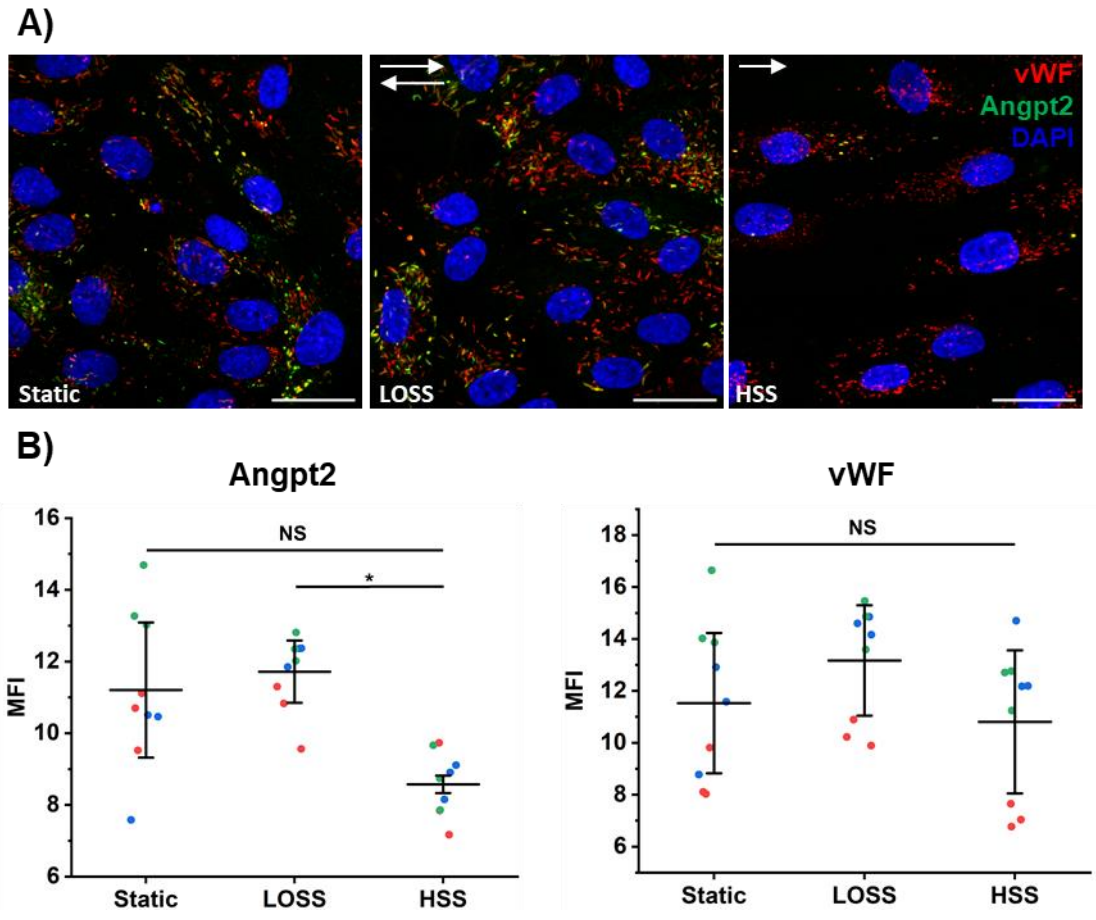

Figure 3.16 - Quantitative analysis of Angpt2 and vWF MFI in HUVECs.
A) Representative immunofluorescent images of Angpt2 (green) and VWF (red: marker of WPBs) in HUVECs under static, HSS or LOSS. Nuclei = DAPI (blue). Arrows indicate direction of flow. Scale bar = 30 µm. B) The graphs show the mean data (MFI: mean fluorescent intensity) of the images depicting Angpt2 and vWF in HUVECs. $n = 3$, * $p < 0.05$ by one-way ANOVA with Bonferroni post-hoc test.

3.9 Summary

This chapter showed the steps involved in optimisation of the Ibidi system for use in the analysis of WPBs under shear stress. It explored the effects of shear stress on WPB length, cargo and gene expression, utilising a published dataset to gain an insight into changes in gene expression *in vivo*.

Optimisation steps of the Ibidi pump system for use in this project included assessing different seeding densities, duration of attachment time, duration of flow, shear stress rates and Ibidi channel heights. To assess the success of each parameter, quantification of cell alignment was used, with the knowledge that HSS should induce uniform alignment of endothelial cells after 24-48 hours. An important finding was that other parameters in the Ibidi system, such as pressure, affected the alignment of cells independent of the shear stress rate. Shear stress applied with the upper limit of pressure in the Ibidi system resulted in reduced alignment compared to the same shear stress applied with lower pressure. This was resolved by using Ibidi channels of lower height (0.4 mm, compared to 0.8 mm). Overall, the Ibidi system induced consistent endothelial cell alignment responses, coupled with an increase in KLF2 mRNA expression compared to LOSS and static conditions, a well-characterised finding identified in previous literature (Dekker *et al.*, 2002).

HUVECs and HAECs were subjected to HSS, LOSS and static conditions for 48 hours. WPBs in endothelial cells subjected to HSS were significantly shorter than those subjected to LOSS and static conditions. There was no observed change in the number of WPBs. Ibidi y-shaped slide did not show any differences in WPB length in different rates of shear stress, thought to be due to the fact that the flow was still laminar and unidirectional. These findings appeared to be replicated in the mouse aorta, however further optimisation is required to draw definitive conclusions from the *in vivo* data.

RT-qPCR revealed no change in mRNA expression of vWF or P-selectin, but showed a decrease in Angpt2 expression in endothelial cells exposed to HSS compared to LOSS and static conditions, consistent with previously published findings (Goettsch *et al.*, 2008). Mean fluorescent intensity measurements of vWF protein levels did not change, whilst Angpt2 levels decreased in cells subjected to HSS. RT-qPCR analysis was coupled with single-cell RNA sequencing analysis on a previously published data set (Andueza *et al.*, 2020). This

highlighted changes in the expression of WPB cargo in steady flow compared to disturbed flow; Plat, Angpt2, Igfbp7, Cd63 and Edn1. This data provides an insight into potential effects of shear stress on WPB cargo, and provides a useful starting point for further investigation.

In summary, this chapter shows that HSS causes a decrease in WPB length, and reduced expression of a number of WPB cargo. The next chapter will focus on whether these shear stress induced changes affect the function of WPBs.

Chapter 4 – The impact of flow on endothelial cell secretome and WPB function

4.1 Introduction

Weibel-Palade bodies contain a variety of molecules, including vWF, P-selectin, Angpt2, endothelin-1 and other factors. These molecules play crucial roles in blood coagulation, inflammation and vascular haemostasis. The contents of WPBs are released in the bloodstream in response to various stimuli and the secretome profile differs based on the nature of stimulus. Notably, potent activators like PMA trigger the non-selective release of WPB contents, whereas histamine induces selective release of specific cargo (Miteva *et al.*, 2019). This selective release is essential for fine-tuning the body's response to different challenges.

Previous research has demonstrated that the morphology of WPBs influences the release of WPB contents secreted into the bloodstream (Ferraro *et al.*, 2016). The preceding chapter detailed a flow-dependent change in WPB size and cargo recruitment. This chapter explores whether these changes affect the overall secretome of endothelial cells, with particular focus on the release of WPB contents and the potential consequences for the function of these cargoes.

The aim of this chapter is to gain a better understanding of how flow-induced changes to WPB morphology and cargo storage affects basal and regulated secretion from endothelial cells.

4.2 The effect of flow on the endothelial cell secretome

Single cell RNA sequencing data and fluorescence intensity measurements described in Chapter 3 have shown that WPB biogenesis and cargo recruitment are dependent on the flow conditions. Here, secretome proteomic analysis was used to determine the effect of flow on basal and regulated endothelial cell secretion, with subsequent analysis of vWF string length upon stimulation with histamine. Cell culture media collected from the Ibidi pump system following 48 hours exposure of HUVECs to either HSS, LOSS or static conditions (basal secretion). Additional media was then collected after acute (10 mins) stimulation with 150 µM histamine (regulated secretion). The collected media was

centrifuged to remove cell debris before freezing and undergoing proteomic analysis by University of Bristol Proteomics Facility.

4.2.1 Overall analysis of protein abundance

Principal component analysis (PCA) is a linear technique used to reduce the dimensionality of the dataset, enabling visualisation of this reduction by projecting the data onto a lower-dimensional space. In this instance, Figure 4.1a represents the first two principal components (PC1 and PC2). PC1 captures the most variance in the data and represents the primary source of variation in the data. PC2 captures the second most significant variance in the data. Subsequently, PC3 and PC4 capture the next most significant variance in the data and are shown in Figure 4.1b. In addition to the four principal components of analysis, the data was split into High (HSS), Oscillatory (LOSS), and static in both basal conditions and histamine stimulated, as defined by the figure legend. A media control with and without histamine was also included in this analysis. Finally, each repeat (F2, F4 and F6) was visualised using ovals with different line features.

Initial observations of Figure 4.1a shows variation between each individual data point, particularly in the PC1 dimension. There is however, no apparent clustering of data points or patterns in the data, indicating a lack of any strong correlation between variables using this method of visualisation. Further analysis of each dataset and specific proteins gives a more in-depth insight as to any differences between individual proteins and whether difference are consistent across repeats.

As well as observing the initial variation between samples, it is also important to consider the sum of raw abundances in each sample set. Figure 4.1c and d depict both the sum of raw abundances and Log2-transformed sum of raw abundances for each sample and in each individual replicate. Of note, pre-exposure to 48h LOSS followed by histamine stimulation (Osc.his) results in an increased abundance of proteins in the secretome compared to all other basal and histamine stimulated conditions and in all three replicates. Further downstream analysis will determine the proteins increased in the secretome of this sample.

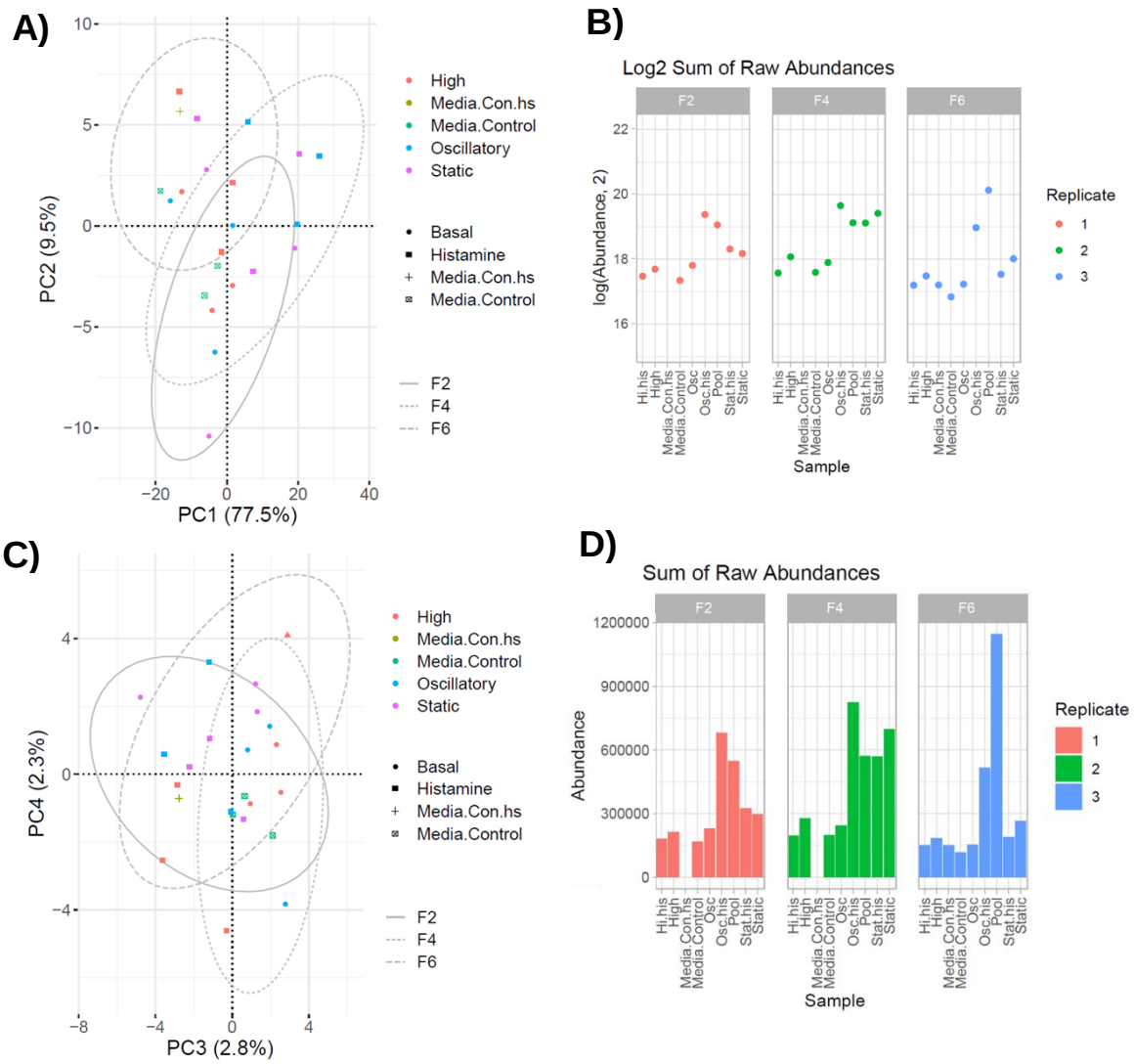

Figure 4.1 – Principal component analysis (PCA) and sum of raw abundances.

A) PCA plots and B) protein abundance conducted on scaled data at various normalisation steps. High = high shear stress, Media.Con.hs = media control histamine, Media.Control = media control without histamine, Oscillatory = low oscillatory shear stress, Static = no flow. Basal = basal levels of glucose, Histamine (.his) = with histamine stimulation. F2 = repeat 1, F4 = repeat 2, F6 = repeat 3.

4.2.1.1 Differential secretion of proteins between conditions

Volcano plots were used to depict the secreted proteins whose expression was significantly ($p < 0.05$) up- or down-regulated by the stated flow conditions (Figure 4.2). The x-axes of these plots represent the fold-change of each protein between conditions and are presented in log form, the 2 red dashed lines indicates a fold change of above or below the *p*-value threshold of 0.05. The y-axes represent the statistical significance of the differences between each condition and is presented as the negative logarithm of the p-value to measure the likelihood that the observed differences are due to random chance. The red dashed line shows the threshold of fold change >1LogFC. In basal (non-stimulated) conditions, no significant difference was observed in the secretion of proteins between LOSS and HSS. Fourteen (14) proteins were significantly different between stimulated static and HSS, with 10 presenting a fold change above the >1LogFC threshold. Similarly, 20 proteins were significantly different between static and LOSS, with 18 reaching the threshold fold-change. Although these changes were initially significant, a false discovery rate (FDR) was applied, which anticipates the expected proportion of false positives among the dataset that are rejected. As a result, once the FDR correction was applied, significance was lost in all comparisons of flow under basal conditions. Similarly, in histamine stimulated static vs HSS and static vs LOSS conditions, although a proportion of proteins reached significance and were above the LogFC threshold, no significance was maintained after FDR correction. In the HSS vs LOSS histamine stimulated comparison, a high proportion of the proteins were significantly increased, and a large proportion also remained significant after FDR correction. In total, 149 proteins were significantly increased in the secretome of cells cultured under LOSS conditions after histamine stimulation compared to HSS. Some of these however, matched exclusively with either a ‘common contaminants’ database or a bovine data (cRFP) and were subsequently removed leaving 43 proteins. Those remaining, alongside their corresponding LogFC, p-values and FDRs, are presented in Table 4.1.

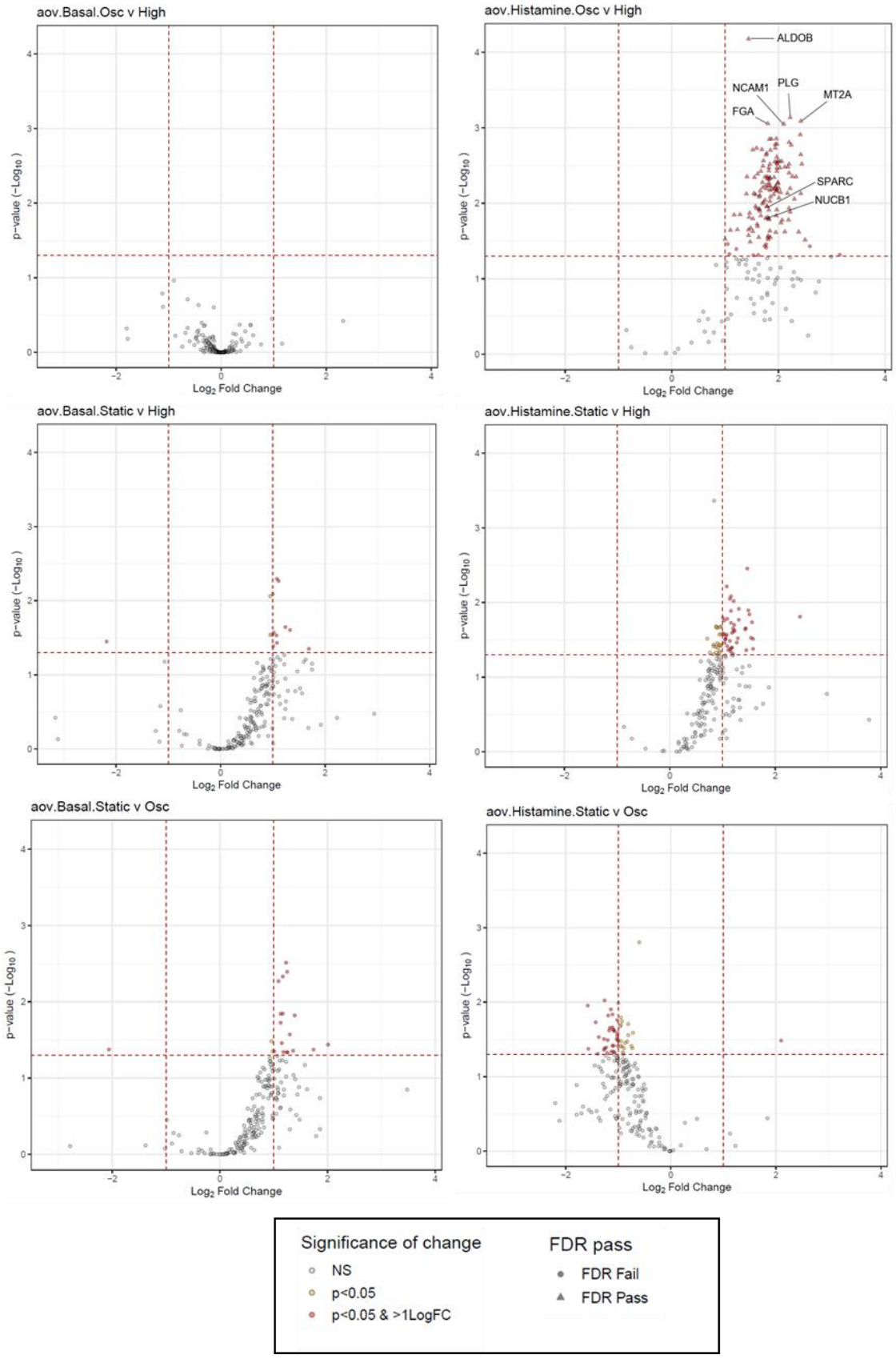
aov.Basal.Osc v High
aov.Histamine.Osc v High
ALDOB
NCAM1
PLG
MT2A
FGA
SPARC
NUCB1
aov.Basal.Static v High
aov.Histamine.Static v High
aov.Basal.Static v Osc
aov.Histamine.Static v Osc
p-value (-Log10)
Log2 Fold Change
Significance of change
NS
p<0.05
p<0.05 & >1LogFC
FDR pass
FDR Fail
FDR Pass

Figure 4.2 - Volcano plots show the log fold change in proteins in basal and stimulated secretomes after exposure to different flow conditions.

Significance of change indicated by colour of points. Plots on the left hand side show protein expression change in media from cells exposed to different flow conditions for 48 hours (basal). Plots on the right hand side show protein expression change in media from cells stimulated with 150 μM histamine for 10 minutes, after pre-exposure to different flow conditions for 48 hours.

Table 4.1 - Proteins increased in the secretome of endothelial cells after exposure to LOSS compared to HSS after histamine stimulation

Accession	Primary Gene names	Protein names	Databases	Contaminant	LogFC	P Value	FDR
P05062	ALDOB	Fructose-bisphosphate aldolase B	Human	FALSE	1.44	6.65E-05	1.50E-02
P02795	MT2A	Metallothionein-2 (MT-2)	Human	FALSE	2.42	8.14E-04	1.78E-02
P20774	OGN	Mimecan (Osteoglycin)	Human	FALSE	1.87	1.40E-03	1.78E-02
P02771	AFP	Alpha-fetoprotein (Alpha-1-fetoprotein) (Alpha-fetoglobulin)	Human	FALSE	1.97	1.63E-03	1.78E-02
P60174	TPI1	Triosephosphate isomerase (TIM)	Human	FALSE	1.85	1.98E-03	1.78E-02
Q15493	RGN	Regucalcin (RC)	Human	FALSE	2.42	2.26E-03	1.78E-02
P54289	CACNA2D1	Voltage-dependent calcium channel subunit alpha-2/delta-1	Human	FALSE	1.77	2.28E-03	1.78E-02
P00441	SOD1	Superoxide dismutase	Human	TRUE	2.44	3.02E-03	1.78E-02
P55287	CDH11	Cadherin-11 (OSF-4)	Human	FALSE	2.18	3.31E-03	1.78E-02
Q96JB1	DNAH8	Dynein axonemal heavy chain 8	Human	FALSE	2.2	3.95E-03	1.82E-02
P68032	ACTC1	Actin, alpha cardiac muscle 1	Human	FALSE	2.26	4.41E-03	1.82E-02
P60712	ACTB	Actin, cytoplasmic 1	Human;cRFP	TRUE	1.79	4.43E-03	1.82E-02
P55290	CDH13	Cadherin-13 (Heart cadherin)	Human	FALSE	2.33	4.44E-03	1.82E-02
P20908	COL5A1	Collagen alpha-1(V) chain	Human	FALSE	1.99	5.31E-03	1.91E-02
Q13162	PRDX4	Peroxiredoxin-4	Human	TRUE	1.85	5.94E-03	1.91E-02
P41271	NBL1	Neuroblastoma suppressor of tumorigenicity 1 (DAN domain family member 1)	Human	FALSE	1.94	6.14E-03	1.91E-02
P18669	PGAM1	Phosphoglycerate mutase 1	Human	FALSE	1.96	6.53E-03	1.91E-02
Q99983	OMD	Osteomodulin	Human	FALSE	2.04	7.19E-03	1.96E-02
Q06828	FMOD	Fibromodulin (FM)	Human	FALSE	1.54	7.40E-03	1.96E-02
Q99497	PARK7	Parkinson disease protein 7 (Maillard deglycase)	Human	FALSE	1.57	7.66E-03	1.96E-02
P52758	RIDA	2-iminobutanoate/2-iminopropanoate deaminase	Human	FALSE	1.85	8.20E-03	2.04E-02
Q14289	PTK2B	Protein-tyrosine kinase 2-beta	Human	FALSE	1.64	8.23E-03	2.04E-02
P55285	CDH6	Cadherin-6 (Kidney cadherin)	Human	FALSE	2.3	8.79E-03	2.13E-02
Q13163	MAP2K5	Dual specificity mitogen-activated protein kinase kinase 5 (MAP kinase kinase 5)	Human	FALSE	1.7	1.01E-02	2.33E-02

Accession	Primary Gene names	Protein names	Databases	Contaminant	LogFC	P Value	FDR
P09486	SPARC	SPARC (Basement-membrane protein 40)	Human	FALSE	1.78	1.10E-02	2.43E-02
Q14118	DAG1	Dystroglycan 1	Human	FALSE	2.2	1.16E-02	2.53E-02
P04424	ASL	Argininosuccinate lyase (ASAL)	Human	FALSE	1.64	1.19E-02	2.54E-02
P13645	KRT10	Keratin, type I cytoskeletal 10 (Cytokeratin-10)	Human	TRUE	1.67	1.46E-02	2.84E-02
Q9BRA2	TXNDC17	Thioredoxin domain-containing protein 17	Human	FALSE	1.8	1.53E-02	2.92E-02
P36871	PGM1	Phosphoglucomutase-1 (PGM 1)	Human	FALSE	1.76	1.58E-02	2.94E-02
Q02818	NUCB1	Nucleobindin-1 (CALNUC)	Human	FALSE	1.82	1.59E-02	2.94E-02
P13497	BMP1	Bone morphogenetic protein 1 (BMP-1)	Human	FALSE	1.44	2.24E-02	3.84E-02
P63103	YWHAZ	14-3-3 protein zeta/delta (Factor activating exoenzyme S)	Human;cRFP	FALSE	1.1	2.27E-02	3.84E-02
P10599	TXN	Thioredoxin (Trx)	Human	TRUE	2.12	2.38E-02	3.92E-02
P81605	DCD	Dermcidin	Human	FALSE	2.38	2.39E-02	3.92E-02
P35908	KRT2	Keratin, type II cytoskeletal 2 epidermal (Cytokeratin-2e)	Human	TRUE	1.81	2.70E-02	4.31E-02
P04264	KRT1	Keratin, type II cytoskeletal 1 (67 kDa cytokeratin) (Cytokeratin-1)	Human	TRUE	2.5	3.04E-02	4.63E-02
Q9H0W9	C11orf54	Ester hydrolase C11orf54	Human	FALSE	1.05	3.46E-02	5.19E-02
Q8IUL8	CILP2	Cartilage intermediate layer protein 2 (CILP-2)	Human	FALSE	2.59	3.71E-02	5.46E-02
Q14789	GOLGB1	Golgin subfamily B member 1	Human	FALSE	1.77	3.85E-02	5.62E-02
Q99435	NELL2	Protein kinase C-binding protein NELL2 (NEL-like protein 2)	Human	FALSE	1.21	4.03E-02	5.85E-02
O75144	ICOSLG	ICOS ligand (B7 homolog 2)	Human	FALSE	1.08	4.70E-02	6.79E-02
Q14314	FGL2	Fibroleukin (Fibrinogen-like protein 2)	Human	FALSE	3.15	4.81E-02	6.89E-02

Accession = Unique identifier for a sequence record. The Uniprot accession for the Master Protein of the group.
Primary Gene names = the primary gene name associated with the protein (retrieved from the Uniprot accession)
Protein names = the full protein name (retrieved from the Uniprot accession)
Databases = The databases that a master candidate protein was identified in. cRFP = Common Repository of FBS Proteins.
Contaminant = Most samples contain contaminant proteins such as keratins, bovine serum proteins and others that are present as a result of sample processing/handling, rather than being genuinely derived from the sample under analysis. These common contaminant proteins were included in the search to avoid miss-assignment of peptides from these proteins to proteins from the species of interest. All proteins which matched exclusively to the contaminants database have been removed. As a result, proteins which are labelled as contaminants (and could therefore match to both the Contaminants database and the database for the species of interest) should be treated with a degree of caution.
LogFC = Log Fold Change – the difference between the mean Log2 Normalised Protein Abundances for each condition.
FDR = False Discovery Rate – corrected p-value (q-value) of a t-test performed on the Log2 Normalised protein abundances.

4.2.2 Analysis of proteins significantly differentially expressed between LOSS and HSS secretomes after histamine stimulation

To gain an initial understanding of the roles of proteins that were identified in the LOSS secretome, PANTHER pathway analysis was performed. The major biological processes identified included; cellular process, metabolic process, biological regulation and response to stimulus, among others, as shown in Figure 4.4. Further analysis into the pathways these processes recruit, indicated that the major pathway activated was the 'blood coagulation' pathway, as well as 'inflammation mediated by chemokine and cytokine pathway' and 'integrin' and 'cadherin signalling' pathways, among others, as shown in Figure 4.4. A primary role of WPBs is to facilitate inflammation and clotting by secreting proteins that induce these pathways. This indicates that a significant proportion of the proteins found in the LOSS secretome may be inherently linked to WPBs. Further investigation into the protein list was performed to gain a more in-depth insight into the proteins that may contribute to the activation of these pathways, and whether they are WPB contents.

The only protein present in Table 4.1 previously confirmed to be a bona fide WPB cargo is vWF. This identification is not surprising given the extensive research performed in this topic, with vWF release well characterised in response to histamine stimulation. Further experiments in this chapter will elucidate the form in which the vWF strings are secreted using high-resolution microscopy of the vWF strings.

The study by van Breevort D et al. 2012 used proximity proteomics to identify a list of proteins 'likely' to reside in WPBs (van Breevoort *et al.*, 2012). Present in this list, as well as in Table 4.1, was secreted protein acidic and cysteine rich (SPARC) and nucleobindin-1 (NUCB1). Further investigation was performed into the potential role of these proteins in WPB biology, particularly in the context of shear stress.

Secreted protein acidic and rich in cysteine (SPARC) is a matricellular protein playing a role in a range of processes including cell migration, cell proliferation, angiogenesis, tissue repair, tissue morphogenesis and wound healing. SPARC-null mice show delayed healing of excision wounds to defects in cell migration

(Basu *et al.*, 2001). The induction of SPARC expression facilitates angiogenesis in both physiological and pathophysiological conditions, mainly by modulating growth factor activity and the functional modulation of integrin activity utilised by endothelial cells (Rivera, Bradshaw and Brekken, 2011). It has also recently been identified recently as a novel regulator of vascular cell function in primary haemostasis (Veith *et al.*, 2022). These findings suggest an important role in the endothelial cell response to either injury or stress, however no direct link between SPARC and Weibel-Palade bodies has been identified, other than the proximity proteomic screen which identified the protein as a potentially novel WPB cargo (van Breevoort *et al.*, 2012). SPARC was a gene identified in the scRNAseq analysis as upregulated in endothelial cells exposed to disturbed flow (see appendix). The proteomic analysis here also shows that exposure to LOSS followed by histamine stimulation results in an increased presence of the SPARC protein in the secretome of endothelial cells (Table 4.1, Figure 4.3 A). Similarly to clusterin, these findings along with their implication in wound healing, implicates functions in line with that of other WPB cargo. Further work is needed to determine whether SPARC resides in WPBs and whether it's upregulation is a direct result of LOSS.

Nucloebindin-1 (NUCB1) was also identified in the proximity screen as a potentially novel WPB cargo (van Breevoort *et al.*, 2012), and was also identified as upregulated in the secretome of cells exposed to LOSS for 48h followed by histamine stimulation (Figure 4.3 B). The gene encoding the protein was also found to be upregulated in the scRNAseq data analysis performed in this project (see appendix). The exact role of NUCB1 in endothelial cells has not been extensively studied, however, there is some evidence of important functions in endothelial cell biology. It is a small, widely expressed, calcium-binding EF-hand protein that, in most cell-types, has been localised to the Golgi area. It was reported in one study to be localised to the cis-Golgi, mediating matrix metalloproteinase-2 (MMP2) and MT1-MMP trafficking along the Golgi apparatus in a Ca^{2+}-dependent manner (Pacheco-Fernandez *et al.*, 2020). Its cellular location and contribution to trafficking through the Golgi implicates a potential role for NUCB1 in WPB biogenesis. It's upregulated gene expression in disturbed flow in the mouse, accompanied by its increased secretion in response to stimulation after exposure to LOSS (compared to HSS), suggests it is regulated in some way

by shear stress. Further work is required to determine whether NUCB1 is involved in the shear stress regulated changes in observed in WPBs.

In addition to the proteins identified in previous WPB literature as being likely WPB cargo, it is possible to speculate potential novel cargo from this proteomic dataset. As these proteins are secreted in response to histamine stimulation, there is a likelihood some of the proteins in Table 4.1 are stored in WPBs. To determine whether the proteins are likely candidates, it is important to consider several key factors such as the Log fold change, P value, false discovery rate and the strength of supporting literature. Table 4.1 has been presented with descending *p*-value, highlighting the proteins with the most significant change. The protein with the highest Log fold change was Fibroleukin (Fibrinogen-like protein 2) (FGL2) indicating a substantial change in abundance and signifies a potential role in these experimental conditions. FGL2 presents as a likely WPB cargo due to its role in inflammation and coagulation. It a multifunctional immunomodulatory protein that is upregulated in response to viral proteins and immune cytokines. It exists in two forms, membrane-associated FGL2 (mFGL2) that acts as a thrombinase, triggering immunogenic coagulation by cleaving thrombin in the non-classical pathway (Rabizadeh *et al.*, 2015; Fu, Liu and Liu, 2023), and soluble FGL2 (sFGL2) which modulates immune responses to tissue injury, viral infection. These functions are consistent with typical WPB cargo and therefore raise the possibility of FGL2 residing in WPBs.

Metallothionein-2 (MT2A) is a zinc and copper binding protein expressed in endothelial cells and has been shown to play important roles in inflammatory diseases (Wang, Schnoor and Yin, 2023). MT2A expression has been shown to increase in response to thrombin and endothelin-1 in vascular endothelial cells (Kaji *et al.*, 1993). One study showed exposure to increasing concentrations of glucose resulted in a rapid increase in MT2A and ET-1 mRNA expression, as well as MT2A protein expression and translocation to the perinuclear area (Apostolova *et al.*, 2001). It's role in inflammation, links to stress mediated changes in regulation and ET-1 and the cytoplasmic localisation of MT2A indicates it may be a potential WPB cargo. Finally, bone morphogenetic protein-1 (BMP1) was upregulated in the secretome of cells exposed to LOSS with histamine compared to those exposed to HSS with histamine stimulation. There is no evidence that it is a WPB cargo protein however, based on its function and

response here it may be a likely candidate protein. Studies have shown BMPs to play a role in the development of cardiovascular diseases such as atherosclerosis. Increased activity is associated with vascular inflammation and calcification (Morrell *et al.*, 2016). BMP1 in particular has been shown to play a role in angiogenesis, with mRNA levels found to be one of the highest in tumour-associated endothelia compared to normal endothelia (Ge *et al.*, 2007). The literature, coupled with the change in levels shown here, implicate BMP1 as a potential novel WPB cargo.

The proteomic analysis of the endothelial cell secretome after exposure to different flow conditions both before and after histamine stimulation has given a useful insight into the effects of flow. Although there were no detectable differences in the secretome between basal conditions, the large increase in proteins secreted after exposure to LOSS with histamine stimulation, compared to HSS, highlights the drastic effect of this type of flow on the cells. Further work is required to confirm whether any of the proteins identified are definitive WPB cargo, but they do seem to evoke similar functions as many of the other WPB cargoes. There were other proteins present in the list that have been shown to be linked to the endothelial response to shear stress. However, there has been no direct link between any of these proteins and WPBs, and were therefore deemed out of scope for further investigation in this project. The full list will hopefully serve as a useful tool for future research in this area.

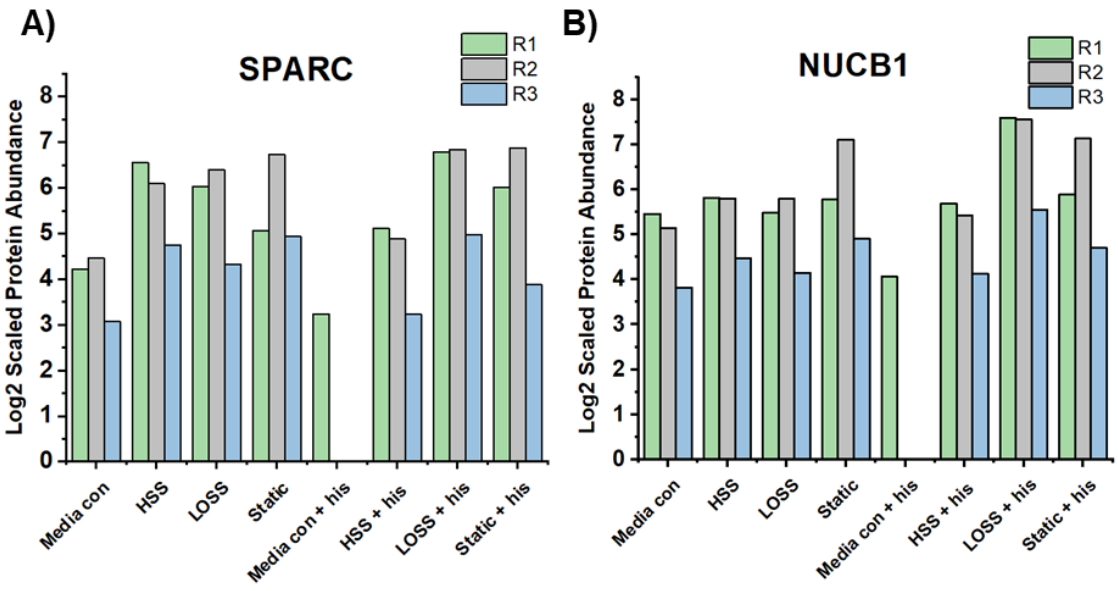

Figure 4.3 – Graphs to show the Log2 scaled abundance for NUCB1 and SPARC across 3 replicates in each flow and stimulated condition.

N = 3 (media control + histamine n=1). Media con = media control. His = histamine.

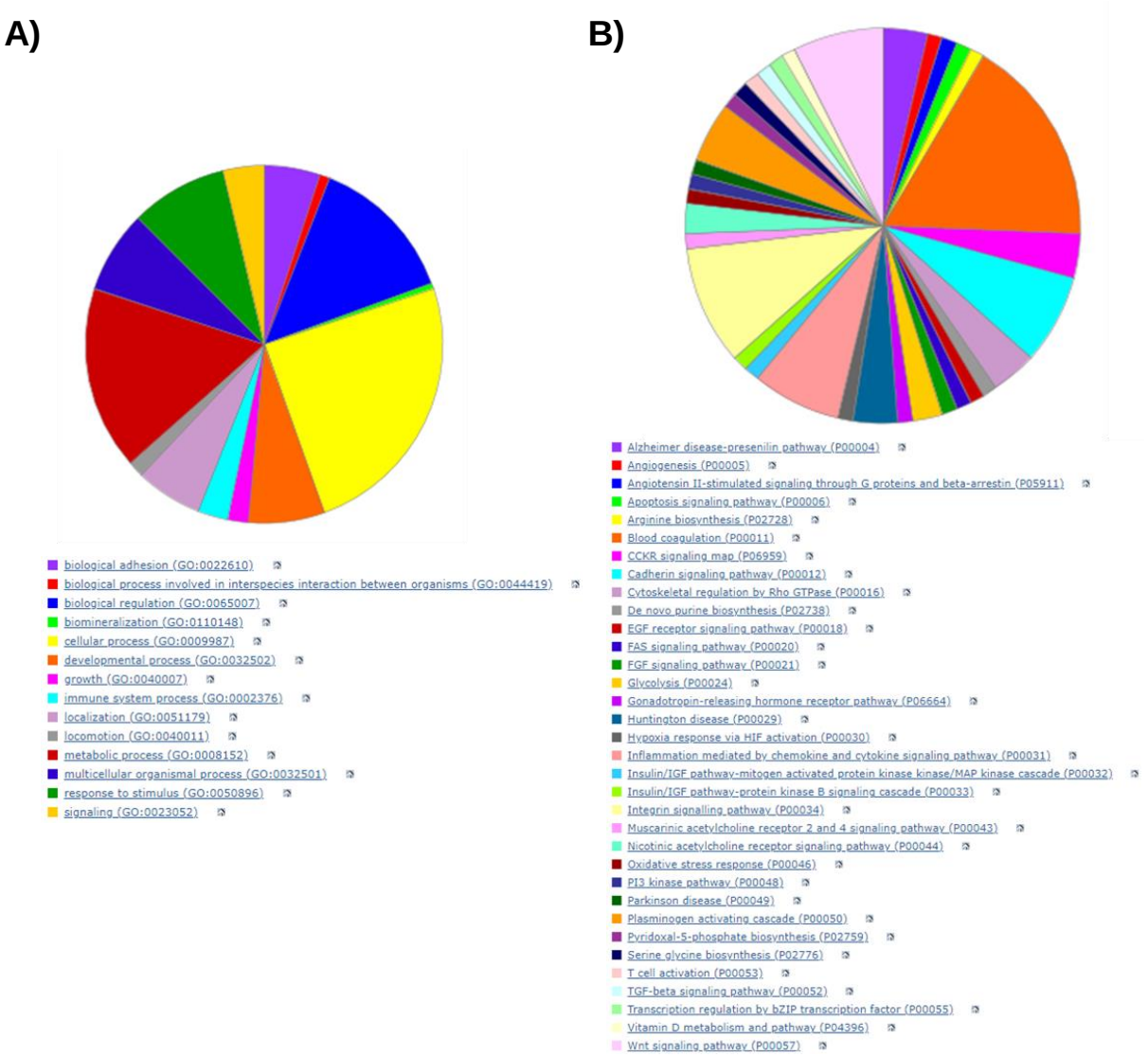

Figure 4.4 – Panther pathway analysis.

Classification of proteins differentially expressed in the secretome of cells exposed to LOSS compared to HSS after histamine stimulation into A) biological processes, and B) biological pathways.

4.3 The effect of flow on WPB Function

Analysis thus far suggests that flow affects the biogenesis of WPBs (size and cargo recruitment) and this impacts secretion. Do these differences impact WPB function? vWF is necessary for WPB biogenesis and, although vWF expression is unchanged by the different flow conditions, the change in WPB size suggests vWF is differentially packed into WPBs and the secretome data indicates LOSS induces increased stimulated vWF secretion. Thereby here, I investigated vWF strings as an indication of vWF function.

4.3.1 vWF Strings

Upon stimulation, WPBs traffic to the cell surface and secrete vWF. Under flow, the vWF uncoils which results in the formation of vWF strings across the endothelial cell surface. There is a positive correlation between vWF string length and WPB length (Ferraro *et al.*, 2016). Moreover, the length of the strings is related to the attraction of platelets. We observed a change in WPB length under different flow conditions and therefore hypothesised that shorter WPBs would result in shorter vWF strings. In this set of experiments, HUVECs were exposed to HSS, LOSS or static conditions for 48 hours before being stimulated with histamine or PMA (positive control) for 10 minutes before fixation and immunofluorescent staining.

Quantification of fluorescent images showed a significant reduction of string length in HUVECs subjected to HSS, and stimulated with histamine, compared to LOSS and static conditions. Static PMA, being a potent endothelial cell activator, was used as a positive control of HUVEC stimulation and subsequent vWF string production. LOSS and static cells stimulated with histamine exhibited strings of similar lengths to the positive control (Figure 4.2). Interestingly, there was no significant change in the number of vWF strings across all conditions.

Figure 4.3a shows the range of string lengths, the majority of vWF strings produced after exposure to HSS and histamine stimulation were approximately 5 - 10 µm in length, compared to the majority of strings produced by HUVECs exposed to LOSS and static residing between 10 – 15 µm. The proportion of vWF strings greater than 50 µm is significantly greater in HUVECs exposed to static and LOSS conditions (689 and 382, respectively), compared to HSS conditions (7). The cumulative frequency graph (Figure 4.3b), highlights the similarity in vWF

string lengths between LOSS, static and static PMA, and the obvious shift in vWF string length in HUVECs exposed to HSS.

The data in this instance validates the original hypothesis, and suggests that HUVECs exposed to HSS are inherently less thrombotic upon stimulation due to a reduction in the average vWF string length, compared to vWF strings secreted by cells exposed to LOSS and static conditions.

A)

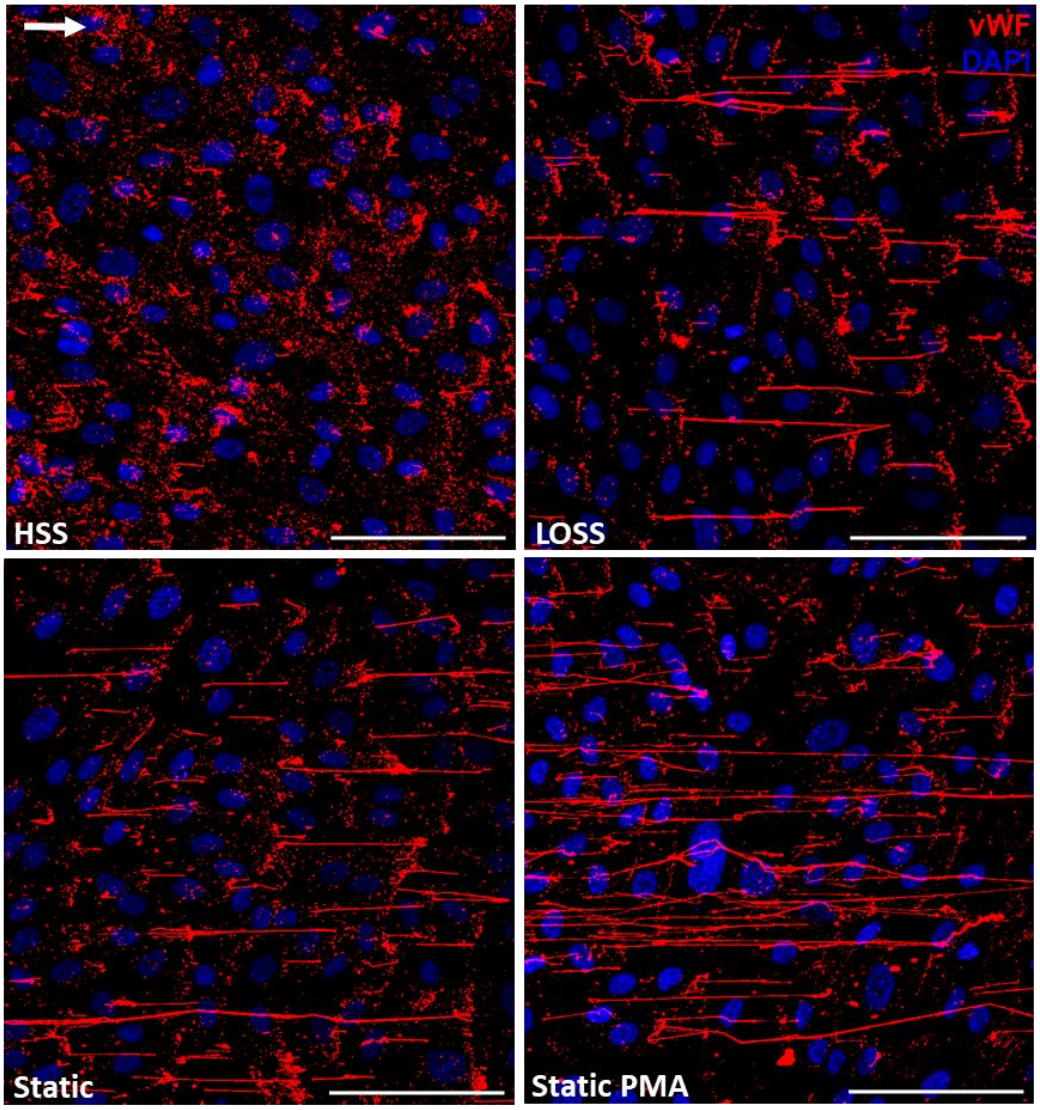
vWF
DAPI
HSS
LOSS
Static
Static PMA

B)

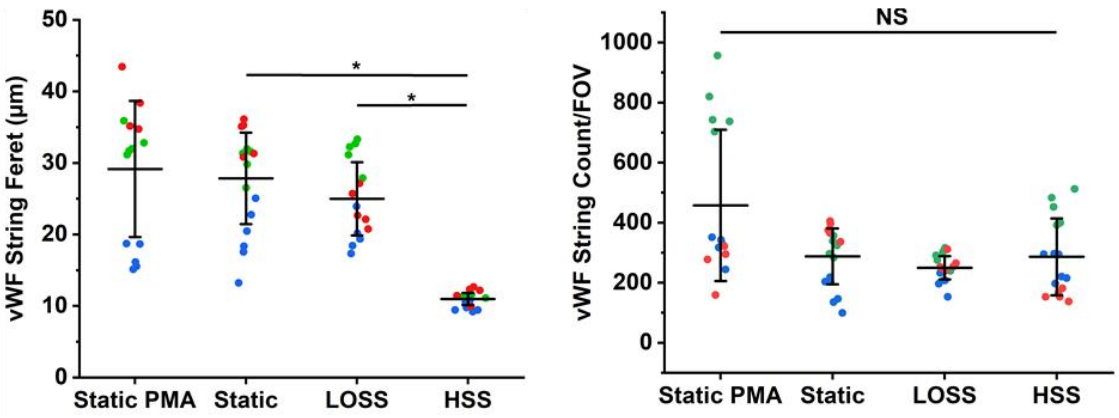
vWF String Feret (µm)
50
40
30
20
10
0
*
*
Static PMA
Static
LOSS
HSS
vWF String Count/FOV
1000
800
600
400
200
0
NS
Static PMA
Static
LOSS
HSS

Figure 4.5 – vWF string length is affected by pre-treatment with shear stress.

A) Representative images (x20 objective, 2x2 tile scan) of vWF strings (red) from HUVECs after 10 minute histamine (or PMA where stated) stimulation after 48h exposure to each flow condition. Scale bar = 100 µm. B) Super plots show mean length of vWF strings and the number of vWF strings per FOV ± SEM in each condition, $n = 3$. Each data point represents the mean value calculated from one image (5 images per condition, per repeat). Each colour represents a separate repeat. * $p < 0.05$ by t-test.

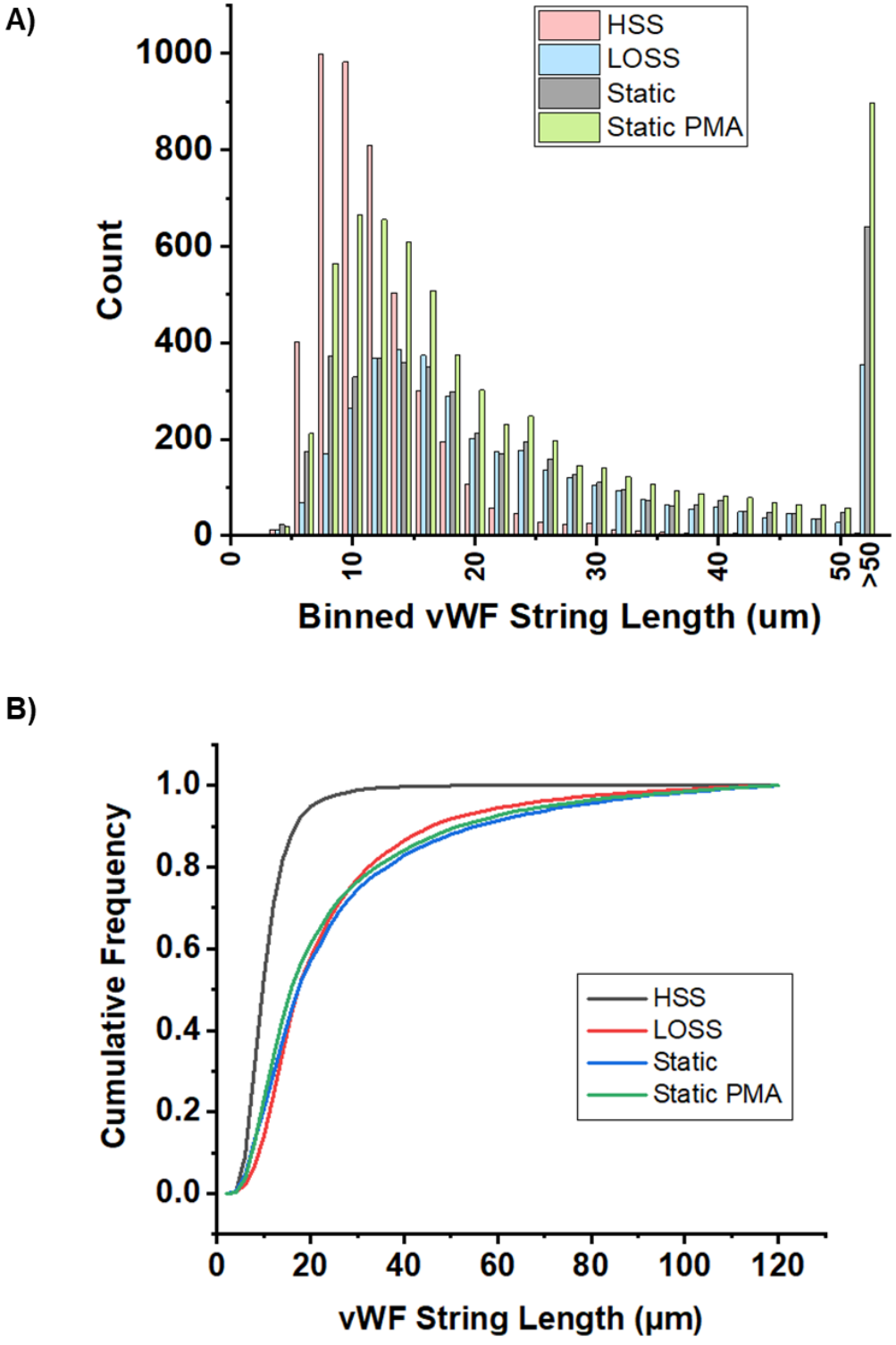

Figure 4.6 - Histogram and Cumulative Frequency graph to show that vWF string length is affected by pre-treatment with shear stress.

A) Histogram shows the distribution of vWF string lengths from 0 to >50 µM. B) Cumulative frequency graph to show the shift in vWF string length after exposure to different flow conditions.

4.4 Summary

This chapter investigated the impact of flow on endothelial cell secretome and function. A proteomic screen was used to analyse the WPB secretome after exposure of HUVEC to HSS, LOSS and static conditions, with and without histamine stimulation.

A significant increase was observed in the abundance of proteins in the secretome of HUVECs pre-exposed to 48h LOSS followed by histamine stimulation, compared to those pre-exposed to HSS and static conditions with the same histamine stimulation. This indicates LOSS results in cells that secrete more protein. Further investigation into this secretome was performed and highlighted a number of pro-inflammatory and pro-thrombotic mediators, most of which however, are yet to be confirmed as WPB cargo. SPARC and Nucleobindin-1 (NUCB1) are 2 proteins previously identified in proximity proteomics as potentially novel WPB contents (van Breevoort *et al.*, 2012), and were all upregulated in the secretome of cells exposed to LOSS with histamine stimulation. These proteins all serve similar functions to WPBs in wound healing, angiogenesis or Golgi transportation. It would therefore not be surprising if any of these proteins were confirmed to be WPB cargoes, however further work is required to confirm this and draw any definitive conclusions.

The primary function of WPBs is to exocytose vWF in the form of strings on the surface of endothelial cells. VWF strings contribute to haemostasis by capturing platelets at sites of vascular injury, facilitating their adhesion, activation, and aggregation. Previous studies have shown vWF string length is proportional to WPB length, however whether this effect was observed as a result of flow induced WPB changes, was not known. LOSS and static conditions induced a significant increase in vWF string length after histamine stimulation, compared to HSS. This indicates an increased function of vWF in regions of the vasculature exposed to LOSS, and areas of cells that are pro-thrombotic compared to cells exposed to HSS. Experiments are currently being performed in the McKeown lab to determine whether the number of platelets adhered to the endothelial cells is decreased as a result of this.

Chapter 5 – Mechanisms of flow mediated changes in WPBs

5.1 Introduction

Previous chapters have identified changes to the morphology and function of WPBs under different flow conditions. The mechanisms by which these changes occur are not well understood. The aim of this chapter is to investigate the potential mechanisms by which these changes occur, investigating Golgi morphology in response to flow, in addition to harnessing Yoda1, a compound that activates Piezo1, to determine whether the process by which cells detect and convert mechanical stimuli into cellular responses, could modulate WPBs.

5.2 Golgi Morphology

Exposure of HUVECs to flow resulted in a population of shorter WPBs, as described in chapter 3. Previous research has shown that the morphology of the Golgi regulates the packaging of vWF 'quanta' into nascent WPBs, where quanta represents a bolus of multimerised vWF (Ferraro *et al.*, 2014). The number of vWF quanta packaged into a nascent WPB is positively correlated with the length of vWF strings formed on the endothelial cell surface upon stimulation (as shown in section 4.3.1 and in previous research (Ferraro *et al.*, 2016)). vWF function is therefore dependent on WPB size. Whether the changes in WPBs seen as a result of shear stress are a result of altered Golgi morphology are not currently known. Golgi apparatus that has become fragmented by addition of statins or nocodazole (Ferraro *et al.*, 2016) does not have the ability to co-package multiple vWF quanta in a single WPB, resulting in shorter WPBs being produced. Ribbon-like Golgi structures however, form longer WPBs that can produce longer vWF strings on the endothelial surface, increasing their function. Binned WPB length analysis under shear stress showed distinct WPBs lengths at defined intervals, indicating that the change in WPB length shown here could be a result of altered Golgi morphology and packaging of vWF quanta (Figure 3.7, Figure 3.8)

To determine whether flow impacts Golgi morphology and thereby could be a mechanism underlying the changes we observe in WPB size, HUVECs were exposed to the previously described flow conditions (i.e. 48h exposure to either HSS, LOSS or static conditions). The Golgi was tagged with anti-GM130

antibody, immunofluorescently labelled and fragmentation quantified. We hypothesised that the Golgi apparatus morphology is more fragmented in HUVECs exposed to HSS. In addition, we hypothesised that the Golgi morphology in HUVECs exposed to LOSS and static conditions would remain relatively intact and non-fragmented (ribbon-like).

Representative images (Figure 5.1a) indicate that the Golgi apparatus appears elongated in HUVECs exposed to HSS. This elongation appears to result in moderate fragmentation of the Golgi, with distinct individual cisternae observed. This fragmentation is particularly apparent in cells highly aligned with the direction of flow. HUVECs exposed to LOSS and static conditions appear to have relatively compact Golgi on one side of the nucleus, with far fewer distinct Golgi cisternae. The fragmentation of the Golgi was quantified using an ImageJ macro (see appendix). The number of (red) objects per cell as a measure of Golgi fragments, is significantly increased in HUVECs exposed to HSS compared to LOSS (Figure 5.1b). Static conditions displayed high variability in this data, with numerous outliers present. Consequently, the statistical test was conducted between only two groups: HSS and LOSS. Further investigation into the mean area of each of these objects shows a tendency for these objects to have a smaller area (Figure 5.1c), consistent with individual cisternae being separated. This finding was however not significant across the 3 conditions.

In conclusion, HSS induced increased Golgi fragmentation compared to LOSS and static conditions. Therefore, the hypothesis was accepted.

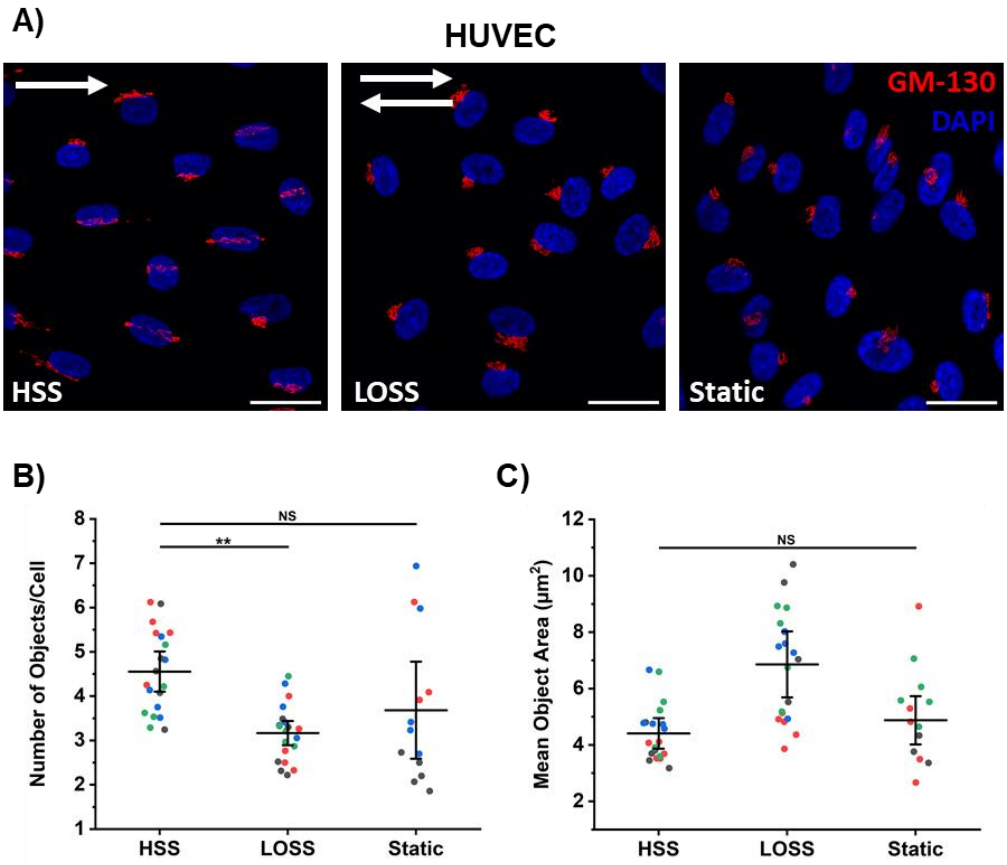

Figure 5.1 - HSS causes increased Golgi Fragmentation compared to LOSS. A) Representative images (x60 objective) of Golgi apparatus (red) in HUVECs from each flow condition. Scale bar = 30 µm. B) Super plot to show mean number of Golgi objects identified per cell ± SEM in each condition, *n* = 3/4. Each data point represents the mean value calculated from one image (10 images per condition, per repeat). Each colour represents a separate repeat. ** $p < 0.01$, NS = not significant by unpaired t-test. C) Super plot to show the mean area of these objects ± SEM in each condition, *n* = 3/4. NS = not significant by Mann-Whitney U Test.

5.3 Chemical activation of Piezo1 and WPB morphology

Piezo1 is a transmembrane protein that functions as a mechanosensitive ion channel, meaning it can respond to mechanical forces, such as shear stress and stretch, by converting this stimuli to cellular processes and functions (Coste *et al.*, 2010; Li *et al.*, 2014). It resides in the plasma membrane of endothelial cells and acts as a sensor of shear stress, resulting in downstream signalling events and the induction of cell alignment (Li *et al.*, 2014). Yoda1 is a small molecule compound that binds to and activates mechanically sensitive ion channel Piezo1 (Syeda *et al.*, 2015; Evans *et al.*, 2018). It rapidly causes Ca^{2+} entry and mimics fluid shear stress induced endothelial activation by initiating AKT and eNOS phosphorylation (Wang *et al.*, 2016). In this instance, we are interested in whether Piezo1 activation using Yoda1, induces similar changes to WPBs that are observed in HSS. This will indicate potential pathways for the mechanism of action, as well as provide a potential model system for the investigation of WPBs under conditions that mimic laminar flow, without the need for any flow apparatus.

5.3.1 Tolerance of Yoda1 in HUVECs

Firstly, an initial experiment was performed to determine the concentration of Yoda1 that could be tolerated by HUVECs in static conditions for 24 hours. Images acquired on the IncuCyte ZOOM imaging software shows that Yoda1 was well-tolerated at concentrations up to and including 1 µM (Figure 5.2). Upon increased Yoda1 concentration to 2 µM, HUVECs exhibited signs of detachment and the subsequent reduction of cell numbers on the slide, with very few cells remaining within the field of view. Consequently, all further experiments involving Yoda1 on static HUVECs utilised concentrations up to and including 1 µM Yoda1.

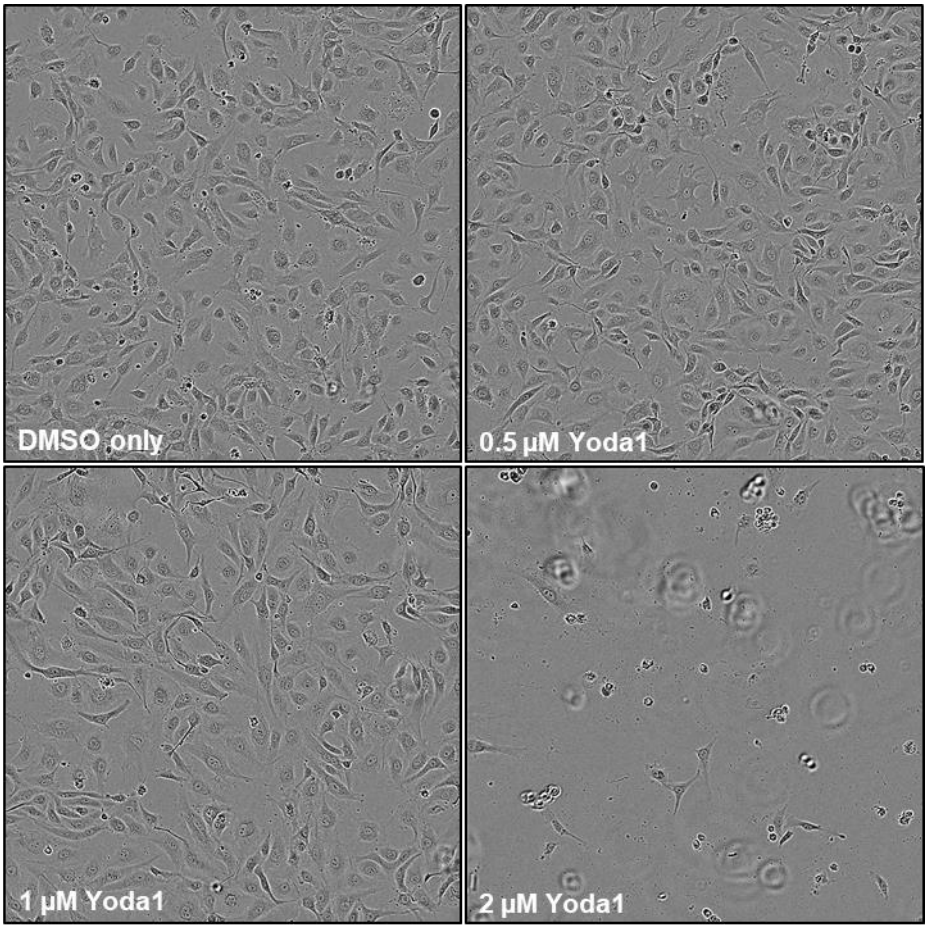

Figure 5.2 – 2 µM Yoda1 results in detachment and a decrease in HUVEC number when cultured under static conditions for 24 hours.

Representative images of HUVECs exposed to different concentrations of Yoda1 for 24 hours in static conditions. Images captured using the IncuCyte ZOOM, $n = 1$.

5.3.2 Yoda1 results in shorter WPBs

An analogue screen was performed using Yoda1, Dooku1 (Yoda1 antagonist, Evans, et al. 2018), compound 2a (inactive Yoda1, Evans, et al. 2018) and DMSO only, to determine their effect on WPB size and number in HUVECs under static conditions for 24 hours. We hypothesised that the addition of Yoda1 would mimic the effects of HSS and result in a population of shorter WPBs. Initially, two repeats were performed in which all 3 compounds were added to HUVECs and WPBs size and number was quantified using the ImageJ macro described previously (see appendix). Initial observations of the representative images and with quantification, indicated that the mean WPB length was shorter in HUVECs subjected to Yoda1 (1 µM), compared to DMSO only. This was accompanied by no change in WPB length in HUVECs exposed to Dooku1 (1 µM) or compound 2a (1 µM), after 2 repeats (Figure 5.3a and b). WPB number per field of view did not change all treatments (Figure 5.3c).

The hypothesis could not be accepted at this stage, due to only 2 repeats being performed. However, these initial changes observed in WPB length gave an indication that Yoda1 may modulate WPBs. This initial screen led to further observations of concentration and time dependency of the compounds, and introduction of a pre-incubation step with the Yoda1-evoked Piezo1 antagonist, Dooku1, and an inactive Yoda1 analogue, compound 2a. Dooku1 should antagonise any changes observed in WPB length, if the changes are a result of Yoda1-evoked Piezo1 channel activation. Compound 2a has a very similar structure to Yoda1, with both chlorine atoms being replaced by fluorine atoms. The chlorine atoms are however essential for Yoda1 activity (Evans *et al.*, 2018), and compound 2a is therefore deemed as an inactive Yoda1 analogue and can be used to show whether any effects observed are a result of Yoda1, and not a similar structured molecules.

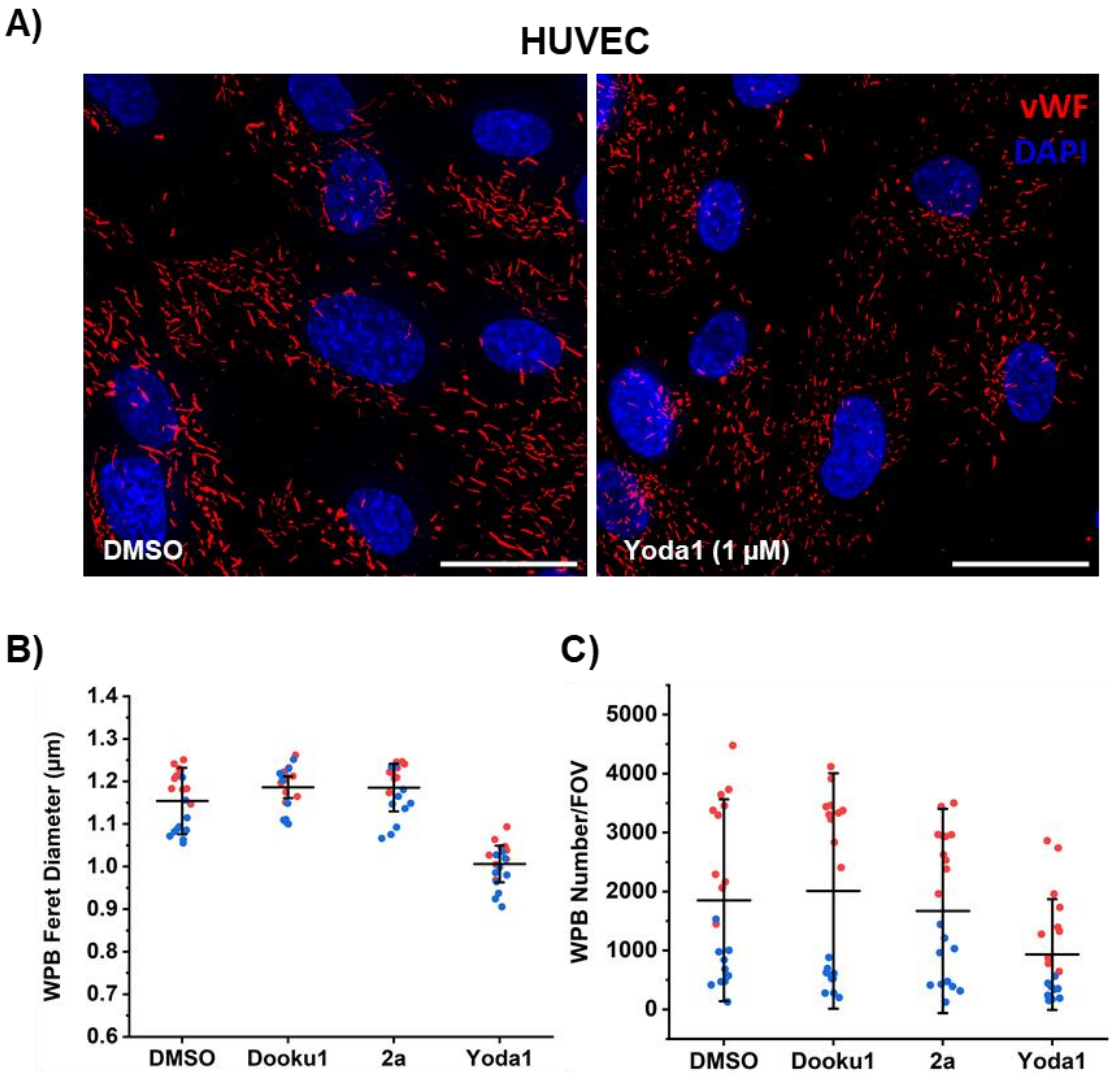

Figure 5.3 – Exposure to Yoda1 appears to result in shorter WPBs in HUVECs.

A) Representative images (x60 objective) of WPBs (red) in HUVECs exposed to DMSO only and Yoda1 (1 µM) in static conditions for 24h. Scale bar = 30 µm. B) Super plot to show mean WPB length ± SEM DMSO only, Dooku1 (1 µM), compound 2a (1 µM) and Yoda1 (1 µM), *n* = 2. Each data point represents the mean WPB length from one image (10 images per condition, per repeat). Each colour represents a separate repeat. C) Super plot to show mean WPB number per field of view (FOV) ± SEM in the same conditions, *n* = 2.

5.3.3 Yoda1 results in decreased WPB length after 24h, and is not affected by the presence of Dooku1

The next set of experiments involved multiple conditions and variables. The first variable was the length of time required to observe significant changes in WPB size from relatively short term time points (5 mins, 30 mins and 2 hours), to a longer term time point (24 hours). The same conditions were repeated in this experiment as shown in Figure 5.3, however, additional experiments were performed using a preincubation step with either Dooku1 (10 µM), compound 2a (10 µM) or DMSO for 10 mins, followed by the addition of Yoda1 in the presence of these compounds. The hypothesis of this experiment was that Yoda1 would lead to decreased WPB size after 24h, and that this effect would inhibited by the preincubation and presence of Yoda1 antagonist, Dooku1, in the media. Compound 2a and DMSO would have no effect of WPB size.

In the shorter time points, WPB size did not change significantly across all conditions (Figure 5.4). Changes were only observed after 24 hours, with Yoda1 (1µM) inducing a significant reduction in WPB size compared to DMSO only. In addition, preincubation with compound 2a, Dooku1 and DMSO had no effect on the change in WPB size after the addition of Yoda1. Additionally, compound 2a (the inactive compound of Yoda1), acted similarly to the DMSO only control in terms of WPB size, and was therefore also significantly different to the response from HUVECs with Yoda1 (1 µM) added, both with and without preincubation.

WPB number did not change across all conditions and across all 4 time-points in this set of analysis (Figure 5.6).

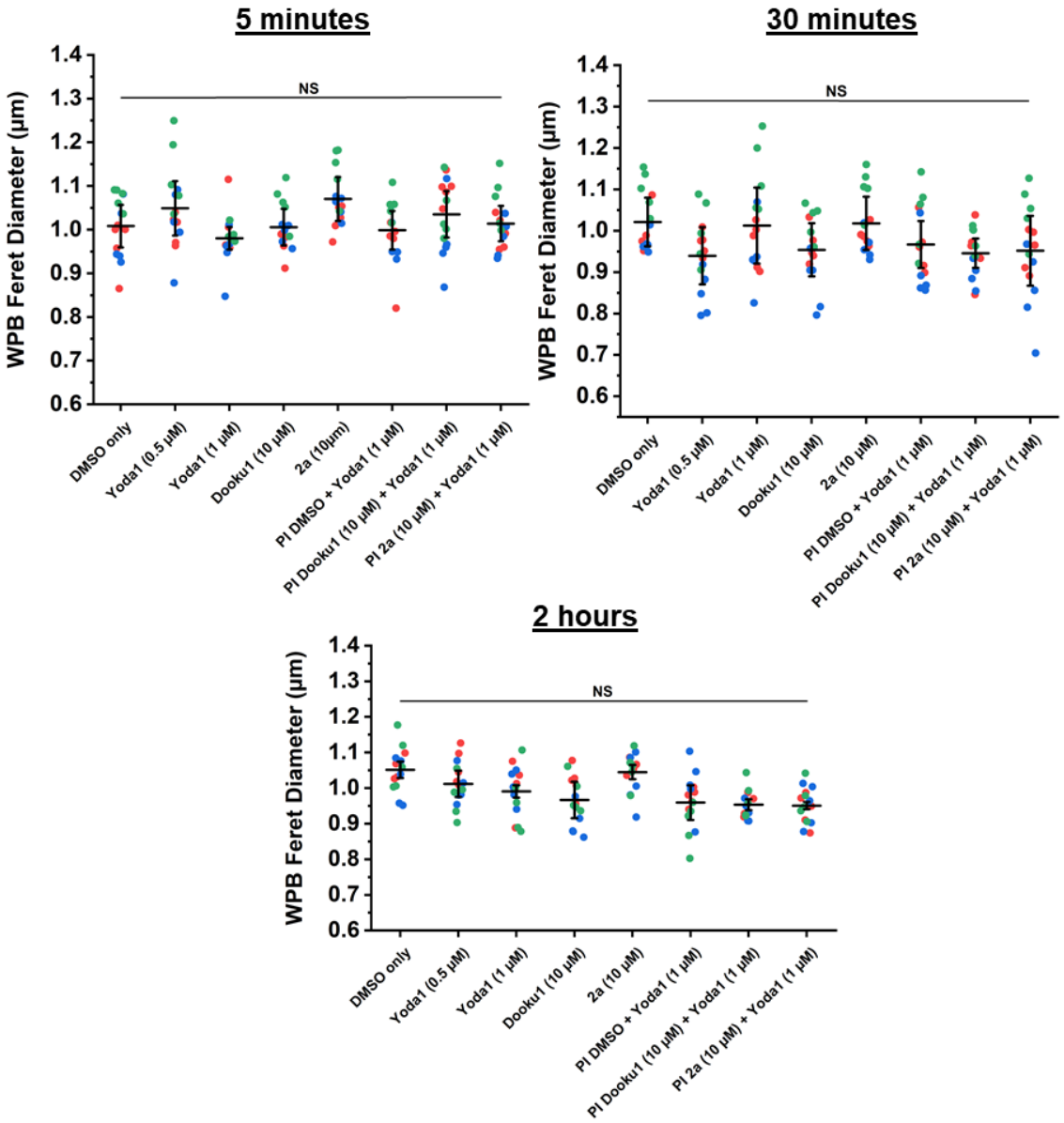

Figure 5.4 - Exposure to Yoda1 and related compounds for up to 2 hours does not affect WPB length.

Super plots show the effect of the different compounds on the mean (± SEM) WPB length at 3 different time points: 5 minutes, 30 minutes and 2 hours. Each data point represents the mean value calculated from one image (5 images per condition, per repeat). Each colour represents a separate repeat. *n* = 3, NS = not significant by Kruskal Wallis test.

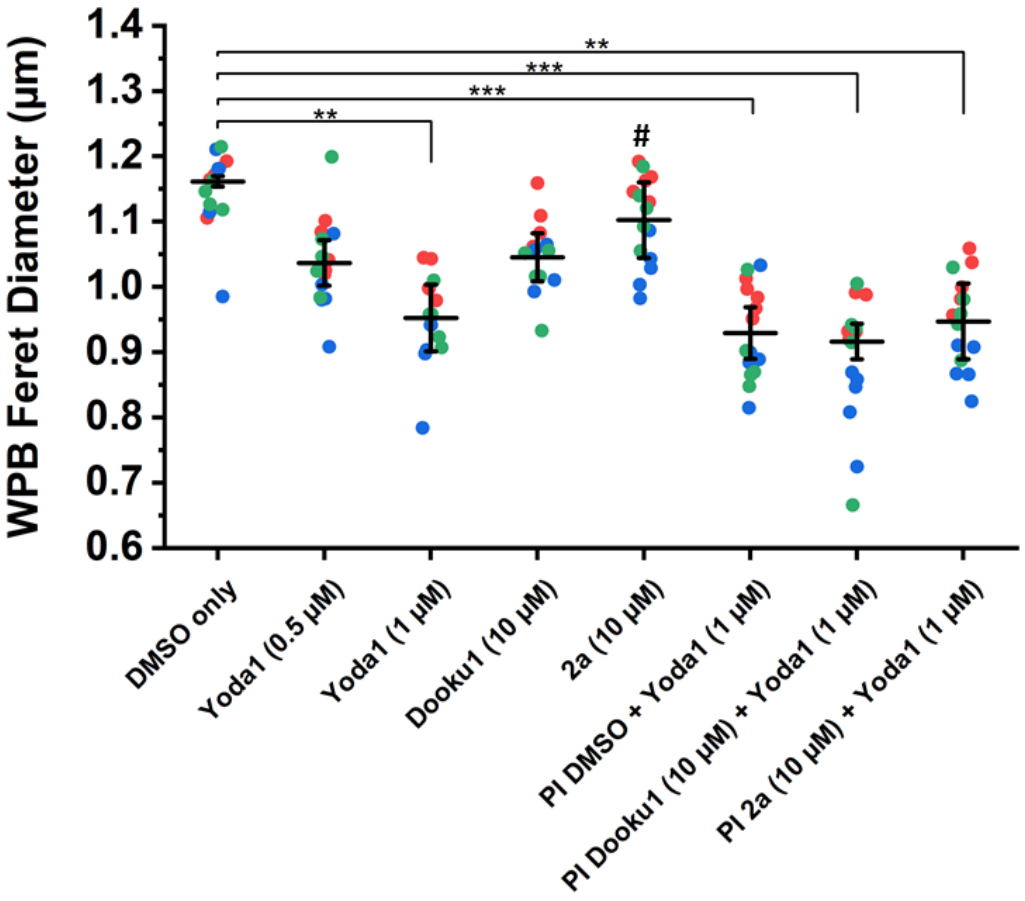

Figure 5.5 - Exposure to Yoda1 for 24h results in a population of shorter WPBs, despite pre-incubation with Yoda1 antagonist, Dooku1.

Super plot shows the effect of the different compounds on the mean (± SEM) WPB length at 24 hours. Each data point represents the mean value calculated from one image (5 images per condition, per repeat). Each colour represents a separate repeat. n = 3, ** p < 0.01, *** p < 0.001 by One-Way ANOVA with Bonferroni post-hoc test. # = Yoda1 also resulted in a population of shorter WPBs compared to compound 2a only. 2a – Yoda1 (* p = 0.048), 2a – PI DMSO + Yoda1 (* p = 0.014), 2a – PI Dooku1 + Yoda1 (** p = 0.0072), 2a - PI 2a + Yoda1 (* p = 0.036). PI = Pre-incubation.

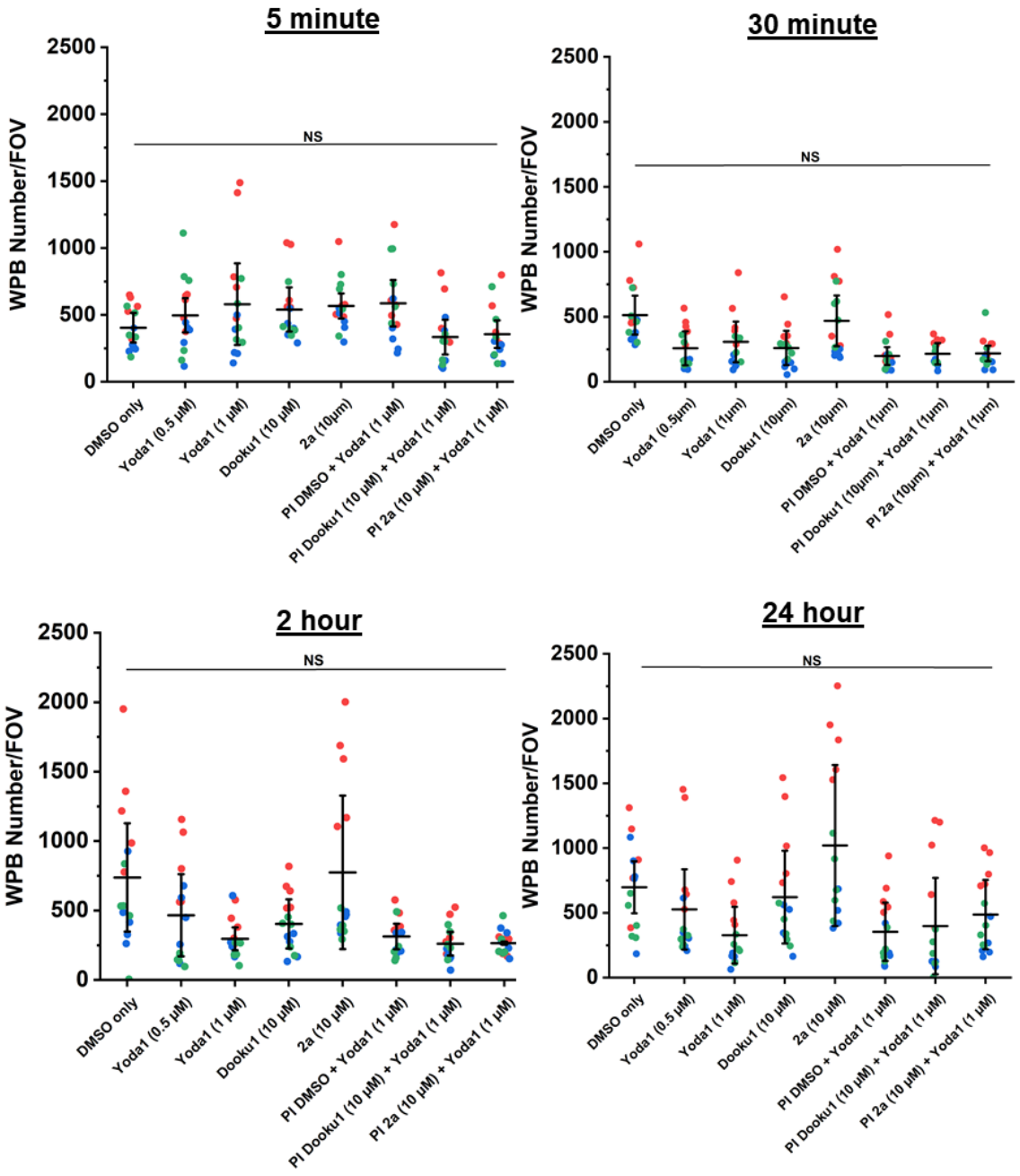

Figure 5.6 – Exposure to Yoda1 and related compounds for up to 24 hours does not affect WPB number.

Super plots show the effect of the different compounds on the mean (± SEM) WPB length at 4 different time points: 5 minutes, 30 minutes, 2 hours and 24 hours. Each data point represents the mean value calculated from one image (5 images per condition, per repeat). Each colour represents a separate repeat. *n* = 3, NS = not significant by Kruskal Wallis test.

5.4 Summary

This chapter aimed to investigate some potential mechanisms that underlie the changes observed in WPB morphology, and the resulting function. Extensive research has been performed previously based on the role of the Golgi apparatus in WPB biogenesis. The Cutler lab has shown that inducing Golgi ribbon ablation through pharmacological interventions, such as nocodazole and statins, leads to the formation of a population of mini-WPBs. We have observed comparable effects, albeit of lesser magnitude, under defined *in vitro* flow conditions.

The Golgi in HUVECs subjected to HSS was significantly more fragmented compared to the Golgi in endothelial cells subjected to LOSS and static conditions. This indicates a potential mechanism for the reduction in WPB length observed in endothelial cells exposed to HSS, however further work will be required to determine whether this is a direct effect, or whether there are other contributing factors.

Endothelial cells rely on mechanosensors in the plasma membrane to sense shear stress. One of those mechanosensors is Piezo1, an ion channel that primarily allows the influx of cations, particularly Ca^{2+} ions, in response to stimuli. We proposed that Yoda1 activation of Piezo1 in static conditions would mimic the effect of HSS and therefore result in shorter WPBs. Indeed, Yoda1-evoked Piezo1 activation for 24 hours resulted in a population of shorter WPBs. This indicates that HSS induced changes in WPB length can be replicated with Yoda1-evoked activation of Piezo1, a useful tool for the study of WPBs without the use of complex flow equipment. It also provides a starting point for investigation into the mechanism of action underlying the Piezo1 activated change in WPB length. Is it related to the morphology of the Golgi, or an independent mechanism?

Chapter 6 – Discussion

The Ibidi pump system serves as a robust *in vitro* method for exploring shear stress effects on WPBs in both HUVECs and HAECs. High shear stress (HSS) induces shorter WPBs compared to low oscillatory shear stress (LOSS) and static conditions, with no change in WPB numbers. Examination of mouse aorta reveals vWF immunofluorescent staining differences between aligned and non-aligned cells, consistent with findings observed *in vitro*. Single-cell RNA sequencing identifies differential expression of WPB cargo and associated genes under disturbed and laminar flow. Proteomic analysis uncovers potentially novel WPB cargoes in cells exposed to LOSS with histamine stimulation. Notably, Golgi apparatus fragmentation is higher under HSS, and Yoda1-induced Piezo1 activation results in shorter WPBs after 24 hours.

6.1 In vitro shear stress modelling

Blood flow within the vasculature is complex and varies significantly depending on the architecture of the vessel and the anatomical location. It is constantly changing direction, velocity and viscosity, presenting as a highly dynamic fluid capable of withstanding both high and low pressure, as well as varying rates of shear stress. This dynamic nature poses a considerable challenge when attempting to replicate blood flow accurately *in vitro*.

Shear stress can be modelled using various *in vitro* methods, and the selection of any particular method depends on several factors. These include the required duration of shear stress, the rate at which it needs to be applied, the necessary throughput of the experiment, and the specific downstream application of analysis required.

6.1.1 Ibidi Pump system

The Ibidi pump system stands out for its capability to facilitate extended applications of shear stress while providing precise control over the rate, rendering it particularly well-suited for longer-term flow experiments. Furthermore, the Ibidi slides are designed to be used for high-resolution fluorescent imaging applications. In the context of my project, I planned to investigate changes to WPBs after prolonged flow exposure i.e. up to 72h, with specific shear stress rates. Analysis would be performed using high-resolution

microscopy on fixed cells. Considering all these requirements, the Ibidi pump system was deemed the most suitable for use in this project.

Following optimisation of the Ibidi pump system (detailed in chapter 3 section 3.1), the method proved to be robust and reproducible, but not without its disadvantages. Firstly, the method was relatively low throughput due to the restricted number of available Ibidi pumps. Typically, each pump can apply a distinct flow rate to a single slide, limiting the number of slides that can be used when employing different flow rates within a single experiment. The method therefore becomes time consuming when generating biological replicates. Furthermore, the limited surface area for cells on the channel slides restricts the downstream applications available, such as Western blot and RT-qPCR. Combining cells from multiple slides is necessary to extract sufficient protein for these applications. Consequently, while the Ibidi pump system excels in its fluorescent imaging applications, its practicality for other analytical applications is somewhat limited.

A key finding during the optimisation of this method was the substantial impact of channel height on cellular response, despite applying the same theoretical shear stress. Initial flow experiments conducted using the Ibidi 0.8 channel (0.8 mm channel height) at 10 dyn/cm^2 revealed a lack of uniform alignment with the direction of flow. Despite adjustments in confluency, attachment time and the flow duration, uniform cell alignment was not achieved. Transitioning to Ibidi slides with a reduced channel height of 0.4 mm whilst maintaining the same shear stress, resulted in uniform alignment of HUVECs with the direction of flow. This finding highlights that, although the specific rate of shear stress is important when studying flow in vitro, other factors such as pressure and shear rate significantly influence the response to flow. As a result, acknowledging and recording these additional factors becomes crucial for understanding the overall cellular response to flow.

6.1.2 Alternative shear stress models

Alternative in vitro methods for applying shear stress offer their own advantages. Rotational methods, such as the orbital shaker or the cone-and-plate method, involve culturing cells on a circular plate and subjecting them to rotational flow. This results in cells on the outer edge of the plate experiencing higher and more

uniform flow, while those closer to the centre of the plate encounter lower and less uniform flow. While this method proves beneficial for downstream applications requiring a larger number of cells, such as Western blotting, it does compromise precise control over shear stress rates applied due to the inherent gradient of shear rates applied across the plate's diameter. Additionally, the plates used for this method are not optimised for fluorescent microscopy, limiting the range of techniques that can be performed downstream of the flow application. Ultimately, an approach involving a combination of multiple shear stress models will achieve the most robust and reproducible data.

6.1.3 HUVECs and HAECs as cell models

The use of Human Umbilical Vein Endothelial Cells (HUVECs) as a model for studying endothelial cells response to shear stress presents both advantages and disadvantages. Firstly, HUVECs are advantageous due to their consistently high population of WPBs, rendering them an excellent model for investigating WPBs. Additionally, they are readily available, exhibit favourable growth characteristics in cell culture and demonstrate robust and reproducible responses to various physiological and pathological stimuli. They do however have a limited lifespan in culture. Senescence increases with each passage, leading to phenotypic variation and variable responses to stimuli. To counteract these effects, experiments were only performed on endothelial cells up to a certain passage number (P7).

Furthermore, HUVECs originate from umbilical vein, where they typically encounter shear stress rates of < 5 dyn/cm^2 (Taylor, 1975; Papaioannou *et al.*, 2006). These shear rates are comparatively lower than those experienced by arterial endothelial cells. Consequently, HUVECs are limited in their representation for all endothelial cells across different tissues and vascular beds, particularly arterial cells that encounter significantly higher shear stress rates. To address this, experiments assessing cell alignment to flow and KLF2 mRNA expression were performed on HUVECs exposed to higher shear stress rates, and their responses were found to align with expectations of arterial endothelial cells. As a result, HUVECs were deemed a suitable model for the study of shear stress and Weibel-Palade bodies.

To further explore the effects of shear stress on WPBs, and to address some of the potential limitations listed above, the experiments were repeated with Human Aortic Endothelial Cells (HAECs) obtained from the ascending and descending aorta of a single donor. These cells experience the high shear stress rates of the aorta and are also the most likely cells to be effected by cardiovascular disease, making them an excellent representative cell population for use in this project. Experimentally, these cells exhibited similar responses to HUVECs in their alignment to the flow direction and observations in WPB size. The extraction of these cells from only a single donor highlights the need to recognise the potential donor variability. This emphasises the importance of incorporating multiple donors in future experiments to ensure changes are observed consistently across donors. Nonetheless, the response of HAECs to HSS reinforces their suitability for studying shear stress and its effect on WPBs, and corroborates findings observed in HUVECs.

6.1.4 Method of quantifying WPBs

The abundance of WPBs in endothelial cells demands a level of automation for efficient detection and quantification of their number and morphology. Previous research in the McKeown lab (Miteva *et al.*, 2019), utilised an ImageJ macro (see appendix) to process raw fluorescent microscopy images for WPB quantification. The same approach was used here, albeit with some modifications to account for a different experimental setup and microscope being used. This method of quantification has proven to be robust, unbiased and effective for observing the effect of shear stress on WPBs. There is however, always room for improvement. A recent study by Laan et al., (2023) utilised the image analysis software, CellProfiler, to automate the segmentation and quantitative analysis of WPB morphology, localisation and content. The benefit of using this software is that it can identify other cellular structures such as the nucleus, the cell membrane, and other organelles, as part of the same analysis workflow. This facilitates more analysis such as distribution from the nucleus, and number of WPBs per cell, without the need for separate analysis workflows, ultimately leading to more efficient analysis (Laan *et al.*, 2023).

An additional piece of software used in the study by Laan et al., (2023) was the ‘OrganelleContentProfiler’, offering a method to measure secondary proteins of interest within, on, or outside of a specific organelle, such as a WPB. This feature

is particularly useful when studying WPBs, as it enables the detection of WPB content changes under different conditions. Given that previous research has shown changes in the coat proteins of WPBs, this analytical approach enables the quantification of such changes, contributing to a more in depth understanding of how different conditions affect WPBs.

In conclusion, the utilisation of advanced image analysis software, such as CellProfiler and OrganelleContentProfiler, presents a promising direction for WPB analysis. These approaches not only enhance the efficiency of the analysis, but also facilitate a more comprehensive analysis workflow. Future research should strongly consider using these platforms for analysing cellular organelles, such as WPBs.

6.2 The effect of shear stress on WPB biogenesis and function

vWF availability drives both the success and rate of WPB biogenesis in endothelial cells. It undergoes rounds of dimerization, multimerisation and tubulation before forming nascent WPBs (Hannah *et al.*, 2002). WPB size is dependent on the number of individual vWF quanta (0.5 µm) that are co-packaged into emerging WPBs at the TGN. From this point onwards, additional WPB cargo and membrane proteins are recruited at various stages. The initial experiments of this project aimed to determine whether shear stress affected the vWF synthesis/availability, and whether this had any effect on WPB biogenesis, cargo and function.

6.2.1 WPB Biogenesis

VWF mRNA expression is unaffected by different flow and static conditions, indicating that vWF synthesis and availability remains constant. In line with this finding, the number of WPBs did not appear to change in the different conditions. Numerous studies have highlighted how conditions such as shear stress influence variations in vWF expression levels (Aird *et al.*, 1997), with varying findings based on the model system and types of stimulus or condition. Slightly more recent *in vitro* studies have shown a 2.4-fold increase in vWF mRNA expression after prolonged (7 day) exposure to high pulsatile flow (12 ± 7 dyn/cm^2) compared to static conditions (Dekker *et al.*, 2002), as well as a 1.84-fold increase in endogenous vWF mRNA expression after exposure to HSS (15 dyn/cm^2) for 26 hours (Hough *et al.*, 2008). Studies in rat aortic endothelial cells

and porcine intima identified differential expression of vWF in distinct endothelial populations based on whether they were exposed to laminar or disturbed flow, with the latter exhibiting more elaborate and homogenous vWF staining compared to the heterogeneous staining pattern observed in endothelial cells exposed to laminar flow (Rand *et al.*, 1987; Senis *et al.*, 1996b). In this project, vWF staining and high resolution microscopy of different regions of the mouse aorta revealed increased vWF intensity in areas of the endothelial cell layer exposed to disturbed flow, as opposed to those exposed to laminar flow. This variation appears consistent with previous *in vivo* findings in the literature, which highlight a marked difference in vWF levels between *in vitro* and *in vivo* environments. *In vitro*, all cells appear to contain or synthesise vWF, to the point where vWF is commonly used as a method of positively identifying endothelial cells (Jaffe, Hoyer and Nachman, 1974). *In vivo* however, often less than 50% of endothelial cells examined stained positively for vWF (Senis *et al.*, 1996b). One possible cause for the homogeneity observed in cell culture could be factors included in the growth medium or plate coating substance. The study by Dekker et al., (2012) for instance, utilised fibronectin coated plates, which is known to promote thrombosis, and would therefore result in an increased production of vWF. Additional optimisation is required to enhance high-resolution imaging of the mouse aorta. This improvement will be crucial for obtaining a more comprehensive understanding of vWF intensity, location and expression. Moreover, it will help identify specific regions of the vasculature where vWF expression is notably increased. On top of this, enhanced imaging will facilitate the more accurate measurement of WPB size, allowing us to determine if shear stress has similar impact *in vivo* as it does in the Ibidi pump system.

WPBs in HUVECs and HAECs subjected to HSS were significantly shorter compared to those exposed to LOSS or static conditions. This is consistent with the study by van Agtmaal et al., (2012), which demonstrated that overexpression of KLF2, the transcription factor well characterised to be upregulated in response to HSS, resulted in a population of shorter WPBs. The HSS applied in the Ibidi system here resulted in elevated KLF2 gene expression and ultimately a population of shorter WPBs. This study was the first instance in which physiological levels of flow have been shown to result in altered WPB length. The study by Dragt et al., (2012) demonstrated that exposure to HSS (10 dyn/cm^2) for

5 days resulted in a decrease in the average number of WPBs per cell compared to static conditions. Interestingly, we found no change in the number of WPBs under the different flow conditions and compared to static conditions.

Research carried out by the Cutler group utilised chemical treatments to induce endothelial cells to produce ‘mini-WPBs’ (Ferraro *et al.*, 2014). The alterations in WPB size under flow conditions appear to be much more subtle than those observed as a result of these treatments. Specifically, in HUVECs, the average WPB length in HSS decreased by approximately 30%, and in HAECs, it decreased by approximately 28% compared to static conditions. This reduction was also notable in comparison to LOSS conditions, with a decrease of approximately 25% in HUVECs and 15% in HAECs in HSS. It is important to emphasise that these findings represent mean measurements, and the inherent heterogeneity within the endothelial cell layer, as demonstrated by Andueza et al. 2020, implies that certain cells may exhibit more pronounced changes in WPB length than others. Consequently, we speculate that the proportion of cells with decreased WPB length may increase in HSS conditions, as opposed to a uniform reduction across all cells. A shift towards a higher proportion of cells containing shorter WPBs could have significant implications in terms of the functionality of WPBs and the thrombotic propensity of the regions of endothelial cells subjected to HSS.

6.2.2 vWF Secretome

Endothelial cells have the ability to regulate their response to stimuli by modulating various stages of WPB exocytosis. Previous research in the McKeown lab demonstrated that differential trafficking of subpopulations of WPBs occurs based on the stimulation. Histamine stimulation for example, results in trafficking of WPBs containing cargo superfluous to the response away from the plasma membrane and to the microtubule organising centre, whilst trafficking WPBs containing the required cargo to the plasma membrane for exocytosis (Miteva *et al.*, 2019). This finding demonstrates the high level of control endothelial cells can exert on WPBs and their involvement in response to stimulation. Other studies have shown endothelial cells can also regulate exocytosis via the fusion event that occurs at the plasma membrane. One such fusion event has been termed a ‘lingering kiss’, which is characterised by transient fusion with the plasma membrane, allowing only small molecular weight

molecules, such as cytokines and chemokines, to be exocytosed (Babich *et al.*, 2008). The study by Babich et al., (2008) demonstrated that the proportion of lingering kiss fusion events was increased during low-level stimulation (25%). This raises the possibility that low-level activation by disturbed flow could promote lingering kiss exocytosis, promoting inflammation whilst restricting the release of pro-thrombotic cargo such as vWF. On the contrary, stimulation of endothelial cells with the secretagogue PMA, results in complete exocytosis of WPB cargo and the unfurling of tightly coiled vWF strings on the endothelial cell surface. In these fusion events, actin rings are often recruited to the site of plasma membrane contact to aid the exocytosis of ultra large vWF strings found in long WPBs (Nightingale *et al.*, 2011; McCormack, Harrison- Lavoie and Cutler, 2020). The objective in this project was to determine whether shear stress had any effect on WPB exocytosis and the resulting secretome under both basal and stimulated conditions.

Despite the subtle reduction of WPB length (compared to the reductions seen with chemical treatments in previous studies (Ferraro *et al.*, 2016)), drastic reductions in vWF string length were observed after histamine stimulation. The overall number of vWF strings remained constant after exposure to the different flow conditions, however the vWF strings exocytosed after exposure to HSS were on average approximately 61% shorter than the strings produced after exposure to static conditions, and 56% shorter than those exocytosed after exposure to LOSS. Only 7 vWF strings were >50 µm in length in HSS, compared to 382 and 689 vWF strings in LOSS and static conditions respectively. The reduction in vWF string length is consistent with previous research investigating the effect of WPB size on vWF string length (Ferraro *et al.*, 2014), however this is the first study to show these changes as a result of different flow conditions. This result demonstrates that exposure to HSS for 48 hours results in a significant decrease in the length of vWF strings exocytosed with histamine stimulation. This indicates that the thrombotic response from endothelial cells after exposure to HSS is drastically reduced. It was once believed that long vWF strings were required in order to response to vascular injury, but this data suggests that these strings may not be normal under physiological laminar flow conditions. Consequently, at regions of disturbed blood flow, WPBs are longer and therefore exocytose significantly longer strings. Thrombus inducing atherosclerotic plaques tend to

form in the regions of the endothelium subjected to disturbed flow, highlighting the potential significance of this finding as a response to blood flow. Subsequent experiments in the McKeown lab are currently being performed to assess the ability of the cells with the different vWF string lengths to bind platelets (unpublished data). Future work is needed to determine whether these changes are also observed with other forms of endothelial cell stimulation, as well as how the different types and rates of flow effect the vWF multimers once they have been exocytosed. In this project, the flow conditions used for stimulation were consistently low and unidirectional, future experiments should investigate how different flow conditions influence the unfurling and function of the vWF strings, not least because shear forces promote stretching of the vWF multimers to expose binding sites for platelets and other integrin's required as part of the response to stimulation (Ruggeri and Mendolicchio, 2015). It is also worth noting here that all experiments performed *in vitro* lack the presence of the circulating proteases, such as ADAMTS13, that is present in the bloodstream and cleaves vWF strings. Consideration should therefore be given if any future experiments analyse the function of these vWF strings *in vitro*, taking into account the possibility that ADAMTS13 would cleave the vWF strings prior to any platelet or leukocyte adhesion *in vivo* (De Ceunynck, De Meyer and Vanhoorelbeke, 2013).

To assess the secretion of other WPB cargo, proteomics was performed on the cell culture media after exposure to HSS, LOSS and static conditions for 48 hours, following by 10 minute stimulation with histamine. The average expression of proteins in both the basal and stimulated conditions was analysed. There were no significant differences in protein expression between any of the conditions in their basal state. This may be due to the high volume of media required to perform a 48h flow experiment, as well as the degradation of proteins that were secreted into the media over the period of the flow experiment. After 10 minute histamine stimulation however, 43 proteins were discovered to be significantly differentially expressed between HSS and LOSS conditions (no significant changes between static and either of the flow conditions). From this list of proteins, we sought to identify any WPB cargo proteins or any proteins known to play a role in the WPB lifecycle or exocytosis. Interestingly, the only confirmed WPB cargo that was differentially expressed was vWF, which was elevated in the secretome of cells subjected to LOSS. Other potential proteins of interest were Basement-

membrane protein 40 (SPARC) and Nucleobindin-1 (NUCB1), as these were all proteins identified as potential WPB cargo proteins in a proteomic screen performed by van Breevort, D et al., (2012). Further research is required to determine whether these are bona fide WPB cargoes, and whether WPB size determines their altered exocytosis, or whether there are alternative regulatory mechanisms within the endothelial cells that promote their secretion after exposure to LOSS.

In summary, these findings indicate that subjecting endothelial cells to LOSS for 48 hours, followed by histamine stimulation (10 min), results in a significant increase in the exocytosis of proteins into cell culture media compared to cells exposed to HSS. This difference is particularly evident in the altered vWF string length, as well as indications of differential expression in other potentially novel WPB cargoes. I hypothesise that the changes in vWF string length are directly correlated with the changes in WPB length as a result of flow. However, to ascertain whether alternative compensatory mechanisms are involved in this exocytosis, additional experiments should be performed.

6.2.3 Additional WPB Cargo

WPB synthesis is driven by its primary cargo, vWF, a protein discussed at length previously. Consequently, this section will focus on the effect of shear stress on additional WPB cargoes that also contribute to the important role of WPBs in cellular function.

Starting at the level of gene expression, single cell RNA sequencing data acquired from a mouse model with endothelial cells subjected to both disturbed and laminar (steady) flow, showed that disturbed flow increased both the average expression and percentage of cells expressing a number of WPB cargo, including Angiopoietin-2 (Angpt2), CD63, Endothelin-1 (Edn1) and Insulin Growth Factor Binding Protein 7 (Igfbp7) (Andueza *et al.*, 2020). The increased expression of Angpt2 in disturbed flow was confirmed in the Ibidi pump system, with Angpt2 mRNA expression and fluorescent staining increasing in endothelial cells subjected to LOSS compared to HSS. Angpt2 is upregulated in multiple inflammatory diseases, and has been well-characterised to contribute to inflammation-related signalling pathways, as well as promoting angiogenesis and therefore disrupting vascular stability (Scholz, Plate and Reiss, 2015). The

protein encoded by the CD63 gene is a member of the tetraspanin family and colocalises with vWF and P-selectin in the WPBs of endothelial cells (Vischer and Wagner, 1993). It plays an important role in the adhesion of leukocytes to endothelial cells, primarily through its role in the regulation of P-selectin trafficking. It acts by promoting clustering and maintenance of P-selectin at the cell surface, and is therefore described as an essential cofactor to leukocyte recruitment by endothelial P-selectin (Doyle *et al.*, 2011). Endothelin-1 is recruited to WPBs at the TGN, and plays an important role in vasoconstriction (Sakamoto *et al.*, 1993). Elevated endothelin-1 in regions of disturbed flow is likely to increase vasoconstriction, increasing the stress on the arterial walls in that area, eventually leading to damage and inflammation of the vessel lining and ultimately, increased susceptibility of atherosclerotic plaque formation (Winkles *et al.*, 1993). Igfbp7 was identified as a WPB cargo more recently (van Breevoort *et al.*, 2012), and emerging evidence suggests that it plays a key role in cell proliferation, adhesion, senescence, and angiogenesis. Higher IGFBP7 expression is found to be linked to an increased risk of cardiovascular events (Lisowska *et al.*, 2019). On the contrary, the scRNAseq results demonstrated a decrease in the average expression and percentage expression of Tissue-Type Plasminogen Activator (PLAT) in disturbed flow compared to steady laminar flow. This protein encoded by this gene is an enzyme that converts plasminogen to plasmin. Increased activity of PLAT leads to hyperfibrinolysis and therefore excessive bleeding. Conversely, the decreased expression observed in disturbed flow leads to hypofibrinolysis, which can result in thrombosis (Collen and Lijnen, 2009). Despite the change in expression shown here, little is known about how shear stress affects recruitment to WPBs and release during the early stages of atherosclerotic plaque development.

Taken together, the significant changes in gene expression of these WPB cargo show a clear propensity towards the promotion of inflammation and thrombosis in disturbed flow compared to laminar (steady) flow in the mouse carotid arteries. Further work using the Ibidi pump and alternative *in vitro* flow methods, as well as optimised imaging of the mouse aorta, may be vital to improve our understanding of whether these changes in gene expression are correlated to changes in recruitment of these cargoes to WPBs and the subsequent secretion under stimulation.

6.3 Mechanisms of changes in WPB length

The mechanism of action that determines WPB length is largely unknown. The final part of this study aimed to investigate some of the effects different flow conditions had on potential mechanisms, including the Golgi morphology, and Piezo1, a well-characterised endothelial cell mechanosensor with links to key intracellular signalling pathways that may induce changes in WPB morphology.

6.3.1 Piezo1 and WPBs

Endothelial cells utilise mechanosensors to detect shear stress, distributed on both apical and basal surfaces of the cell, as well as within cell-cell junctions and intracellular compartments. Mechanosensors include the cation channels Piezo1 and P2X purinoceptor 4, as well as integrins, primary cilia, glycocalyx, caveolae, G-protein coupled receptors and G-proteins.

Piezo1 is a mechanosensitive cation channel that responds to mechanical forces. More specifically, the onset of shear stress results in activation of Piezo1 and calcium influx in endothelial cells (Li *et al.*, 2014; Ranade *et al.*, 2014). Whilst the immediate response of WPBs to calcium-mediated stimulation has been studied extensively, many of the long term effects of elevated intracellular calcium on WPBs have yet to be investigated, particularly not that of Piezo1 mediated elevation. Whilst Piezo1 causes an initial influx of calcium into the cell, this peak is followed by a gradual decline until an equilibrium is met. There is evidence that Piezo1 interacts with other calcium ion channel receptors on the cell surface, such as TRPV4, to cause more of sustained calcium influx (Swain and Liddle, 2021). Nonetheless, Piezo1 causes an increase in intracellular calcium in endothelial cells and this has a number of potential implications on WPBs.

In this project, the Piezo1 agonist, Yoda1, was applied to cells under static conditions to activate the channel, along with related compounds, including the Yoda1 antagonist, Dooku1, and an inactive Yoda1 compound (compound 2a). Analysis after 24 hours revealed that Yoda1, unlike Dooku1 or compound 2a, induced a response similar to that seen under HSS conditions, causing a consistent decrease in the average WPB length. Subsequent experiments at earlier time points demonstrated that these changes were only observed after 24 hours. Notably, the addition of Yoda1 after preincubation and in the presence of Dooku1 (and compound 2a) had no inhibitory effect on the Yoda1-induced

decrease in WPB Length. The relatively short half-life of Dooku1 (5 hours) (https://www.smolecule.com/products/s2977394) might have contributed to this lack of antagonistic effect by the 24-hour time point.

These preliminary results suggest that Piezo1 activation indeed plays a role in regulating WPB length. Future work is required to delineate the specific downstream effects involved, however, the wide range of cellular effects of Piezo1 activation raises numerous potential possibilities.

Piezo1-mediated changes in transcription may influence WPB biogenesis, contents and ultimately function. The study by Shinge S et al., (2021) demonstrated that laminar flow activates Piezo1 and therefore increases calcium influx and subsequent endothelial nitric oxide synthase (eNOS) generation (Shinge *et al.*, 2021). This activation further induces the expression of KLF2 and KLF4 through the MAPK pathway while deactivating AP-1. KLF2 upregulation as a result of HSS (shown in this project) or as an over-expression mode, showed that elevated KLF2 results in shorter WPBs (van Agtmaal *et al.*, 2012), providing a potential mechanism between Piezo1 activation and WPB length.

Piezo1 also has an important role in the organisation of the actin cytoskeletal in response to shear stress. When Piezo1 is depleted, endothelial cells exhibit reduced or complete ablation of alignment with the direction of flow (Li *et al.*, 2014). Piezo1 is therefore a critical component in endothelial cell organisation, which has implication in WPB biogenesis and trafficking. In terms of WPB biogenesis, Golgi morphology is well-characterised to influence WPB size (Ferraro *et al.*, 2014) and is strongly connected to the actin cytoskeleton. Piezo1 and the regulation of alignment therefore has the potential to modulate WPB length during biogenesis via Golgi morphology. In addition, the actin cytoskeleton plays an important role in the distribution and trafficking of WPBs.

The distribution and trafficking of WPBs is also highly dependent on the actin cytoskeleton of endothelial cells. WPBs recruit a set of effector proteins (MyRIP, Munc13-4, Slp4-a) that act as a tether to the actin cytoskeleton, which is necessary for the peripheral distribution of WPBs as well as anchoring the WPBs during exocytosis (Schillemans *et al.*, 2019). Piezo1 activation leads to cytoskeletal changes through calcium-dependent regulation of actin-regulating proteins. Under shear stress, Piezo1 activation is critical for actin filament alignment with the direction of flow, and endothelial cells depleted of Piezo1 do

not align (Santana Nunez *et al.*, 2023). Although the direct effect of actin alignment under shear stress on WPBs has not been shown, the strong links and reliance of WPBs on actin dynamics, indicates that Piezo1 mediated actin alignment under shear stress is likely to modulate WPB distribution and trafficking.

Research performed in osteoblasts showed that increased intracellular calcium due to Piezo1 activation promotes AMP-activated protein kinase (AMPK) activation (Zong *et al.*, 2023), similar to observations in endothelial cells under HSS (Dixit *et al.*, 2008). Studies have shown that elevated AMPK phosphorylation is concurrent with increased GBF1 phosphorylation, which in turn permits a "normal" rate of anterograde vWF trafficking and limits the excessive copackaging observed in GBF1-depleted cells (Lopes-da-Silva *et al.*, 2019). It is therefore possible to speculate that in cells exposed to disturbed, atherogenic flow, or static conditions, reduced AMPK phosphorylation could lead to slower anterograde trafficking of vWF, resulting in longer WPBs and providing another potential mechanism for the observed change in WPB size. Further work is required to understand whether this is a direct downstream effects of Piezo1 activation in endothelial cells.

6.3.2 Golgi Morphology

The research conducted by Ferraro et al. (2014) demonstrated that the size of vWF quanta (0.5 µm) always remains constant, with variations in WPB length depending upon the number of co-packaged vWF quanta within an emerging WPB. This research also demonstrated that changes in Golgi morphology affects its ability to co-package vWF quanta. Under static conditions, Golgi cisternae are linked together to form a ribbon-lie structure. The close proximity of each cisternae facilitates multimerisation of several vWF quanta at the TGN, resulting in elongated WPBs. Pharmacological treatments, such as nocodazole, were used to unlink the Golgi ribbon to cause distinct separation of Golgi cisternae. When this unlinking occurs, multimerisation of VWF quanta is inhibited resulting in a population of smaller WPBs, termed ‘mini’ WPBs (Ferraro *et al.*, 2014).

In this project, the objective was to investigate whether different flow conditions altered the Golgi morphology, serving as a potential mechanism behind the observed changes in WPB Length. Exposure to HSS resulted in an increased

number of Golgi objects per cell compared to LOSS conditions (Figure 5.1). While this change was not as significant as that observed with pharmacological treatments, it suggests that shear stress may play an important role in Golgi morphology and consequently, WPB multimerisation at the TGN. Regions of endothelial cells exposed to HSS may exhibit increased Golgi fragmentation.

Further research is needed to ascertain the mechanism by which shear stress alters Golgi morphology. The study by van Agtmaal et al., (2012) demonstrated that neither virus-mediated overexpression of KLF2, or knockdown of KLF2, had any effect on the Golgi morphology. KLF2 is a primary transcription factor involved in gene expression changes in response to flow. The change in Golgi morphology under flow must therefore occur independent of any signalling pathways and be more related to structure changes. The way in which the Golgi appears to stretch across the nucleus under HSS, suggests that this may be a secondary affect caused by the alignment of cells with the direction of flow. The actin and microtubule network are tightly linked to the overall structure of the Golgi, both of which undergo drastic rearrangements under HSS (Malek and Izumo, 1996; Ravichandran, Goud and Manneville, 2020). We therefore speculate that cell alignment during HSS induces cytoskeletal rearrangement that causes moderate Golgi ribbon unlinking and reduced multimerisation of vWF quanta in nascent WPBs. This hypothesis would indicate endothelial cells under HSS contain fragmented Golgi and therefore result in WPBs with a reduced length. It will be important in the future to establish whether this occurs after longer-term exposure to flow (<48h), or whether the Golgi adapts and returns to a more compact morphology.

In addition, and to reinforce these findings, it would have been beneficial to include a positive control that induces Golgi fragmentation alongside the flow conditions. A suitable positive control could involve either a pharmacological treatment known to induce significant fragmentation, such as nocodazole or statins, or the depletion of Golgi matrix proteins such as GM130 or Giantin. Both methods have been successfully used in previous studies (Ferraro *et al.*, 2014, 2016). Although Golgi fragmentation appears more pronounced with pharmacological treatments compared to shear stress-induced fragmentation, comparing the extent of Golgi fragmentation under high shear stress (HSS) conditions with a robust Golgi fragmentation model would be valuable.

Another experiment that would have validated the role of KLF2 involves determining whether the change in WPB size results from KLF2-mediated Golgi fragmentation by depleting KLF2. Ferraro et al. (2016) demonstrated that KLF2 depletion using siRNA increased WPB size, and this effect was not reversed by statin treatment, a known Golgi fragmentation-inducing agent. If KLF2 is knocked down, does Golgi fragmentation still occur under HSS conditions, leading to smaller WPBs? If statins are applied under low shear stress (LOSS) and static conditions, does WPB size decrease, or does oscillatory flow induce longer WPBs through a different mechanism? These experiments would have been insightful if more time had been available and should be considered for future research in this area.

6.4 Implications for disease states and therapeutics

The increase of WPB length in endothelial cells exposed to disturbed flow, coupled with the elevated secretion of pro-inflammatory and pro-thrombotic mediators upon stimulation, highlights the important role of WPBs in increasing the susceptibility of vascular regions to the development of atherosclerosis and thrombosis. Unfortunately, disturbed flow will always be present in the vasculature due to the architecture of the blood vessels, so any potential therapeutic treatments will be targeted towards mitigating the effects induced by disturbed flow in these regions.

There are a large number of anti-thrombotic therapies already in widespread use, however none of the compounds are specifically or intentionally targeted towards WPBs. The study by Ferraro et al., 2020 assessed the modulation of WPB size as an antithrombotic strategy by testing these compounds already approved for use. The study tested 1280 human licensed drugs and found 37 compounds that caused a reduction in WPB size. Some of these compounds targeted mechanisms previously described, such as the Golgi morphology, but a large proportion altered WPB size with by way of an unknown mechanism (Ferraro *et al.*, 2020). This suggests that there are numerous additional cellular pathways that can modulate WPB size, an exciting prospect in the search for therapeutic targets to regulate this process.

Research has also been performed on ADAMTS13, a circulating zinc-containing protease that cleaves ULVWF multimers that are released into the circulation

from WPBs (Gandhi *et al.*, 2012). Deficiency of ADAMTS13 results in thrombotic thrombocytopenic purpura, a life-threatening disorder in which the blood clots excessively due to excessive plasma levels of ULVWF. On the contrary, increasing circulating levels of ADAMTS13 could therefore be used as a method of reducing blood clots. Initial studies have utilised administration of recombinant ADAMTS13, which has exhibit promising anti-thrombotic changes in preclinical studies (Chauhan *et al.*, 2006). Mouse studies have also shown ADAMTS13 also reduces vascular inflammation and the development of early atherosclerosis (Gandhi *et al.*, 2012). This may therefore become a promising pharmacological agent for the treatment of cardiovascular disease.

There is a fine-balance between disease prevention and disrupting endothelial cells to the point at which they can no longer performed their required function. However, the large number of anti-thrombotic and anti-inflammatory drugs already in use is hugely promising when considering they likely already target WPBs in some way. Understanding how WPBs are affected with these treatments, and how they can be optimised further to prevent CVD is essential for developing effective therapeutic strategies with minimal side effects.

Chapter 7 – Conclusion and Future Directions

7.1 Summary of Key Findings

The aim of this project was to investigate the effect of shear stress on WPB biogenesis, cargo and secretion using an *in vitro* flow system. The key findings from this project are as follows:

- The Ibidi pump system is a robust *in vitro* method for studying the effect of shear stress on WPBs.
- Endothelial cell alignment depends upon more than just the rate of shear stress. Other parameters, such as flow rate and pressure, must be taken into account.
- HSS results in a population of shorter WPBs, compared to WPBs in cells exposed to LOSS and static conditions in both HUVECs and HAECs.
- Different shear stress rates do not change the number of WPBs in HUVECs or HAECs.
- Shear stress applied to cells cultured on the Ibidi y-shaped slide does not induce any change in WPB length or number.
- Initial observations of different regions of mouse aorta identified morphological changes in vWF immunofluorescent staining between aligned and non-aligned cells.
- Single-cell RNA sequencing analysis identified WPB cargo and WPB associated genes differentially expressed in cells exposed to disturbed flow compared to cells exposed to laminar flow.
- Proteomic analysis identified 4 potentially novel WPB cargoes that were differentially expressed in the secretome of cells exposed to LOSS with histamine stimulation, compared to cells exposed to HSS with histamine stimulation.
- Proteomic analysis revealed no change in proteins secreted in basal conditions (no stimulation).
- HSS results in shorter vWF strings upon stimulation with histamine, compared to vWF strings formed from cells exposed to LOSS and static conditions.
- The Golgi apparatus is significantly more fragmented under HSS, compared to LOSS and static conditions.

- Yoda1-evoked Piezo1 activation results in a population of shorter WPBs after 24 hours.

7.2 Future Work

The work performed in this project has provided an insight into the effects of shear stress on WPB morphology, cargo and function, and begins to explore some of the potential mechanisms involved in this regulation. The single cell RNA sequencing data and proteomic analysis data sets will hopefully provide useful information for those studying endothelial cell gene expression and secretome in response to different flow conditions going forward. Future work is required to address emerging questions with regards to the effect of shear stress on WPBs and its potential contribution to atherosclerosis.

7.2.1 Functional characterisation of novel WPB cargoes

Functional studies should be performed to elucidate the roles of the newly identified potentially novel WPB cargoes identified in van Breevort et al. 2012, particularly those that have been shown in this project to be regulated by shear stress. Genetic and pharmacological tools will need to be employed to modulate the expression of these cargoes and observe the resultant effects on WPBs, investigating further how these cargoes contribute to key endothelial functions such as haemostasis, angiogenesis, and vascular permeability.

7.2.2 Intracellular signalling pathways of Piezo1 activation

Investigate the intracellular signalling pathways activated by Yoda1-induced Piezo1 activation. Employ molecular biology techniques and signalling pathway inhibitors to decipher the downstream signalling events triggered by Piezo1. Investigate how these pathways integrate with known regulators of WPBs, shedding light on the molecular mechanisms orchestrating Piezo1-mediated changes in WPB morphology and function.

7.2.3 *In vivo* vWF staining in mouse aorta

In vitro findings have been shown in two cell types, HUVECs and HAECs. This gives a good indication of the WPB response, however, the in vivo mouse environment is much more complex and representative of WPBs and their responses in humans. There is therefore a requirement to improve and advance

the vWF staining and subsequent imaging of aligned and non-aligned cells in the Current methods used to extract and prepare the mouse aorta renders them susceptible to damage. Advancements in this process, i.e. mounting the intact aorta for imaging, would omit these pitfalls in the preparation methodology. We have made initial observations in this project of WPB morphology alterations in aligned and non-aligned cells of the aorta. Future work should start to induce stimulation to the mouse aorta to elicit the functional ability of WPBs in each of these regions.

7.3 Conclusion

The investigation into the effects of shear stress on endothelial cells has revealed distinct responses in WPBs. Different flow conditions influence WPB length, cargo, and secretome composition. HSS emerges as a key regulating factor, inducing shorter WPBs, shorter vWF strings, and fragmenting the Golgi apparatus, ultimately resulting in anti-thrombotic and anti-inflammatory population of cells. Potential mechanisms that underlie these changes include Golgi fragmentation and Piezo1 activation. In addition, chemical activation of Piezo1 mimics HSS that could present both a tool for studying the effects of HSS, as well as providing a potential mechanism of action for the reduction in WPB length. RNA sequencing and proteomic analysis shed light on potentially novel WPB cargo, whilst demonstrating the effect of shear stress on bona fide WPB cargo. These findings offer a comprehensive view of the impact different types of flow have on endothelial cells and their WPBs, paving the way for future studies in vascular biology and potential therapeutic targets.

References

van Agtmaal, E.L. *et al.* (2012) 'The shear stress-induced transcription factor KLF2 affects dynamics and angiopoietin-2 content of Weibel-Palade bodies', *PloS One*, 7(6), p. e38399. Available at: https://doi.org/10.1371/journal.pone.0038399.

Aird, W.C. *et al.* (1997) 'Vascular Bed–specific Expression of an Endothelial Cell Gene Is Programmed by the Tissue Microenvironment', *The Journal of Cell Biology*, 138(5), pp. 1117–1124.

Akwii, R.G. *et al.* (2019) 'Role of Angiopoietin-2 in Vascular Physiology and Pathophysiology', *Cells*, 8(5), p. 471. Available at: https://doi.org/10.3390/cells8050471.

Ando, J. and Yamamoto, K. (2009) 'Vascular Mechanobiology Endothelial Cell Responses to Fluid Shear Stress: Endothelial Cell Responses to Fluid Shear Stress', *Circulation Journal*, 73(11), pp. 1983–1992. Available at: https://doi.org/10.1253/circj.CJ-09-0583.

Andueza, A. *et al.* (2020) 'Endothelial Reprogramming by Disturbed Flow Revealed by Single-Cell RNA and Chromatin Accessibility Study', *Cell Reports*, 33(11). Available at: https://doi.org/10.1016/j.celrep.2020.108491.

Apostolova, M.D. *et al.* (2001) 'High-glucose-induced metallothionein expression in endothelial cells: an endothelin-mediated mechanism', *American Journal of Physiology-Cell Physiology*, 281(3), pp. C899–C907. Available at: https://doi.org/10.1152/ajpcell.2001.281.3.C899.

Babich, V. *et al.* (2008) 'Selective release of molecules from Weibel-Palade bodies during a lingering kiss', *Blood*, 111(11), pp. 5282–5290. Available at: https://doi.org/10.1182/blood-2007-09-113746.

Barbee, K.A. *et al.* (1995) 'Subcellular distribution of shear stress at the surface of flow-aligned and nonaligned endothelial monolayers', *American Journal of Physiology-Heart and Circulatory Physiology*, 268(4), pp. H1765–H1772. Available at: https://doi.org/10.1152/ajpheart.1995.268.4.H1765.

Basatemur, G.L. *et al.* (2019) 'Vascular smooth muscle cells in atherosclerosis', *Nature Reviews Cardiology*, 16(12), pp. 727–744. Available at: https://doi.org/10.1038/s41569-019-0227-9.

Basu, A. *et al.* (2001) 'Impaired wound healing in mice deficient in a matricellular protein SPARC (osteonectin, BM-40)', *BMC Cell Biology*, 2, p. 15. Available at: https://doi.org/10.1186/1471-2121-2-15.

Bhattacharya, R. *et al.* (2005) 'Inhibition of Vascular Permeability Factor/Vascular Endothelial Growth Factor-mediated Angiogenesis by the Kruppel-like Factor KLF2*', *Journal of Biological Chemistry*, 280(32), pp. 28848–28851. Available at: https://doi.org/10.1074/jbc.C500200200.

Bierings, R. *et al.* (2012) 'The interplay between the Rab27A effectors Slp4-a and MyRIP controls hormone-evoked Weibel-Palade body exocytosis', *Blood*,

120(13), pp. 2757–2767. Available at: https://doi.org/10.1182/blood-2012-05-429936.

Birukov, K.G. *et al.* (2002) 'Shear stress-mediated cytoskeletal remodeling and cortactin translocation in pulmonary endothelial cells', *American Journal of Respiratory Cell and Molecular Biology*, 26(4), pp. 453–464. Available at: https://doi.org/10.1165/ajrcmb.26.4.4725.

Bonfanti, R. *et al.* (1989) 'PADGEM (GMP140) is a component of Weibel-Palade bodies of human endothelial cells', *Blood*, 73(5), pp. 1109–1112.

Bortot, M. *et al.* (2019) 'Turbulent Flow Promotes Cleavage of VWF (von Willebrand Factor) by ADAMTS13 (A Disintegrin and Metalloproteinase With a Thrombospondin Type-1 Motif, Member 13)', *Arteriosclerosis, Thrombosis, and Vascular Biology*, 39(9), pp. 1831–1842. Available at: https://doi.org/10.1161/ATVBAHA.119.312814.

van Breevoort, D. *et al.* (2012) 'Proteomic Screen Identifies IGFBP7 as a Novel Component of Endothelial Cell-Specific Weibel-Palade Bodies', *Journal of Proteome Research*, 11(5), pp. 2925–2936. Available at: https://doi.org/10.1021/pr300010r.

Carmeliet, P. *et al.* (1999) 'Targeted Deficiency or Cytosolic Truncation of the VE-cadherin Gene in Mice Impairs VEGF-Mediated Endothelial Survival and Angiogenesis', *Cell*, 98(2), pp. 147–157. Available at: https://doi.org/10.1016/S0092-8674(00)81010-7.

Carmeliet, P. (2005) 'Angiogenesis in life, disease and medicine', *Nature*, 438(7070), pp. 932–936. Available at: https://doi.org/10.1038/nature04478.

Chachisvilis, M., Zhang, Y.-L. and Frangos, J.A. (2006) 'G protein-coupled receptors sense fluid shear stress in endothelial cells', *Proceedings of the National Academy of Sciences*, 103(42), pp. 15463–15468. Available at: https://doi.org/10.1073/pnas.0607224103.

Chaterjee, Shampa (2018) *Frontiers | Endothelial Mechanotransduction, Redox Signaling and the Regulation of Vascular Inflammatory Pathways*. Available at: https://www.frontiersin.org/articles/10.3389/fphys.2018.00524/full (Accessed: 4 November 2023).

Chauhan, A.K. *et al.* (2006) 'Systemic antithrombotic effects of ADAMTS13', *Journal of Experimental Medicine*, 203(3), pp. 767–776. Available at: https://doi.org/10.1084/jem.20051732.

Chiu, Y.-J., McBeath, E. and Fujiwara, K. (2008) 'Mechanotransduction in an extracted cell model: Fyn drives stretch- and flow-elicited PECAM-1 phosphorylation', *Journal of Cell Biology*, 182(4), pp. 753–763. Available at: https://doi.org/10.1083/jcb.200801062.

Chlench, S. *et al.* (2007) 'Regulation of Foxo-1 and the angiopoietin-2/Tie2 system by shear stress', *FEBS letters*, 581(4), pp. 673–680. Available at: https://doi.org/10.1016/j.febslet.2007.01.028.

Choi, S.J. and Lillicrap, D. (2020) 'A sticky proposition: The endothelial glycocalyx and von Willebrand factor', *Journal of Thrombosis and Haemostasis*, 18(4), pp. 781–785. Available at: https://doi.org/10.1111/jth.14743.

Chuntharpursat-Bon, E. *et al.* (2023) 'PIEZO1 and PECAM1 interact at cell-cell junctions and partner in endothelial force sensing', *Communications Biology*, 6(1), pp. 1–18. Available at: https://doi.org/10.1038/s42003-023-04706-4.

Cines, D.B. *et al.* (1998) 'Endothelial cells in physiology and in the pathophysiology of vascular disorders', *Blood*, 91(10), pp. 3527–3561.

Coan, D.E. *et al.* (1993) 'Effect of shear stress upon localization of the Golgi apparatus and microtubule organizing center in isolated cultured endothelial cells', *Journal of Cell Science*, 104(4), pp. 1145–1153.

Collen, D. and Lijnen, H. r. (2009) 'The Tissue-Type Plasminogen Activator Story', *Arteriosclerosis, Thrombosis, and Vascular Biology*, 29(8), pp. 1151–1155. Available at: https://doi.org/10.1161/ATVBAHA.108.179655.

Conway, D.E. and Schwartz, M.A. (2013) 'Flow-dependent cellular mechanotransduction in atherosclerosis', *Journal of Cell Science*, 126(22), pp. 5101–5109. Available at: https://doi.org/10.1242/jcs.138313.

Cooke, J.P. (2000) 'The endothelium: a new target for therapy', *Vascular Medicine (London, England)*, 5(1), pp. 49–53. Available at: https://doi.org/10.1177/1358836X0000500108.

Corson, M.A. *et al.* (1996) 'Phosphorylation of Endothelial Nitric Oxide Synthase in Response to Fluid Shear Stress', *Circulation Research*, 79(5), pp. 984–991. Available at: https://doi.org/10.1161/01.RES.79.5.984.

Coste, B. *et al.* (2010) 'Piezo1 and Piezo2 Are Essential Components of Distinct Mechanically Activated Cation Channels', *Science*, 330(6000), pp. 55–60. Available at: https://doi.org/10.1126/science.1193270.

Das, H. *et al.* (2006) 'Kruppel-like factor 2 (KLF2) regulates proinflammatory activation of monocytes', *Proceedings of the National Academy of Sciences*, 103(17), pp. 6653–6658. Available at: https://doi.org/10.1073/pnas.0508235103.

Davies, P.F. (2009) 'Hemodynamic shear stress and the endothelium in cardiovascular pathophysiology', *Nature Clinical Practice Cardiovascular Medicine*, 6(1), pp. 16–26. Available at: https://doi.org/10.1038/ncpcardio1397.

Davies, P.F., Robotewskyj, A. and Griem, M.L. (1994) 'Quantitative studies of endothelial cell adhesion. Directional remodeling of focal adhesion sites in response to flow forces.', *The Journal of Clinical Investigation*, 93(5), pp. 2031–2038. Available at: https://doi.org/10.1172/JCI117197.

Davies, P.F., Spaan, Jos.A. and Krams, R. (2005) 'Shear Stress Biology of the Endothelium', *Annals of Biomedical Engineering*, 33(12), pp. 1714–1718. Available at: https://doi.org/10.1007/s10439-005-8774-0.

De Ceunynck, K., De Meyer, S.F. and Vanhoorelbeke, K. (2013) 'Unwinding the von Willebrand factor strings puzzle', *Blood*, 121(2), pp. 270–277. Available at: https://doi.org/10.1182/blood-2012-07-442285.

Deanfield, J.E., Halcox, J.P. and Rabelink, T.J. (2007) 'Endothelial Function and Dysfunction', *Circulation*, 115(10), pp. 1285–1295. Available at: https://doi.org/10.1161/CIRCULATIONAHA.106.652859.

Dekker, R.J. *et al.* (2002) 'Prolonged fluid shear stress induces a distinct set of endothelial cell genes, most specifically lung Krüppel-like factor (KLF2)', *Blood*, 100(5), pp. 1689–1698. Available at: https://doi.org/10.1182/blood-2002-01-0046.

Dekker, R.J. *et al.* (2006) 'KLF2 provokes a gene expression pattern that establishes functional quiescent differentiation of the endothelium', *Blood*, 107(11), pp. 4354–4363. Available at: https://doi.org/10.1182/blood-2005-08-3465.

Dewey, C.F., Jr. *et al.* (1981) 'The Dynamic Response of Vascular Endothelial Cells to Fluid Shear Stress', *Journal of Biomechanical Engineering*, 103(3), pp. 177–185. Available at: https://doi.org/10.1115/1.3138276.

Diamond, S.L. *et al.* (1990) 'Tissue plasminogen activator messenger RNA levels increase in cultured human endothelial cells exposed to laminar shear stress', *Journal of Cellular Physiology*, 143(2), pp. 364–371. Available at: https://doi.org/10.1002/jcp.1041430222.

Dixit, M. *et al.* (2008) 'Shear stress-induced activation of the AMP-activated protein kinase regulates FoxO1a and angiopoietin-2 in endothelial cells', *Cardiovascular Research*, 77(1), pp. 160–168. Available at: https://doi.org/10.1093/cvr/cvm017.

Dong, J. *et al.* (2002) 'ADAMTS-13 rapidly cleaves newly secreted ultralarge von Willebrand factor multimers on the endothelial surface under flowing conditions', *Blood*, 100(12), pp. 4033–4039. Available at: https://doi.org/10.1182/blood-2002-05-1401.

Doyle, E.L. *et al.* (2011) 'CD63 is an essential cofactor to leukocyte recruitment by endothelial P-selectin', *Blood*, 118(15), pp. 4265–4273. Available at: https://doi.org/10.1182/blood-2010-11-321489.

Dragt, B.S. *et al.* (2012) 'Effect of laminar shear stress on the distribution of Weibel-Palade bodies in endothelial cells', *Thrombosis Research*, 130(5), pp. 741–745. Available at: https://doi.org/10.1016/j.thromres.2012.08.301.

Eikenboom, J.C.J. (2001) 'Congenital von Willebrand disease type 3: clinical manifestations, pathophysiology and molecular biology', *Best Practice & Research Clinical Haematology*, 14(2), pp. 365–379. Available at: https://doi.org/10.1053/beha.2001.0139.

Emeis, J.J. *et al.* (1997) 'An Endothelial Storage Granule for Tissue-Type Plasminogen Activator', *The Journal of Cell Biology*, 139(1), pp. 245–256. Available at: https://doi.org/10.1083/jcb.139.1.245.

Evans, E.L. *et al.* (2018) 'Yoda1 analogue (Dooku1) which antagonizes Yoda1-evoked activation of Piezo1 and aortic relaxation', *British Journal of Pharmacology*, 175(10), pp. 1744–1759. Available at: https://doi.org/10.1111/bph.14188.

Federici, A.B. *et al.* (1989) 'Binding of von Willebrand factor to glycoproteins Ib and IIb/IIIa complex: affinity is related to multimeric size', *British Journal of Haematology*, 73(1), pp. 93–99. Available at: https://doi.org/10.1111/j.1365-2141.1989.tb00226.x.

Ferraro, F. *et al.* (2014) 'A Two-Tier Golgi-Based Control of Organelle Size Underpins the Functional Plasticity of Endothelial Cells', *Developmental Cell*, 29(3), pp. 292–304. Available at: https://doi.org/10.1016/j.devcel.2014.03.021.

Ferraro, F. *et al.* (2016) 'Weibel-Palade body size modulates the adhesive activity of its von Willebrand Factor cargo in cultured endothelial cells', *Scientific Reports*, 6(1), pp. 1–15. Available at: https://doi.org/10.1038/srep32473.

Ferraro, F. *et al.* (2020) 'Modulation of endothelial organelle size as an antithrombotic strategy', *Journal of Thrombosis and Haemostasis*, 18(12), pp. 3296–3308. Available at: https://doi.org/10.1111/jth.15084.

Fiedler, U. *et al.* (2004a) 'The Tie-2 ligand Angiopoietin-2 is stored in and rapidly released upon stimulation from endothelial cell Weibel-Palade bodies', *Blood*, 103(11), pp. 4150–4156. Available at: https://doi.org/10.1182/blood-2003-10-3685.

Fiedler, U. *et al.* (2004b) 'The Tie-2 ligand Angiopoietin-2 is stored in and rapidly released upon stimulation from endothelial cell Weibel-Palade bodies', *Blood*, 103(11), pp. 4150–4156. Available at: https://doi.org/10.1182/blood-2003-10-3685.

Fiedler, U. *et al.* (2006) 'Angiopoietin-2 sensitizes endothelial cells to TNF-alpha and has a crucial role in the induction of inflammation', *Nature Medicine*, 12(2), pp. 235–239. Available at: https://doi.org/10.1038/nm1351.

Fleming, I. (2010) 'Molecular mechanisms underlying the activation of eNOS', *Pflügers Archiv - European Journal of Physiology*, 459(6), pp. 793–806. Available at: https://doi.org/10.1007/s00424-009-0767-7.

Fu, L., Liu, Z. and Liu, Y. (2023) 'Fibrinogen-like protein 2 in inflammatory diseases: A future therapeutic target', *International Immunopharmacology*, 116, p. 109799. Available at: https://doi.org/10.1016/j.intimp.2023.109799.

Galbraith, C.G., Skalak, R. and Chien, S. (1998) 'Shear stress induces spatial reorganization of the endothelial cell cytoskeleton', *Cell Motility*, 40(4), pp. 317–330. Available at: https://doi.org/10.1002/(SICI)1097-0169(1998)40:4<317::AID-CM1>3.0.CO;2-8.

Galbusera, M. *et al.* (1997) 'Fluid Shear Stress Modulates von Willebrand Factor Release From Human Vascular Endothelium', *Blood*, 90(4), pp. 1558–1564. Available at: https://doi.org/10.1182/blood.V90.4.1558.

Galley, H.F. and Webster, N.R. (2004) 'Physiology of the endothelium', *British Journal of Anaesthesia*, 93(1), pp. 105–113. Available at: https://doi.org/10.1093/bja/aeh163.

Gandhi, C. *et al.* (2012) 'ADAMTS13 reduces vascular inflammation and the development of early atherosclerosis in mice', *Blood*, 119(10), pp. 2385–2391. Available at: https://doi.org/10.1182/blood-2011-09-376202.

Ge, G. *et al.* (2007) 'Bone morphogenetic protein 1 processes prolactin to a 17-kDa antiangiogenic factor', *Proceedings of the National Academy of Sciences of the United States of America*, 104(24), pp. 10010–10015. Available at: https://doi.org/10.1073/pnas.0704179104.

Gebrane-Younès, J. *et al.* (1991) 'Heterogeneous distribution of Weibel-Palade bodies and von Willebrand factor along the porcine vascular tree.', *The American Journal of Pathology*, 139(6), pp. 1471–1484.

Giblin, J.P., Hewlett, L.J. and Hannah, M.J. (2008) 'Basal secretion of von Willebrand factor from human endothelial cells', *Blood*, 112(4), pp. 957–964. Available at: https://doi.org/10.1182/blood-2007-12-130740.

Gimbrone Michael A. and García-Cardeña Guillermo (2016) 'Endothelial Cell Dysfunction and the Pathobiology of Atherosclerosis', *Circulation Research*, 118(4), pp. 620–636. Available at: https://doi.org/10.1161/CIRCRESAHA.115.306301.

Givens, C. and Tzima, E. (2016) 'Endothelial Mechanosignaling: Does One Sensor Fit All?', *Antioxidants & Redox Signaling*, 25(7), pp. 373–388. Available at: https://doi.org/10.1089/ars.2015.6493.

Goehring, N.W. and Hyman, A.A. (2012) 'Organelle growth control through limiting pools of cytoplasmic components', *Current biology: CB*, 22(9), pp. R330-339. Available at: https://doi.org/10.1016/j.cub.2012.03.046.

Goettsch, W. *et al.* (2008) 'Flow-dependent regulation of angiopoietin-2', *Journal of Cellular Physiology*, 214(2), pp. 491–503. Available at: https://doi.org/10.1002/jcp.21229.

Gudi, S. *et al.* (2003) 'Rapid activation of Ras by fluid flow is mediated by Galpha(q) and Gbetagamma subunits of heterotrimeric G proteins in human endothelial cells', *Arteriosclerosis, Thrombosis, and Vascular Biology*, 23(6), pp. 994–1000. Available at: https://doi.org/10.1161/01.ATV.0000073314.51987.84.

Gudi, S.R.P., Clark, C.B. and Frangos, J.A. (1996) 'Fluid Flow Rapidly Activates G Proteins in Human Endothelial Cells', *Circulation Research*, 79(4), pp. 834–839. Available at: https://doi.org/10.1161/01.RES.79.4.834.

Haberichter, S.L. *et al.* (2005) 'Re-establishment of VWF-dependent Weibel-Palade bodies in VWD endothelial cells', *Blood*, 105(1), pp. 145–152. Available at: https://doi.org/10.1182/blood-2004-02-0464.

Hannah, M.J. *et al.* (2002) 'Biogenesis of Weibel–Palade bodies', *Seminars in Cell & Developmental Biology*, 13(4), pp. 313–324. Available at: https://doi.org/10.1016/S1084-9521(02)00061-7.

Hannah, M.J. *et al.* (2003) 'Weibel-Palade bodies recruit Rab27 by a content-driven, maturation-dependent mechanism that is independent of cell type', *Journal of Cell Science*, 116(19), pp. 3939–3948. Available at: https://doi.org/10.1242/jcs.00711.

Henry, C.B. and Duling, B.R. (2000) 'TNF-alpha increases entry of macromolecules into luminal endothelial cell glycocalyx', *American Journal of Physiology. Heart and Circulatory Physiology*, 279(6), pp. H2815-2823. Available at: https://doi.org/10.1152/ajpheart.2000.279.6.H2815.

Holthenrich, A. *et al.* (2019) 'Proximity proteomics of endothelial Weibel-Palade bodies identifies novel regulator of von Willebrand factor secretion', *Blood*, 134(12), pp. 979–982. Available at: https://doi.org/10.1182/blood.2019000786.

Hough, C. *et al.* (2008) 'Influence of a GT repeat element on shear stress responsiveness of the VWF gene promoter', *Journal of Thrombosis and Haemostasis*, 6(7), pp. 1183–1190. Available at: https://doi.org/10.1111/j.1538-7836.2008.03011.x.

Huber, D. *et al.* (2002) 'Tissue-type plasminogen activator (t-PA) is stored in Weibel-Palade bodies in human endothelial cells both in vitro and in vivo', *Blood*, 99(10), pp. 3637–3645. Available at: https://doi.org/10.1182/blood.V99.10.3637.

Iomini, C. *et al.* (2004) 'Primary cilia of human endothelial cells disassemble under laminar shear stress', *The Journal of Cell Biology*, 164(6), pp. 811–817. Available at: https://doi.org/10.1083/jcb.200312133.

Jaffe, E.A., Hoyer, L.W. and Nachman, R.L. (1974) 'Synthesis of von Willebrand Factor by Cultured Human Endothelial Cells', *Proceedings of the National Academy of Sciences*, 71(5), pp. 1906–1909. Available at: https://doi.org/10.1073/pnas.71.5.1906.

James, P.D. *et al.* (2007) 'The mutational spectrum of type 1 von Willebrand disease: results from a Canadian cohort study', *Blood*, 109(1), pp. 145–154. Available at: https://doi.org/10.1182/blood-2006-05-021105.

Jilma-Stohlawetz, P. *et al.* (2016) 'Acquired von Willebrand factor deficiency caused by LVAD is ADAMTS-13 and platelet dependent', *Thrombosis Research*, 137, pp. 196–201. Available at: https://doi.org/10.1016/j.thromres.2015.11.002.

Jin, L. *et al.* (2020) 'Insulin Growth Factor Binding Protein 7 (IGFBP7)-Related Cancer and IGFBP3 and IGFBP7 Crosstalk', *Frontiers in Oncology*, 10. Available at: https://www.frontiersin.org/articles/10.3389/fonc.2020.00727 (Accessed: 26 January 2023).

Kaji, T. *et al.* (1993) 'Metallothionein induction by cadmium, cytokines, thrombin and endothelin-1 in cultured vascular endothelial cells', *Life Sciences*, 53(15), pp. 1185–1191. Available at: https://doi.org/10.1016/0024-3205(93)90536-C.

Kaufmann, J.E. *et al.* (2000) 'Vasopressin-induced von Willebrand factor secretion from endothelial cells involves V2 receptors and cAMP', *The Journal of Clinical Investigation*, 106(1), pp. 107–116. Available at: https://doi.org/10.1172/JCI9516.

Kellermair, J. *et al.* (2020) 'High-molecular-weight von Willebrand Factor multimer ratio differentiates true-severe from pseudo-severe classical low-flow, low-gradient aortic stenosis', *European Heart Journal - Cardiovascular Imaging*, 21(10), pp. 1123–1130. Available at: https://doi.org/10.1093/ehjci/jeaa056.

Knop, M. *et al.* (2004) 'Rab3D and annexin A2 play a role in regulated secretion of vWF, but not tPA, from endothelial cells', *The EMBO Journal*, 23(15), pp. 2982–2992. Available at: https://doi.org/10.1038/sj.emboj.7600319.

Kobayashi, T. *et al.* (2000) 'The Tetraspanin CD63/lamp3 Cycles between Endocytic and Secretory Compartments in Human Endothelial Cells', *Molecular Biology of the Cell*, 11(5), pp. 1829–1843.

Krüger-Genge, A. *et al.* (2019) 'Vascular Endothelial Cell Biology: An Update', *International Journal of Molecular Sciences*, 20(18), p. 4411. Available at: https://doi.org/10.3390/ijms20184411.

Ku, D.N. *et al.* (1985) 'Pulsatile flow and atherosclerosis in the human carotid bifurcation. Positive correlation between plaque location and low oscillating shear stress.', *Arteriosclerosis: An Official Journal of the American Heart Association, Inc.*, 5(3), pp. 293–302. Available at: https://doi.org/10.1161/01.ATV.5.3.293.

Laan, S.N.J. *et al.* (2023) 'Automated segmentation and quantitative analysis of organelle morphology, localization and content using CellProfiler', *PLOS ONE*, 18(6), p. e0278009. Available at: https://doi.org/10.1371/journal.pone.0278009.

Lan, Q., Mercurius, K.O. and Davies, P.F. (1994) 'Stimulation of transcription factors NF kappa B and AP1 in endothelial cells subjected to shear stress', *Biochemical and Biophysical Research Communications*, 201(2), pp. 950–956. Available at: https://doi.org/10.1006/bbrc.1994.1794.

Li, J. *et al.* (2014) 'Piezo1 integration of vascular architecture with physiological force', *Nature*, 515(7526), pp. 279–282. Available at: https://doi.org/10.1038/nature13701.

Li, S. *et al.* (1999) 'Distinct roles for the small GTPases Cdc42 and Rho in endothelial responses to shear stress', *The Journal of Clinical Investigation*, 103(8), pp. 1141–1150. Available at: https://doi.org/10.1172/JCI5367.

Libby, P., Ridker, P.M. and Hansson, G.K. (2011) 'Progress and challenges in translating the biology of atherosclerosis', *Nature*, 473(7347), pp. 317–325. Available at: https://doi.org/10.1038/nature10146.

Lisowska, A. *et al.* (2019) 'Insulin-like growth factor-binding protein 7 (IGFBP 7) as a new biomarker in coronary heart disease', *Advances in Medical Sciences*, 64(1), pp. 195–201. Available at: https://doi.org/10.1016/j.advms.2018.08.017.

Lopes-da-Silva, M. *et al.* (2019) 'A GBF1-Dependent Mechanism for Environmentally Responsive Regulation of ER-Golgi Transport', *Developmental Cell*, 49(5), pp. 786-801.e6. Available at: https://doi.org/10.1016/j.devcel.2019.04.006.

Lui-Roberts, W.W.Y. *et al.* (2005) 'An AP-1/clathrin coat plays a novel and essential role in forming the Weibel-Palade bodies of endothelial cells', *Journal of Cell Biology*, 170(4), pp. 627–636. Available at: https://doi.org/10.1083/jcb.200503054.

Mahmoud, M.M. *et al.* (2016) 'TWIST1 Integrates Endothelial Responses to Flow in Vascular Dysfunction and Atherosclerosis', *Circulation Research*, 119(3), pp. 450–462. Available at: https://doi.org/10.1161/CIRCRESAHA.116.308870.

Maisonpierre, P.C. *et al.* (1997) 'Angiopoietin-2, a Natural Antagonist for Tie2 That Disrupts in vivo Angiogenesis', *Science*, 277(5322), pp. 55–60. Available at: https://doi.org/10.1126/science.277.5322.55.

Malek, A.M. and Izumo, S. (1996) 'Mechanism of endothelial cell shape change and cytoskeletal remodeling in response to fluid shear stress', *Journal of Cell Science*, 109(4), pp. 713–726.

Manneville, J.-B. *et al.* (2003) 'Interaction of the actin cytoskeleton with microtubules regulates secretory organelle movement near the plasma membrane in human endothelial cells', *Journal of Cell Science*, 116(19), pp. 3927–3938. Available at: https://doi.org/10.1242/jcs.00672.

McCormack, J.J., Harrison-Lavoie, K.J. and Cutler, D.F. (2020) 'Human endothelial cells size-select their secretory granules for exocytosis to modulate their functional output', *Journal of Thrombosis and Haemostasis*, 18(1), pp. 243–254. Available at: https://doi.org/10.1111/jth.14634.

McEver, R.P. *et al.* (1989) 'GMP-140, a platelet alpha-granule membrane protein, is also synthesized by vascular endothelial cells and is localized in Weibel-Palade bodies.', *The Journal of Clinical Investigation*, 84(1), pp. 92–99. Available at: https://doi.org/10.1172/JCI114175.

Methia, N. *et al.* (2001) 'Localized reduction of atherosclerosis in von Willebrand factor-deficient mice', *Blood*, 98(5), pp. 1424–1428. Available at: https://doi.org/10.1182/blood.v98.5.1424.

Michaux, G. *et al.* (2006) 'P-selectin binds to the D'-D3 domains of von Willebrand factor in Weibel-Palade bodies', *Blood*, 107(10), pp. 3922–3924. Available at: https://doi.org/10.1182/blood-2005-09-3635.

Michaux, G. and Cutler, D.F. (2004) 'How to Roll an Endothelial Cigar: The Biogenesis of Weibel-Palade Bodies', *Traffic*, 5(2), pp. 69–78. Available at: https://doi.org/10.1111/j.1600-0854.2004.00157.x.

Miteva, K.T. *et al.* (2019) 'Rab46 integrates Ca^{2+} and histamine signaling to regulate selective cargo release from Weibel-Palade bodies', *The Journal of Cell Biology*, 218(7), pp. 2232–2246. Available at: https://doi.org/10.1083/jcb.201810118.

Morawietz, H. *et al.* (2000) 'Regulation of the endothelin system by shear stress in human endothelial cells', *The Journal of Physiology*, 525(Pt 3), pp. 761–770. Available at: https://doi.org/10.1111/j.1469-7793.2000.00761.x.

Morrell, N.W. *et al.* (2016) 'Targeting BMP signalling in cardiovascular disease and anaemia', *Nature Reviews Cardiology*, 13(2), pp. 106–120. Available at: https://doi.org/10.1038/nrcardio.2015.156.

Nauli, S.M. *et al.* (2008) 'Endothelial Cilia Are Fluid Shear Sensors That Regulate Calcium Signaling and Nitric Oxide Production Through Polycystin-1', *Circulation*, 117(9), pp. 1161–1171. Available at: https://doi.org/10.1161/CIRCULATIONAHA.107.710111.

Nightingale, T.D. *et al.* (2009) 'Rab27a and MyRIP regulate the amount and multimeric state of VWF released from endothelial cells', *Blood*, 113(20), pp. 5010–5018. Available at: https://doi.org/10.1182/blood-2008-09-181206.

Nightingale, T.D. *et al.* (2011) 'Actomyosin II contractility expels von Willebrand factor from Weibel-Palade bodies during exocytosis', *The Journal of Cell Biology*, 194(4), pp. 613–629. Available at: https://doi.org/10.1083/jcb.201011119.

Nightingale, T.D. *et al.* (2018) 'Tuning the endothelial response: differential release of exocytic cargos from Weibel-Palade bodies', *Journal of Thrombosis and Haemostasis*, 16(9), pp. 1873–1886. Available at: https://doi.org/10.1111/jth.14218.

Nikmanesh, M., Shi, Z.-D. and Tarbell, J.M. (2012) 'Heparan sulfate proteoglycan mediates shear stress-induced endothelial gene expression in mouse embryonic stem cell-derived endothelial cells', *Biotechnology and Bioengineering*, 109(2), pp. 583–594. Available at: https://doi.org/10.1002/bit.23302.

Otte, L.A. *et al.* (2009) 'Rapid changes in shear stress induce dissociation of a G alpha(q/11)-platelet endothelial cell adhesion molecule-1 complex', *The Journal of Physiology*, 587(Pt 10), pp. 2365–2373. Available at: https://doi.org/10.1113/jphysiol.2009.172643.

Øynebråten, I. *et al.* (2004) 'Rapid chemokine secretion from endothelial cells originates from 2 distinct compartments', *Blood*, 104(2), pp. 314–320. Available at: https://doi.org/10.1182/blood-2003-08-2891.

Pacheco-Fernandez, N. *et al.* (2020) 'Nucleobindin-1 regulates ECM degradation by promoting intra-Golgi trafficking of MMPs', *The Journal of Cell Biology*, 219(8), p. e201907058. Available at: https://doi.org/10.1083/jcb.201907058.

Pahakis, M.Y. *et al.* (2007) 'The role of endothelial glycocalyx components in mechanotransduction of fluid shear stress', *Biochemical and Biophysical Research Communications*, 355(1), pp. 228–233. Available at: https://doi.org/10.1016/j.bbrc.2007.01.137.

Papaioannou, T.G. *et al.* (2006) 'Assessment of vascular wall shear stress and implications for atherosclerotic disease', *International Journal of Cardiology*, 113(1), pp. 12–18. Available at: https://doi.org/10.1016/j.ijcard.2006.03.035.

Parmar, K.M. *et al.* (2006) 'Integration of flow-dependent endothelial phenotypes by Kruppel-like factor 2', *Journal of Clinical Investigation*, 116(1), pp. 49–58. Available at: https://doi.org/10.1172/JCI24787.

Pedicini, L. *et al.* (2021) 'Affinity-based proteomics reveals novel binding partners for Rab46 in endothelial cells', *Scientific Reports*, 11(1), p. 4054. Available at: https://doi.org/10.1038/s41598-021-83560-y.

Pickett, J.A. and Edwardson, J.M. (2006) 'Compound Exocytosis: Mechanisms and Functional Significance', *Traffic*, 7(2), pp. 109–116. Available at: https://doi.org/10.1111/j.1600-0854.2005.00372.x.

Rabizadeh, E. *et al.* (2015) 'The cell-membrane prothrombinase, fibrinogen-like protein 2, promotes angiogenesis and tumor development', *Thrombosis Research*, 136(1), pp. 118–124. Available at: https://doi.org/10.1016/j.thromres.2014.11.023.

Ranade, S.S. *et al.* (2014) 'Piezo1, a mechanically activated ion channel, is required for vascular development in mice', *Proceedings of the National Academy of Sciences*, 111(28), pp. 10347–10352. Available at: https://doi.org/10.1073/pnas.1409233111.

Rand, J.H. *et al.* (1987) 'Distribution of von Willebrand factor in porcine intima varies with blood vessel type and location.', *Arteriosclerosis: An Official Journal of the American Heart Association, Inc.*, 7(3), pp. 287–291. Available at: https://doi.org/10.1161/01.ATV.7.3.287.

Ravichandran, Y., Goud, B. and Manneville, J.-B. (2020) 'The Golgi apparatus and cell polarity: Roles of the cytoskeleton, the Golgi matrix, and Golgi membranes', *Current Opinion in Cell Biology*, 62, pp. 104–113. Available at: https://doi.org/10.1016/j.ceb.2019.10.003.

Reininger, A.J. (2015) 'The function of ultra-large von Willebrand factor multimers in high shear flow controlled by ADAMTS13', *Hamostaseologie*, 35(3), pp. 225–233. Available at: https://doi.org/10.5482/HAMO-14-12-0077.

Rivera, L.B., Bradshaw, A.D. and Brekken, R.A. (2011) 'The regulatory function of SPARC in vascular biology', *Cellular and molecular life sciences : CMLS*, 68(19), pp. 3165–3173. Available at: https://doi.org/10.1007/s00018-011-0781-8.

Rizzo, Victor *et al.* (1998) '*In Situ* Flow Activates Endothelial Nitric Oxide Synthase in Luminal Caveolae of Endothelium with Rapid Caveolin Dissociation and Calmodulin Association*', *Journal of Biological Chemistry*, 273(52), pp. 34724–34729. Available at: https://doi.org/10.1074/jbc.273.52.34724.

Rizzo, V. *et al.* (1998) 'Rapid mechanotransduction in situ at the luminal cell surface of vascular endothelium and its caveolae', *The Journal of Biological Chemistry*, 273(41), pp. 26323–26329. Available at: https://doi.org/10.1074/jbc.273.41.26323.

Rubanyi, G.M. (1993) 'The Role of Endothelium in Cardiovascular Homeostasis and Diseases', *Journal of Cardiovascular Pharmacology*, 22, p. S1.

Ruggeri, Z.M. and Mendolicchio, G.L. (2015) ‘Interaction of von Willebrand factor with platelets and the vessel wall’, *Hämostaseologie*, 35(3), pp. 211–224. Available at: https://doi.org/10.5482/HAMO-14-12-0081.

Russell, F., Skepper, J. and Davenport, A. (1998) ‘Evidence Using Immunoelectron Microscopy for Regulated and Constitutive Pathways in the Transport and Release of Endothelin’, *Journal of Cardiovascular Pharmacology*, 31(3), pp. 424–430.

Russell Fraser D., Skepper Jeremy N., and Davenport Anthony P. (1998) ‘Human Endothelial Cell Storage Granules’, *Circulation Research*, 83(3), pp. 314–321. Available at: https://doi.org/10.1161/01.RES.83.3.314.

Sadler, J.E. *et al.* (2006) ‘Update on the pathophysiology and classification of von Willebrand disease: a report of the Subcommittee on von Willebrand Factor’, *Journal of Thrombosis and Haemostasis*, 4(10), pp. 2103–2114. Available at: https://doi.org/10.1111/j.1538-7836.2006.02146.x.

Sakamoto, Y. *et al.* (1993) ‘Immunoelectron microscopy on the localization of endothelin in the umbilical vein of perinatal rabbits’, *The Anatomical Record*, 237(4), pp. 482–488. Available at: https://doi.org/10.1002/ar.1092370407.

Sanders, Y.V. *et al.* (2013) ‘Reduced prevalence of arterial thrombosis in von Willebrand disease’, *Journal of Thrombosis and Haemostasis*, 11(5), pp. 845–854. Available at: https://doi.org/10.1111/jth.12194.

Santana Nunez, D. *et al.* (2023) ‘Piezo1 induces endothelial responses to shear stress via soluble adenylyl Cyclase-IP3R2 circuit’, *iScience*, 26(5), p. 106661. Available at: https://doi.org/10.1016/j.isci.2023.106661.

Schillemans, M. *et al.* (2019) ‘Exocytosis of Weibel–Palade bodies: how to unpack a vascular emergency kit’, *Journal of Thrombosis and Haemostasis*, 17(1), pp. 6–18. Available at: https://doi.org/10.1111/jth.14322.

Schnyder-Candrian, S. *et al.* (2000) ‘Localization of α1,3-fucosyltransferase VI in Weibel–Palade bodies of human endothelial cells’, *Proceedings of the National Academy of Sciences*, 97(15), pp. 8369–8374. Available at: https://doi.org/10.1073/pnas.97.15.8369.

Scholz, A., Plate, K.H. and Reiss, Y. (2015) ‘Angiopoietin-2: a multifaceted cytokine that functions in both angiogenesis and inflammation’, *Annals of the New York Academy of Sciences*, 1347, pp. 45–51. Available at: https://doi.org/10.1111/nyas.12726.

Senis, Y.A. *et al.* (1996a) ‘Changes in the pattern of distribution of von Willebrand factor in rat aortic endothelial cells following thrombin generation in vivo’, *British Journal of Haematology*, 93(1), pp. 195–203. Available at: https://doi.org/10.1046/j.1365-2141.1996.4661005.x.

Senis, Y.A. *et al.* (1996b) ‘Changes in the pattern of distribution of von Willebrand factor in rat aortic endothelial cells following thrombin generation in vivo’, *British Journal of Haematology*, 93(1), pp. 195–203. Available at: https://doi.org/10.1046/j.1365-2141.1996.4661005.x.

Shinge, S.A.U. *et al.* (2021) ' Mechanosensitive Piezo1 Channel Evoked-Mechanical Signals in Atherosclerosis ', *Journal of Inflammation Research*, 14, pp. 3621–3636. Available at: https://doi.org/10.2147/JIR.S319789.

Shyy, J.Y.-J. and Chien, S. (2002) 'Role of Integrins in Endothelial Mechanosensing of Shear Stress', *Circulation Research*, 91(9), pp. 769–775. Available at: https://doi.org/10.1161/01.RES.0000038487.19924.18.

Siedlecki, C.A. *et al.* (1996) 'Shear-dependent changes in the three-dimensional structure of human von Willebrand factor', *Blood*, 88(8), pp. 2939–2950.

Sporn, L.A., Marder, V.J. and Wagner, D.D. (1986) 'Inducible secretion of large, biologically potent von Willebrand factor multimers', *Cell*, 46(2), pp. 185–190. Available at: https://doi.org/10.1016/0092-8674(86)90735-X.

Springer, T.A. (2014) 'von Willebrand factor, Jedi knight of the bloodstream', *Blood*, 124(9), pp. 1412–1425. Available at: https://doi.org/10.1182/blood-2014-05-378638.

Stenmark, H. (2009) 'Rab GTPases as coordinators of vesicle traffic', *Nature Reviews Molecular Cell Biology*, 10(8), pp. 513–525. Available at: https://doi.org/10.1038/nrm2728.

Suri, C. *et al.* (1996) 'Requisite Role of Angiopoietin-1, a Ligand for the TIE2 Receptor, during Embryonic Angiogenesis', *Cell*, 87(7), pp. 1171–1180. Available at: https://doi.org/10.1016/S0092-8674(00)81813-9.

Swain, S.M. and Liddle, R.A. (2021) 'Piezo1 acts upstream of TRPV4 to induce pathological changes in endothelial cells due to shear stress', *Journal of Biological Chemistry*, 296. Available at: https://doi.org/10.1074/jbc.RA120.015059.

Syeda, R. *et al.* (2015) 'Chemical activation of the mechanotransduction channel Piezo1', *eLife*, 4, p. e07369. Available at: https://doi.org/10.7554/eLife.07369.

Taylor, D.E.M. (1975) 'BLOOD FLOW IN ARTERIES. 2nd ed. By D. A. McDonald. Edward Arnold, London, 1974. Pp. xviii+496. £12', *Quarterly Journal of Experimental Physiology and Cognate Medical Sciences*, 60(1), pp. 65–65. Available at: https://doi.org/10.1113/expphysiol.1975.sp002291.

Thurston, G. *et al.* (2000) 'Angiopoietin-1 protects the adult vasculature against plasma leakage', *Nature Medicine*, 6(4), pp. 460–463. Available at: https://doi.org/10.1038/74725.

Titani, K. *et al.* (1986) 'Amino acid sequence of human von Willebrand factor', *Biochemistry*, 25(11), pp. 3171–3184. Available at: https://doi.org/10.1021/bi00359a015.

Traub, O. and Berk, B.C. (1998) 'Laminar Shear Stress: Mechanisms by Which Endothelial Cells Transduce an Atheroprotective Force', *Arteriosclerosis, Thrombosis, and Vascular Biology*, 18(5), pp. 677–685. Available at: https://doi.org/10.1161/01.ATV.18.5.677.

Tressel, S.L. *et al.* (2007) 'Laminar Shear Inhibits Tubule Formation and Migration of Endothelial Cells by an Angiopoietin-2–Dependent Mechanism', *Arteriosclerosis, Thrombosis, and Vascular Biology*, 27(10), pp. 2150–2156. Available at: https://doi.org/10.1161/ATVBAHA.107.150920.

Tsai, H.-M. *et al.* (1991) 'The high molecular weight form of endothelial cell von Willebrand factor is released by the regulated pathway', *British Journal of Haematology*, 79(2), pp. 239–245. Available at: https://doi.org/10.1111/j.1365-2141.1991.tb04528.x.

Tzima, E. *et al.* (2001) 'Activation of integrins in endothelial cells by fluid shear stress mediates Rho-dependent cytoskeletal alignment', *The EMBO Journal*, 20(17), pp. 4639–4647. Available at: https://doi.org/10.1093/emboj/20.17.4639.

Tzima, E. *et al.* (2003) 'Localized Cdc42 Activation, Detected Using a Novel Assay, Mediates Microtubule Organizing Center Positioning in Endothelial Cells in Response to Fluid Shear Stress', *Journal of Biological Chemistry*, 278(33), pp. 31020–31023. Available at: https://doi.org/10.1074/jbc.M301179200.

Utgaard, J.O. *et al.* (1998) 'Rapid Secretion of Prestored Interleukin 8 from Weibel-Palade Bodies of Microvascular Endothelial Cells', *The Journal of Experimental Medicine*, 188(9), pp. 1751–1756. Available at: https://doi.org/10.1084/jem.188.9.1751.

Van der Heiden, K. *et al.* (2008) 'Endothelial primary cilia in areas of disturbed flow are at the base of atherosclerosis', *Atherosclerosis*, 196(2), pp. 542–550. Available at: https://doi.org/10.1016/j.atherosclerosis.2007.05.030.

Veith, C. *et al.* (2022) 'SPARC, a Novel Regulator of Vascular Cell Function in Pulmonary Hypertension', *Circulation*, 145(12), pp. 916–933. Available at: https://doi.org/10.1161/CIRCULATIONAHA.121.057001.

Vischer Ulrich M., Barth Holger, and Wollheim Claes B. (2000) 'Regulated von Willebrand Factor Secretion Is Associated With Agonist-Specific Patterns of Cytoskeletal Remodeling in Cultured Endothelial Cells', *Arteriosclerosis, Thrombosis, and Vascular Biology*, 20(3), pp. 883–891. Available at: https://doi.org/10.1161/01.ATV.20.3.883.

Vischer, U.M. and Wagner, D.D. (1993) 'CD63 is a component of Weibel-Palade bodies of human endothelial cells', *Blood*, 82(4), pp. 1184–1191.

Vischer, U.M. and Wollheinn, C.B. (1997) 'Epinephrine Induces von Willebrand Factor Release from Cultured Endothelial Cells: Involvement of Cyclic AMP-dependent Signalling in Exocytosis', *Thrombosis and Haemostasis*, 77(6), pp. 1182–1188. Available at: https://doi.org/10.1055/s-0038-1656135.

Voorberg, J. *et al.* (1990) 'Domains involved in multimer assembly of von willebrand factor (vWF): multimerization is independent of dimerization.', *The EMBO Journal*, 9(3), pp. 797–803. Available at: https://doi.org/10.1002/j.1460-2075.1990.tb08176.x.

Voorberg, J. *et al.* (1991) 'Assembly and routing of von Willebrand factor variants: the requirements for disulfide-linked dimerization reside within the carboxy-

terminal 151 amino acids.', *Journal of Cell Biology*, 113(1), pp. 195–205. Available at: https://doi.org/10.1083/jcb.113.1.195.

Wagner, D.D. (1990) 'Cell Biology of von Willebrand Factor', *Annual Review of Cell Biology*, 6(1), pp. 217–242. Available at: https://doi.org/10.1146/annurev.cb.06.110190.001245.

Wagner, D.D. *et al.* (1991) 'Induction of specific storage organelles by von Willebrand factor propolypeptide', *Cell*, 64(2), pp. 403–413. Available at: https://doi.org/10.1016/0092-8674(91)90648-I.

Wagner, D.D. and Frenette, P.S. (2008) 'The vessel wall and its interactions', *Blood*, 111(11), pp. 5271–5281. Available at: https://doi.org/10.1182/blood-2008-01-078204.

Wagner, D.D. and Marder, V.J. (1984) 'Biosynthesis of von Willebrand protein by human endothelial cells: processing steps and their intracellular localization.', *Journal of Cell Biology*, 99(6), pp. 2123–2130. Available at: https://doi.org/10.1083/jcb.99.6.2123.

Wagner, D.D., Olmsted, J.B. and Marder, V.J. (1982) 'Immunolocalization of von Willebrand protein in Weibel-Palade bodies of human endothelial cells.', *The Journal of Cell Biology*, 95(1), pp. 355–360. Available at: https://doi.org/10.1083/jcb.95.1.355.

Wang, S. *et al.* (2016) 'Endothelial cation channel PIEZO1 controls blood pressure by mediating flow-induced ATP release', *The Journal of Clinical Investigation*, 126(12), pp. 4527–4536. Available at: https://doi.org/10.1172/JCI87343.

Wang, X.-L., Schnoor, M. and Yin, L.-M. (2023) 'Metallothionein-2: An emerging target in inflammatory diseases and cancers', *Pharmacology & Therapeutics*, 244, p. 108374. Available at: https://doi.org/10.1016/j.pharmthera.2023.108374.

Weibel, E.R. (2012) 'Fifty years of Weibel–Palade bodies: the discovery and early history of an enigmatic organelle of endothelial cells1', *Journal of Thrombosis and Haemostasis*, 10(6), pp. 979–984. Available at: https://doi.org/10.1111/j.1538-7836.2012.04718.x.

Weibel, E.R. and Palade, G.E. (1964) 'NEW CYTOPLASMIC COMPONENTS IN ARTERIAL ENDOTHELIA', *The Journal of Cell Biology*, 23(1), pp. 101–112. Available at: https://doi.org/10.1083/jcb.23.1.101.

Weinbaum, S., Tarbell, J.M. and Damiano, E.R. (2007) 'The structure and function of the endothelial glycocalyx layer', *Annual Review of Biomedical Engineering*, 9, pp. 121–167. Available at: https://doi.org/10.1146/annurev.bioeng.9.060906.151959.

Whincup, P.H. *et al.* (2002) 'von Willebrand factor and coronary heart disease. Prospective study and meta-analysis', *European Heart Journal*, 23(22), pp. 1764–1770. Available at: https://doi.org/10.1053/euhj.2001.3237.

Wieberdink, R.G. *et al.* (2010) ‘High von Willebrand Factor Levels Increase the Risk of Stroke’, *Stroke*, 41(10), pp. 2151–2156. Available at: https://doi.org/10.1161/STROKEAHA.110.586289.

Winkles, J.A. *et al.* (1993) ‘Endothelin-1 and Endothelin Receptor mRNA Expression in Normal and Atherosclerotic Human Arteries’, *Biochemical and Biophysical Research Communications*, 191(3), pp. 1081–1088. Available at: https://doi.org/10.1006/bbrc.1993.1327.

Xiong, Y. *et al.* (2013) ‘Hypertensive stretch regulates endothelial exocytosis of Weibel-Palade bodies through VEGF receptor 2 signaling pathways’, *Cell Research*, 23(6), pp. 820–834. Available at: https://doi.org/10.1038/cr.2013.56.

Yamamoto, K. *et al.* (1998) ‘Tissue Distribution and Regulation of Murine von Willebrand Factor Gene Expression In Vivo’, *Blood*, 92(8), pp. 2791–2801. Available at: https://doi.org/10.1182/blood.V92.8.2791.

Zannettino, A.C.W. *et al.* (2005) ‘Osteoprotegerin (OPG) is localized to the Weibel-Palade bodies of human vascular endothelial cells and is physically associated with von Willebrand factor’, *Journal of Cellular Physiology*, 204(2), pp. 714–723. Available at: https://doi.org/10.1002/jcp.20354.

Zenner, H.L. *et al.* (2007) ‘High-pressure freezing provides insights into Weibel-Palade body biogenesis’, *Journal of Cell Science*, 120(12), pp. 2117–2125. Available at: https://doi.org/10.1242/jcs.007781.

Zhao, Q. *et al.* (2016) ‘Ion Permeation and Mechanotransduction Mechanisms of Mechanosensitive Piezo Channels’, *Neuron*, 89(6), pp. 1248–1263. Available at: https://doi.org/10.1016/j.neuron.2016.01.046.

Zografou, S. *et al.* (2012) ‘A complete Rab screening reveals novel insights in Weibel–Palade body exocytosis’, *Journal of Cell Science*, 125(20), pp. 4780–4790. Available at: https://doi.org/10.1242/jcs.104174.

Zong, B. *et al.* (2023) ‘Mechanosensitive Piezo1 channel in physiology and pathophysiology of the central nervous system’, *Ageing Research Reviews*, 90, p. 102026. Available at: https://doi.org/10.1016/j.arr.2023.102026.

Appendix

ImageJ Macro – Endothelial Cell Alignment Quantification

```
imageTitle=getTitle();//returns a string with the image title

run("Rotate 90 Degrees Left");

run("Difference of Gaussians", "  sigma1=20 sigma2=1");

run("32-bit");

run("OrientationJ Distribution", "tensor=2.0 gradient=4 orientation=off
radian=off histogram=off table=on min-coherency=0.0 min-energy=0.0 ");

saveAs("Results", "C:\\ "+imageTitle+".txt");

selectWindow("OJ-Histogram-1-slice-1");

close();

selectWindow(imageTitle);

close();
```

ImageJ Macro – WPB Number and Feret diameter

```
imageTitle=getTitle();//returns a string with the image title

run("Split Channels");

selectWindow("C1-"+imageTitle)

close();

selectWindow("C2-"+imageTitle);

setOption("ScaleConversions", true);

run("8-bit");

run("Subtract Background...", "rolling=3 sliding");

run("Auto Local Threshold", "method=Bernsen radius=15 parameter_1=0
parameter_2=0 white");

run("Analyze Particles...", "size=0.1-3.00 show=Masks clear add");

run("Set Measurements...", "area perimeter feret's redirect=None
decimal=9");

roiManager("Measure");

saveAs("Results", "C:\\"+imageTitle+".txt");

selectWindow("C2-"+imageTitle);

close();

selectWindow("Mask of C2-"+imageTitle);

close();

close("Results");

close("ROI Manager");
```

ImageJ Macro – WPB Distribution

```
//macro to create distance map on 512 x 512 pixel image

imageTitle=getTitle();//returns a string with the image title

run("Split Channels");

selectWindow("C2-"+imageTitle);

close();

selectWindow("C1-"+imageTitle);

close();

selectWindow("C3-"+imageTitle);

rename("nuclei");

run("Command From Macro",
"command=[de.csbdresden.stardist.StarDist2D], args=['input':'nuclei',
'modelChoice':'Versatile (fluorescent nuclei)',
'normalizeInput':'true', 'percentileBottom':'1.0',
'percentileTop':'99.8', 'probThresh':'0.5', 'nmsThresh':'0.4',
'outputType':'Both', 'nTiles':'1', 'excludeBoundary':'2',
'roiPosition':'Automatic', 'verbose':'false',
'showCsbdeepProgress':'false', 'showProbAndDist':'false'],
process=[false]");

selectWindow("Label Image");

run("Auto Threshold", "method=MinError(I) white");

setOption("BlackBackground", true);

run("Convert to Mask");

run("Invert");

run("Distance Map");

close("ROI Manager");

close("nuclei");

run("Brightness/Contrast...");

setMinAndMax(0, 150);

run("Apply LUT");
```

```
run("Size...", "width=2048 height=2048 depth=1 constrain average
interpolation=Bilinear"); //end up with distance map with nuclei
identified using StarDist (much more robust than previous method)



//macro to identify WPBs

imageTitle=getTitle();//returns a string with the image title

run("Split Channels");

selectWindow("C2-"+imageTitle);

setOption("ScaleConversions", true);

run("8-bit");

run("Subtract Background...", "rolling=3 sliding");

run("Auto Local Threshold", "method=Bernsen radius=15 parameter_1=0
parameter_2=0 white");

run("Set Measurements...", "area mean min integrated redirect=[Label
Image] decimal=3");

selectWindow("C2-" + imageTitle);


run("Analyze Particles...", "size=0.1-3.00 display");

saveAs("Results", "C:\\"+imageTitle+".txt");

selectWindow("Label Image");

close();

selectWindow("C2-"+imageTitle);

close();

selectWindow("C1-"+imageTitle);

close();

close("Results");
```

ImageJ Macro – vWF String Analysis

```
imageTitle=getTitle();//returns a string with the image title

run("Split Channels");

selectWindow("C1-"+imageTitle)

close();

selectWindow("C2-"+imageTitle);

setOption("ScaleConversions", true);

run("8-bit");

run("Auto Local Threshold", "method=Phansalkar radius=15 parameter_1=0
parameter_2=0 white");

run("Analyze Particles...", "size=2-Infinity circularity=0.00-0.20
show=Masks clear add");

saveAs("Results", "C:\\ "+imageTitle+".txt");

selectWindow("C2-"+imageTitle);

close();

selectWindow("Mask of C2-"+imageTitle);

close();

close("Results");

close("ROI Manager");
```

ImageJ Macro – Golgi Fragmentation

```
imageTitle=getTitle();

run("Split Channels");

selectWindow("C1-"+imageTitle)

close();

selectWindow("C2-"+imageTitle);

close();

selectWindow("C3-"+imageTitle);

setOption("ScaleConversions", true);

run("8-bit");

run("Grays");

run("Subtract Background...", "rolling=20");

run("Auto Threshold", "method=IsoData white");

run("Set Measurements...", "area perimeter feret's redirect=None
decimal=9");

run("Analyze Particles...", "size=0.20-Infinity display");

saveAs("Results", "C:\\ "+imageTitle+".txt");

close("Results");

selectWindow("C3-"+imageTitle);

close();
```

Appendix Table - WPB associated proteins differentially expressed in scRNAseq dataset

This table shows a list of potential WPB associated proteins identified in the literature that were either upregulated or downregulated in scRNAseq data (Andueza et al., 2020) in response to disturbed flow (E8), compared to laminar flow (E2). These potential WPB proteins were identified from proximity and affinity-based proteomics (van Breevoort *et al.*, 2012; Pedicini *et al.*, 2021). Red highlighted avg_log2FC values indicate higher expression in E8 (disturbed flow), green highlighted avg_log2FC values indicate higher expression in E2 (laminar/steady flow). Pct.1 and pct.2 represent percentage expression, green being the highest and red being the lowest of the colour scale.

WPB Associated Protein	Gene Short Name	p_val	avg_log2FC	pct.1 (E2)	pct.2 (E8)	p_val_adj
SPARC	SPARC	0	-2.054844149	0.992	1	0
Fibronectin	FN1	3.21E-288	-2.004374564	0.852	0.982	1.04E-283
Thioredoxin domain-containing protein 5	TXNDC5	0	-1.891869252	0.756	0.978	0
Matrix Gla protein	MGP	1.14E-215	-1.209438071	0.998	1	3.68E-211
Serpin H1	SERPINH1	9.15E-289	-1.190068394	0.914	0.987	2.95E-284
Plasminogen activator inhibitor 1	SERPINE1	5.17E-96	-1.149448938	0.498	0.763	1.67E-91
Caldesmon	CALD1	3.87E-168	-1.119364888	0.865	0.956	1.25E-163
Heat shock 70 kDa protein 4	HSPA4	1.17E-168	-0.935047825	0.705	0.904	3.76E-164
Collagen alpha-1(III) chain	COL3A1	5.50E-151	-0.675247418	0.062	0.447	1.78E-146
Endothelial protein C receptor	PROCR	5.05E-124	-0.666390291	0.945	0.986	1.63E-119
Cell surface glycoprotein MUC18	MCAM	1.54E-136	-0.662054811	0.345	0.717	4.96E-132
Fascin	FSCN1	4.68E-232	-0.612528096	0.001	0.463	1.51E-227
40S ribosomal protein SA	RPSA	7.55E-239	-0.575883594	0.998	1	2.44E-234
Cathepsin Z	CTSZ	4.32E-121	-0.527042684	0.909	0.964	1.40E-116
Ral guanine nucleotide dissociation stimulator	RALGDS	2.01E-135	-0.4979127	0.182	0.579	6.49E-131
Heat shock cognate 71 kDa protein	HSPA8	6.52E-128	-0.471122538	0.996	0.999	2.10E-123

WPB Associated Protein	Gene Short Name	p_val	avg_log2FC	pct.1 (E2)	pct.2 (E8)	p_val_adj
Tubulin beta-2C chain	TUBB4B	2.94E-72	-0.467309022	0.938	0.978	9.50E-68
Transgelin-2	TAGLN2	2.04E-87	-0.464840743	0.984	0.993	6.57E-83
Oxidation resistance protein 1	OXR1	3.77E-70	-0.461521527	0.542	0.741	1.22E-65
ADP-ribosylation factor 5	ARF5	2.97E-104	-0.439445975	0.941	0.97	9.59E-100
Lysosomal Pro-X carboxypeptidase	PRCP	2.18E-71	-0.417812336	0.438	0.684	7.03E-67
Cytosol aminopeptidase	LAP3	2.81E-55	-0.41707633	0.707	0.849	9.08E-51
Tubulin beta-3 chain	TUBB3	6.97E-76	-0.407543114	0.083	0.336	2.25E-71
Beta-hexosaminidase subunit alpha	HEXA	2.34E-57	-0.389387865	0.838	0.915	7.54E-53
Alpha-actinin-1	ACTN1	1.12E-39	-0.388835149	0.904	0.935	3.62E-35
Ras-related protein Rab-34	RAB34	2.67E-82	-0.373008994	0.216	0.512	8.64E-78
ADP-ribosylation factor-like protein 1	ARL1	5.46E-55	-0.370714175	0.85	0.915	1.76E-50
Vinculin	VCL	2.31E-33	-0.363298249	0.796	0.868	7.46E-29
Epididymal secretory protein E1	NPC2	1.39E-66	-0.361582003	0.936	0.972	4.48E-62
Integrin beta-5	ITGB5	2.43E-55	-0.357943899	0.293	0.531	7.83E-51
Tubulin beta-2A chain	TUBB2A	3.44E-24	-0.34970423	0.885	0.931	1.11E-19
40S ribosomal protein S20	RPS20	6.49E-146	-0.348893103	0.999	1	2.09E-141
Protein PRRC1	PRRC1	4.35E-58	-0.337650117	0.391	0.618	1.40E-53
Nascent polypeptide associated complex subunit alpha	NACA	7.82E-84	-0.329757123	0.983	0.995	2.52E-79
Myristoylated alanine-rich C-kinase substrate	MARCKS	2.35E-49	-0.32693914	0.323	0.551	7.59E-45
Tubulin beta-6 chain	TUBB6	3.89E-64	-0.322284062	0.16	0.414	1.26E-59
Endoplasmin	HSP90B1	1.10E-40	-0.320362526	0.982	0.988	3.56E-36
Coatomer subunit epsilon	COPE	5.05E-39	-0.31670147	0.826	0.876	1.63E-34
Forkhead box protein O1	FOXO1	2.67E-38	-0.31656808	0.615	0.745	8.62E-34
Annexin A5	ANXA5	5.74E-59	-0.312824791	0.978	0.991	1.85E-54
Glyceraldehyde-3-phosphate dehydrogenase	GAPDH	1.35E-44	-0.3067244	0.939	0.971	4.37E-40
Protein disulfide-isomerase A4	PDIA4	2.21E-35	-0.304153332	0.735	0.823	7.12E-31
Gap junction alpha-1 protein	GJA1	3.73E-88	-0.302380691	0.052	0.314	1.20E-83

WPB Associated Protein	Gene Short Name	p_val	avg_log2FC	pct.1 (E2)	pct.2 (E8)	p_val_adj
26S proteasome non-ATPase regulatory subunit 11	PSMD11	5.78E-34	-0.28833782	0.759	0.859	1.87E-29
Elongation factor 1-alpha 1	EEF1A1	6.18E-77	-0.267093358	1	1	2.00E-72
Mothers against decapentaplegic homolog 1	SMAD1	2.15E-35	-0.261157617	0.399	0.584	6.94E-31
Annexin A6	ANXA6	4.10E-29	-0.25900486	0.645	0.757	1.32E-24
Elongation factor 1-gamma	EEF1G	2.45E-37	-0.258821903	0.941	0.967	7.92E-33
Syntaxin-12	STX12	4.53E-28	0.252799173	0.806	0.71	1.46E-23
Lamin-B receptor	LBR	1.42E-34	0.256908554	0.664	0.472	4.58E-30
EPAC/Rap guanine nucleotide exchange factor 3	RAPGEF3	1.40E-34	0.263379223	0.567	0.365	4.53E-30
Rab GDP dissociation inhibitor beta	GDI2	1.86E-35	0.264566952	0.94	0.917	6.01E-31
Torsin-1A-interacting protein 1	TOR1AIP1	1.33E-25	0.270259405	0.864	0.782	4.31E-21
Extended synaptotagmin-1	ESYT1	5.42E-39	0.271058688	0.583	0.368	1.75E-34
Erythrocyte initiation factor 4A-I	EIF4A1	1.20E-44	0.272989331	0.983	0.98	3.88E-40
Ras GTPase-activating-like protein IQGAP1	IQGAP1	3.08E-35	0.278556353	0.976	0.946	9.94E-31
Moesin	MSN	2.49E-36	0.28988994	0.979	0.974	8.05E-32
Apha-actinin-4	ACTN4	2.47E-42	0.301232087	0.987	0.977	7.96E-38
Toll-interacting protein	TOLLIP	1.87E-56	0.308114397	0.572	0.303	6.04E-52
Amyloid beta A4 precursor protein-binding family B member 2	APBB2	1.32E-36	0.314593329	0.844	0.736	4.27E-32
Synaptic vesicle membrane protein VAT-1 homolog	VAT1	1.46E-38	0.315150159	0.733	0.571	4.72E-34
Mitogen-activated protein kinase kinase kinase 11	MAP3K11	1.64E-34	0.317025919	0.631	0.449	5.28E-30
UDP-N-acetylhexosamine pyrophosphorylase-like protein 1	UAP1L1	2.41E-50	0.319790484	0.566	0.317	7.77E-46
14-3-3 protein zelta/delta	YWHAZ	2.27E-52	0.330570019	0.963	0.923	7.33E-48
Guanine nucleotide-binding protein G(I)/G(S)/G(T) subunit beta-1	GNB1	1.38E-53	0.337727615	0.958	0.926	4.47E-49
Thioredoxin-related transmembrane protein 1	TMX1	3.78E-46	0.348090179	0.87	0.786	1.22E-41
BAG family molecular chaperone regulator 5	BAG5	6.44E-54	0.367379184	0.713	0.5	2.08E-49
SUN domain-containing protein 2	SUN2	6.10E-60	0.368385008	0.605	0.334	1.97E-55
Tropomyosin alpha-4 chain	TPM4	2.02E-69	0.379041092	0.966	0.935	6.51E-65
Ras-related protein 1	RAP1B	9.27E-60	0.379225198	0.932	0.879	2.99E-55

WPB Associated Protein	Gene Short Name	p_val	avg_log2FC	pct.1 (E2)	pct.2 (E8)	p_val_adj
Nucleobindin-1	NUCB1	1.77E-64	0.393150717	0.921	0.849	5.71E-60
Junction plakoglobin	JUP	1.89E-68	0.402429862	0.673	0.403	6.09E-64
PRA1 family protein 3	ARL6IP5	1.15E-79	0.44729427	0.946	0.897	3.70E-75
Amyloid-like protein 2	APLP2	7.26E-108	0.46907243	0.987	0.982	2.34E-103
Integrin beta-1	ITGB1	9.72E-124	0.484055876	0.993	0.991	3.14E-119
Carboxypeptidase D	CPD	3.76E-90	0.507107382	0.892	0.734	1.21E-85
Amyloid beta A4 protein	APP	2.99E-140	0.539489343	0.985	0.971	9.66E-136
Transforming protein RhoA	RHOA	9.41E-161	0.569422717	0.986	0.983	3.04E-156
Heat shock protein HSP 90-alpha	HSP90AA1	2.44E-139	0.571381894	0.984	0.95	7.88E-135
Plasmalemma vesicle-associated protein	PLVAP	1.18E-29	0.577649708	0.696	0.567	3.81E-25
Rab effector MyRIP	MYRIP	8.33E-161	0.588973766	0.616	0.125	2.69E-156
Annexin A2	ANXA2	6.62E-135	0.645635379	0.982	0.955	2.14E-130
Polyubiquitin-C	UBC	6.33E-163	0.69594926	0.999	0.999	2.04E-158
Guanine nucleotide-binding protein G(k) subunit alpha	GNAI3	4.59E-143	0.698394079	0.91	0.726	1.48E-138
Lysosome membrane protein 2	SCARB2	1.48E-149	0.730899671	0.841	0.565	4.78E-145
NADH-cytochrome b5 reductase 3	CYB5R3	3.15E-157	0.770136877	0.952	0.865	1.02E-152
EGF-containing fibulin-like extracellular matrix protein 1	EFEMP1	4.11E-154	0.77969234	0.885	0.577	1.33E-149
S-adenosylmethionine synthase isoform type-2	MAT2A	8.43E-156	0.799812	0.927	0.751	2.72E-151
Nuclease-sensitive element binding protein 1	YBX1	1.63E-275	0.817741762	0.994	0.992	5.25E-271
S100 Calcium-Binding Protein A10/Calpactin I light chain	S100A10	7.87E-129	0.839305603	0.989	0.952	2.54E-124
Annexin A3	ANXA3	1.10E-271	0.912017191	0.993	0.982	3.55E-267
Jun proto-oncogene, Activator Protein-1	JUN	6.04E-145	0.965354769	0.999	0.997	1.95E-140
Protein-glutamine gamma-glutamyltransferase 2	TGM2	1.50E-225	0.987507476	0.967	0.807	4.86E-221
Platelet endothelial cell adhesion molecule	PECAM1	0	1.002736143	1	0.998	0
Intercellular adhesion molecule 2	ICAM2	0	1.181973253	0.987	0.958	0
Podocalyxin	PODXL	5.10E-299	1.31065203	0.915	0.406	1.65E-294
Kruppel-like factor 2	KLF2	0	1.383565849	1	0.982	0

WPB Associated Protein	Gene Short Name	p_val	avg_log2FC	pct.1 (E2)	pct.2 (E8)	p_val_adj
Kruppel-like factor 4	KLF4	0	1.899031579	0.999	0.91	0